NASA/CR-2008-215334

Constitutive Soil Properties for Unwashed Sand and Kennedy Space Center

Michael A. Thomas, Daniel E. Chitty, Martin L. Gildea, and Casey M. T'Kindt
Applied Research Associates, Inc., Albuquerque, New Mexico

July 2008

The NASA STI Program Office . . . in Profile

Since its founding, NASA has been dedicated to the advancement of aeronautics and space science. The NASA Scientific and Technical Information (STI) Program Office plays a key part in helping NASA maintain this important role.

The NASA STI Program Office is operated by Langley Research Center, the lead center for NASA's scientific and technical information. The NASA STI Program Office provides access to the NASA STI Database, the largest collection of aeronautical and space science STI in the world. The Program Office is also NASA's institutional mechanism for disseminating the results of its research and development activities. These results are published by NASA in the NASA STI Report Series, which includes the following report types:

- TECHNICAL PUBLICATION. Reports of completed research or a major significant phase of research that present the results of NASA programs and include extensive data or theoretical analysis. Includes compilations of significant scientific and technical data and information deemed to be of continuing reference value. NASA counterpart of peer-reviewed formal professional papers, but having less stringent limitations on manuscript length and extent of graphic presentations.

- TECHNICAL MEMORANDUM. Scientific and technical findings that are preliminary or of specialized interest, e.g., quick release reports, working papers, and bibliographies that contain minimal annotation. Does not contain extensive analysis.

- CONTRACTOR REPORT. Scientific and technical findings by NASA-sponsored contractors and grantees.

- CONFERENCE PUBLICATION. Collected papers from scientific and technical conferences, symposia, seminars, or other meetings sponsored or co-sponsored by NASA.

- SPECIAL PUBLICATION. Scientific, technical, or historical information from NASA programs, projects, and missions, often concerned with subjects having substantial public interest.

- TECHNICAL TRANSLATION. English-language translations of foreign scientific and technical material pertinent to NASA's mission.

Specialized services that complement the STI Program Office's diverse offerings include creating custom thesauri, building customized databases, organizing and publishing research results ... even providing videos.

For more information about the NASA STI Program Office, see the following:

- Access the NASA STI Program Home Page at ***http://www.sti.nasa.gov***

- E-mail your question via the Internet to help@sti.nasa.gov

- Fax your question to the NASA STI Help Desk at (301) 621-0134

- Phone the NASA STI Help Desk at (301) 621-0390

- Write to:
  NASA STI Help Desk
  NASA Center for AeroSpace Information
  7115 Standard Drive
  Hanover, MD 21076-1320

NASA/CR-2008-215334

Constitutive Soil Properties for Unwashed Sand and Kennedy Space Center

Michael A. Thomas, Daniel E. Chitty, Martin L. Gildea, and Casey M. T'Kindt
Applied Research Associates, Inc., Albuquerque, New Mexico

National Aeronautics and
Space Administration

Langley Research Center
Hampton, Virginia 23681-2199

Prepared for Langley Research Center
under Contract NNL07AA00B

July 2008

Acknowledgments

Applied Research Associates, Inc (ARA) conducted this soil study under contract to NASA Langley Research Center's (LaRC) prime contractor for engineering support, ATK Space. ATK Space is the TEAMS (Technology Engineering and Aerospace Mission Support) prime contractor. Dr. Ralph Buehrle, LaRC, sponsored the study. The study was conducted for LaRC's Landing Systems ADP group, charged with evaluating Crew Exploration Vehicle (CEV) terrain landing designs. The two sites selected for this study, LaRC's gantry facility and Kennedy Space Center, were identified by LaRC.

LaRC is evaluating terrain landing events for the Orion CEV. The current terrain landing design involves parachuting the CEV to a defined landing zone, deploying airbags prior to contact, and releasing the airbag pressures to cushion the capsule during landing. This report provides constitutive soil properties for landing simulations. The primary author is Michael A. Thomas, with contributions from Daniel E. Chitty, Martin L. Gildea, and Casey M. T'Kindt. All are engineers with ARA.

Available from:

NASA Center for AeroSpace Information (CASI)
7115 Standard Drive
Hanover, MD 21076-1320
(301) 621-0390

National Technical Information Service (NTIS)
5285 Port Royal Road
Springfield, VA 22161-2171
(703) 605-6000

National Aeronautics and
Space Administration

Langley Research Center
Hampton, Virginia 23681-2199

Prepared for Langley Research Center
under Contract NNL07AA00B

July 2008

Abstract

Accurate soil models are required for numerical simulations of land landings for the Orion Crew Exploration Vehicle. This report provides constitutive material models for one soil, unwashed sand, from NASA Langley's gantry drop test facility and three soils from Kennedy Space Center (KSC). The four soil models are based on mechanical and compressive behavior observed during geotechnical laboratory testing of remolded soil samples. The test specimens were reconstituted to measured in situ density and moisture content. Tests included: triaxial compression, hydrostatic compression, and uniaxial strain. A fit to the triaxial test results defines the strength envelope. Hydrostatic and uniaxial tests define the compressibility. The constitutive properties are presented in the format of *LS-DYNA Material Model 5: Soil and Foam*. However, the laboratory test data provided can be used to construct other material models.

The four soil models are intended to be specific to the soil conditions discussed in the report. The unwashed sand model represents clayey sand at high density. The KSC models represent three distinct coastal sand conditions: low density dry sand, high density in-situ moisture sand, and high density flooded sand. It is possible to approximate other sands with these models, but the results would be unverified without geotechnical tests to confirm similar soil behavior.

Table of Contents

1 Introduction

Langley Research Center (LaRC) was tasked with modeling Crew Exploration Vehicle (CEV) -soil interaction. Two sites of modeling interest were identified. The first is a test soil located at LaRC's gantry facility. Mock-up CEV craft were dropped on an "unwashed sand" soil. The second site is comprised of the soils surrounding Pad 39 A and B at Kennedy Space Center (KSC). LaRC is interested in determining soil factors influence the design of the CEV capsule during soil impact. The models presented in this report are geared toward CEV-soil interaction models. The KSC models are able to model the higher stresses expected for landing without airbag systems.

This report quantifies soil conditions at each site and provides soil constitutive properties to support LaRC's numerical modeling of the CEV landing. For this modeling, LaRC is using LS-DYNA, a 3-dimensional finite element software program. Applied Research Associates (ARA) performed soil sampling on field visits to each site. The soil samples were shipped to ARA's geotechnical laboratory for a series of laboratory tests. The tests were designed to yield the required constitutive inputs for LS-DYNA's Material Model 5: Soil and Foam. The unwashed sand at LaRC's gantry comprises of a single soil model. KSC's range of variation is characterized to the best possible extent within three models.

The unwashed sand soil can be described as mostly sand material mixed with some clay. The clay provides cohesion to the granular sand particles. The KSC sands can be described as quartzite/feldspar sands with common material constituents and grain size distribution.

The soil characterization began with field visits to each of the sites. The general field plan consisted of rapidly surveying the area to observe the total number of soil types, then performing in situ measurements and collecting soil samples. After the rapid surveys, the site's soils were sampled within the restrictions of scope. Four soil models are presented in this report. Soil sampling at LaRC's gantry reflected the production of one soil model to represent the uniform drop test soil. KSC sampling was predicated on three soil models to represent three distinct soil conditions near Pad 39 A and B.

This document is intended as a stand-alone second phase report. It supplements the 1 Feb 2008 report titled "Constitutive Soil Properties for Cuddeback Lake, CA and Carson Sink, NV." Comparisons to Cuddeback and Carson Sink models are made throughout this report.

2 LS-DYNA Material Model 5 Description

LS-DYNA Material Model 5 was identified by LaRC for modeling the soils in preliminary calculations. The constitutive properties derived in this report are tailored for constructing this type of model. This section describes the physical meaning of each of the model inputs. Section 3 addresses how each of the model inputs were obtained from material testing.

Because soil strength is pressure dependent, a pressure dependent material model is necessary for constitutive modeling. In LS-DYNA, Material Model 5: Soil and Foam is the most basic of the pressure dependent strength models available. It is also the oldest LS-DYNA pressure dependent model and therefore has accumulated a considerable amount of user experience and feedback. As a result, the model is quite robust given its simple inputs.

Defining the model requires shear and unloading bulk moduli, three coefficients that define the quadratic shear failure surface, a pressure cutoff value that defines the maximum tension allowed, and 10 points on a pressure-volume strain curve to define compressibility. Table 2-1 defines these inputs. Based on LaRC preference for their numerical modeling, the material model inputs are provided in pounds and inches.

The elastic shear modulus, *G*, describes shear deformation when the soil is initially loaded. The bulk unloading modulus, BULK, describes the expansion of the soil when the load is reduced. These two parameters are necessary because the loading and unloading behavior of soil is not equal due to permanent deformations.

The a_0, a_1, and a_2 inputs define a quadratic fit to a strength curve. The strength curve is defined as a yield surface plotted in J_2' vs. pressure space. Pressure is the mean stress, the average of all the principle stresses on the material. Pressure is positive in compression. J_2' is the second invariant of the stress deviator. Material tests define points on the yield surface, and the quadratic fit is LS-DYNA's approximation of material strength. In the LS-DYNA manual, the second invariant of the stress deviator is denoted J_2. In this report, the more common notation, J_2', is used to represent the same quantity.

Volumetric strain behavior is defined by the natural log of the relative volume and is negative in compression. Relative volume is the ratio of the current soil cell volume to the initial volume at the start of the calculation. The volumetric strain is represented as a 10 point curve in pressure vs. volume strain space. Each point on the curve is obtained from material testing at the given pressure.

The LS-DYNA Theory Manual describes Material Model 5 in more detail. Appendix A contains excerpts from the manual.

Table 2-1. LS-DYNA Material Model 5 Inputs.

Input	Obtained from soil test:	Description
MID	N/A	LS-DYNA's material identification number. A unique number identifying an input set of material properties. A number must be assigned.
RO	Nuclear density field test	Mass density. Obtained from dividing weight density (mass/unit volume) by gravity.
G	Uniaxial strain	Elastic shear modulus. The slope of the shear stress vs. shear strain curve. Can be computed from constrained modulus and Poisson's ratio from a uniaxial test.
BULK	Hydrostatic compression	Unloading bulk modulus. It is the slope of the mean stress vs. strain curve when the pressure is reduced (unloaded) from a higher pressure load. Can also be obtained from uniaxial strain unloading.
A0	Triaxial compression	A quadratic fit coefficient. In a J_2' vs. p (second invariant of stress difference vs. pressure) plot, a_0 represents the intersection of the shear failure envelope's (or yield surface) quadratic fit and the J_2' axis. a_0 coefficient is the Y-intercept. The J_2' vs. p plot is derived from stress difference vs. normal stress.
A1	Triaxial compression	a_1 is a quadratic fit coefficient. It is the initial slope coefficient of the shear failure envelope's quadratic fit.
A2	Triaxial compression	a_2 is a quadratic fit coefficient. It is the curvature coefficient of the shear failure envelope's quadratic fit.
PC	Triaxial compression	"Pressure cut-off." Maximum tension stress allowed, representing tensile fracture. It is the mean stress intercept of the shear failure envelope.
VCR	This is a flag variable. VCR=0	VCR=0 turns on volumetric crushing, defined by the 10 points on the pressure-volume curve. VCR=1 turns off. The pressure-volume curve defines the deformation of the material at 10 pressures.
REF	This is a flag variable. REF=0	This option controls the use of reference geometry to initialize the pressure. REF=0 is recommended. This option does not initialize the deviatoric stress state.
EPS1, P1	EPS1=0, P1=0	This is the first point on the pressure volume curve; at zero loading there is zero volume change. EPS is the natural logarithmic volume strain = (ln [1 - ε_{volume}]), where ε_{volume} = (initial volume – current volume)/initial volume
EPS2, P2	Uniaxial strain	2nd pressure-volume point
EPS3, P3	Uniaxial strain	3rd pressure-volume point
EPS4, P4	Uniaxial strain	4th pressure-volume point
EPS5, P5	Uniaxial strain	5th pressure-volume point
EPS6, P6	Uniaxial strain	6th pressure-volume point
EPS7, P7	Uniaxial strain	7th pressure-volume point
EPS8, P8	Uniaxial strain	8th pressure-volume point
EPS9, P9	Uniaxial strain	9th pressure-volume point
EPS10, P10	Uniaxial strain	10th pressure-volume point

3 Methodology for Obtaining Constitutive Soil Properties

This section describes the methodology for deriving LS-DYNA material model inputs from laboratory test data.

3.1 Geotechnical Laboratory Tests

ARA operates a specialized geotechnical laboratory in South Royalton, VT where the soil samples were shipped for testing. The types of tests conducted for this effort are listed and explained below:

- Grain density
- Grain size distribution
- Moisture content
- Atterberg limits
- Hydrostatic compression
- Uniaxial strain
- Triaxial compression

3.1.1 Grain Density

A given volume of soil is comprised of solid particles and void space. The grain density (ρ_g) of a soil is the density of the solid particles. Knowing the grain density of a soil allows one to perform accurate saturation and void volume calculations. Soils typically have a grain density of 2.7 +/- 0.1 g/cm^3. Although not specifically used in constitutive modeling, the grain density is a basic piece of information useful for characterizing the soil as a whole.

The grain density is measured according to the procedures defined by ASTM D854-83. This test is performed using a pycnometer, a special-purpose glass flask with a drilled ground glass stopper that allows it to be filled with the same volume of water with density ρ_w. First, the weight of a 100-ml pycnometer is determined. Second, the pycnometer is filled with distilled, de-aired water to its fill point and re-weighed, (m_a). Then, the water is dumped, and an oven dried soil sample is placed in the dried pycnometer and weighed to determine the mass of the oven-dried sand sample (m_o). Distilled, de-aired water is added to the pycnometer again to slightly above the soil sample. The air entrapped in the sample soil is removed by vacuum. More de-aired, distilled water is added to the pycnometer until reaching the same fill point, and the mass of pycnometer, soil, and water (m_b) is recorded. Finally, the grain density of the soil is computed, including temperature corrections, which are not shown, by the following:

$$\rho_g = \frac{\rho_w m_0}{\left[m_0 + \left(m_a - m_b\right)\right]}$$ **Equation 3-1**

3.1.2 Grain size distribution

A given soil contains a variety of particle sizes. The relative proportions of all particle sizes is captured by defining grain size distribution. The distribution is a good indicator of general soil behavior. A soil with mostly fine grains will have poor drainage, retain water for long periods of time, exhibit cohesive strength, and have very low shear strengths at high moisture contents. The low shear strength in fine grained soils is due to pore pressures building up during loading because of the poor drainage. This pore pressure reduces the effective shear stress, carried by grain-to-grain contact in the soil. Grain size distribution is also essential in recommending surrogate soils to replace a soil of interest. Soils with similar grain size distributions tend to have similar behavior. The grain size distribution is not specifically used in LS-DYNA, but it offers great insight into what the soil is comprised of, and how it will behave with varying moisture levels.

Wet or dry sieve analysis can be used to obtain grain size distribution, also a basic test. Dry grain size distribution tests on soils are performed with the material in the oven-dried condition. The sample is broken up and shaken through a stack of sieves that are graduated from coarse at the top to fine at the bottom. The material retained on each sieve is then weighed, and the results are presented in terms of the percent passing (or percent finer than) each sieve size as a function of the logarithm of the grain size. The sieves used for this characterization effort were US standard meshes of No. 5, 10, 20, 30, 40, 70, 100, 140, and 200. Wet sieving flushes the soil with water, further breaking up cohesive particles that would otherwise not pass through a sieve. Once flushed, the retained soil is dried and weighed. Dry sieving is less reliable because cohesive blocks of soil grains can distort the distribution. However, wet sieving is much more time consuming because the retained soil must be completely dried.

3.1.3 Moisture content

The moisture content of a soil is another basic test and key property. It is the gravimetric ratio of water to dry soil material. Although not a direct input to LS-DYNA's Material Model 5, water plays an important role in soil strength and knowing the moisture content in conjunction with grain density allows one to compute saturation and air void volumes in the soil. Soils have an optimum moisture content, at which soil strength is maximized. Any moisture content lower or above this optimum value will reduce the soil strength. At lower values, removing water also removes some cohesion strength. At higher values, the extra water causes pore pressures to build up in the soil, reducing its effective strength. Approximate moisture content (w%) can be obtained through field testing with a nuclear density gage, and verified through laboratory testing. Laboratory testing to obtain moisture content is performed by first weighing a set of soil samples. Then the samples are oven dried and weighed again to measure the difference caused by the loss of water. The difference in weight is m_w. The oven dried weight is m_s. Individual moisture content is calculated for each sample, and the results are averaged. The formula for calculating water content is:

$$w\% = \frac{m_w}{m_s} \qquad \textbf{Equation 3-2}$$

3.1.4 Atterberg limits

The Atterberg limits test defines the degree to which a soil behaves plastically, and is used to classify silts and clays. Fine grained soils can exist in any of several states depending on the amount of water in the soil. As water is added to a dry soil, each particle is covered with a film of adsorbed water. As more water is added, the thickness of the water film covering the particle increases, permitting the particles to slide past one another more easily, thus affecting the engineering properties, e.g., shear strength of the soil. The Atterberg limits test defines the boundaries of four states in terms of limits as follows:

- Liquid Limit – the boundary between the liquid and plastic states.
- Plastic Limit – the boundary between the plastic and semi-solid states.
- Shrinkage Limit – the boundary between the semi-solid and solid states.

These limits are further refined in terms of the water content associated with these boundaries. The water contents at which different clays pass from one state to another vary considerably, and thus can be used for identification and comparison of different clays.

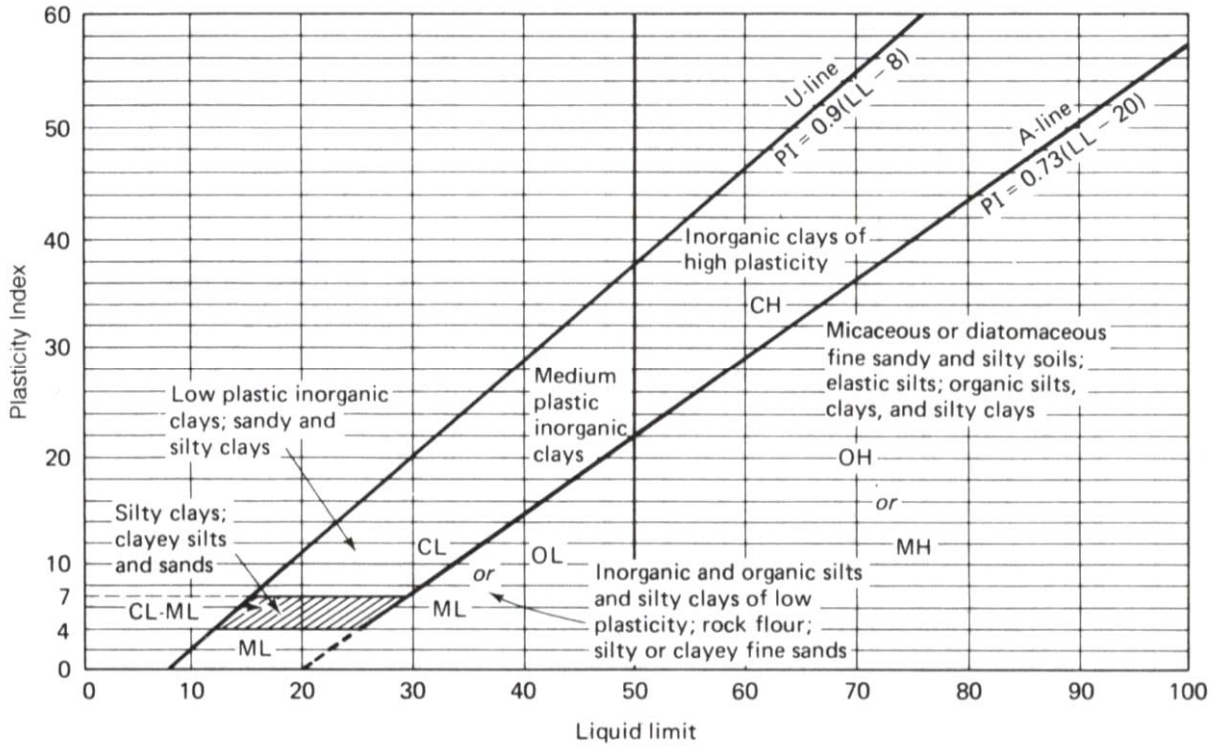

Figure 3-1: Cassagrande's plasticity chart, showing several representative soil types. (Developed from Cassagrande, 1948, and Howard, 1977.)

In order to determine these limits for each soil, we followed ASTM Method D4318-05, which prescribes the current standard test methodology. Based on the results of these tests, standard soil classifications were determined based on Cassagrande's plasticity chart shown in Figure 3-1.

The A-line (lower line in Figure 3.1) generally separates the more claylike materials from silty materials, and the organics from the inorganics. The U-line indicates the upper bound for general clays. Only special clays, such as quick clays, plot above the U-line.

3.1.5 Triaxial compression

The results of triaxial compression tests are used to define the strength envelope, or yield surface as it's referred to in LS-DYNA, of the soil. The following paragraphs describe the triaxial testing machine, how the sample is tested, and how the coefficients of the shear failure surface, a_0, a_1, and a_2 are derived from laboratory test data.

3.1.5.1. Triaxial test apparatus

All of the mechanical property tests were performed in a triaxial compression test apparatus, which is illustrated schematically in Figure 3-2. For each test, a cylindrical specimen of soil is first prepared inside a fluid-tight membrane to prevent infiltration of the confining fluid (air). In the triaxial apparatus, it is possible to apply two independently controlled components of load to the test specimen, as appropriate to each individual test. Pressurized fluid (air) in the vessel is used to impose a hydrostatic stress, simulating the effect of adjacent soil in the field. The other component of load is derived from a piston, which extends through a seal in the top of the pressure vessel, loading the cylindrical specimen in the axial direction. Electronic instrumentation is used to measure both the applied loads and the resulting deformations of the soil specimens. The following paragraphs describe in more detail how the test specimens were prepared, instrumented, and tested.

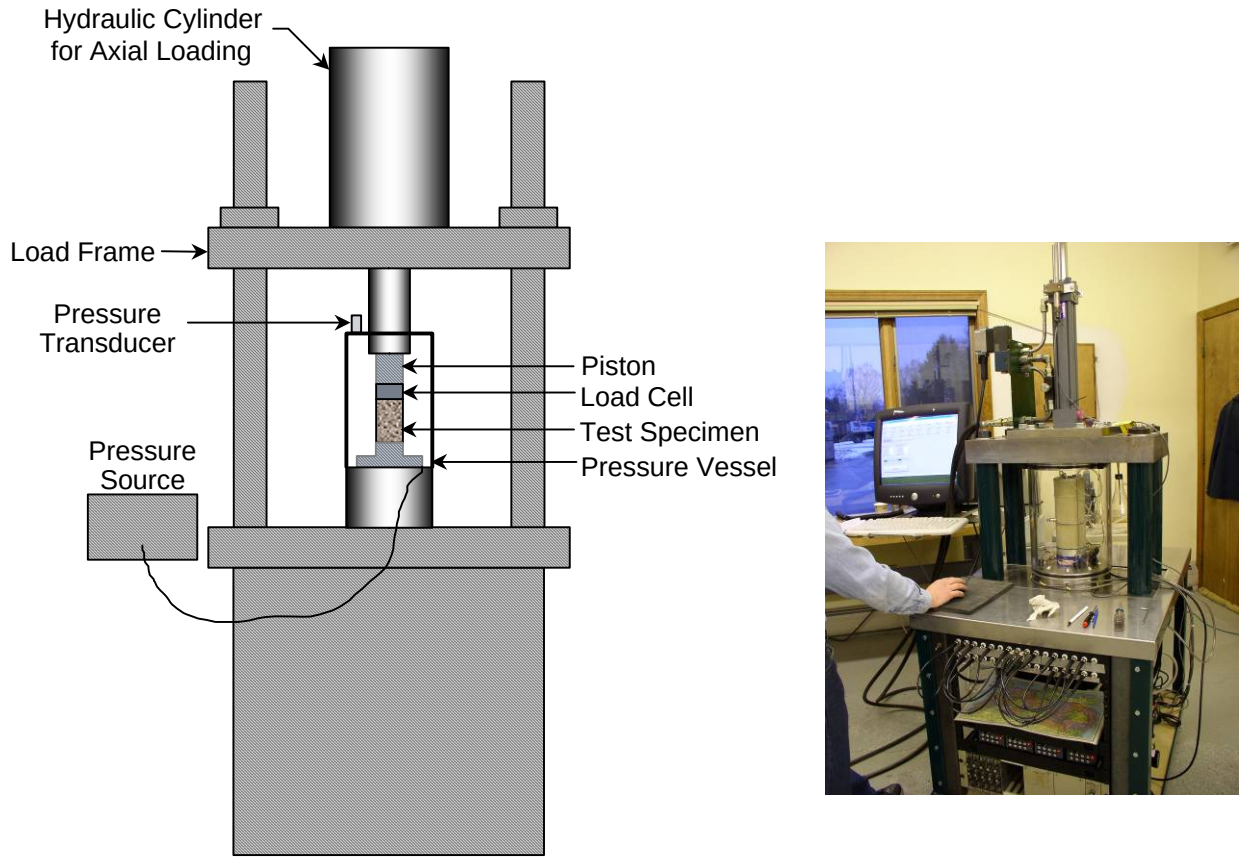

Figure 3-2: Schematic and photograph of a triaxial compression test apparatus.

3.1.5.2. Soil specimen preparation

The first step in the test process is to pack the soil to the measured field density inside the latex rubber membrane that separates the specimen material from the confining fluid. The membrane lines the inside of a steel cylinder mold, which can be removed by splitting in half. The soil is placed in the mold in measured lifts and compacted to the field density. The soil sample reconstitution is described in more detail in the individual material chapters. Once the mold is filled, the top cap is installed in the same manner as the bottom cap, and final measurements of the specimen dimensions and mass are made. The sample is then placed in the triaxial apparatus. Figure 3-3 illustrates how the membranes are sealed on each end to hardened steel endcaps through which the axial load was applied. The membrane was then sealed to the bottom cap using sealant and O-rings. Figure 3-4 is a "ready to test" photograph.

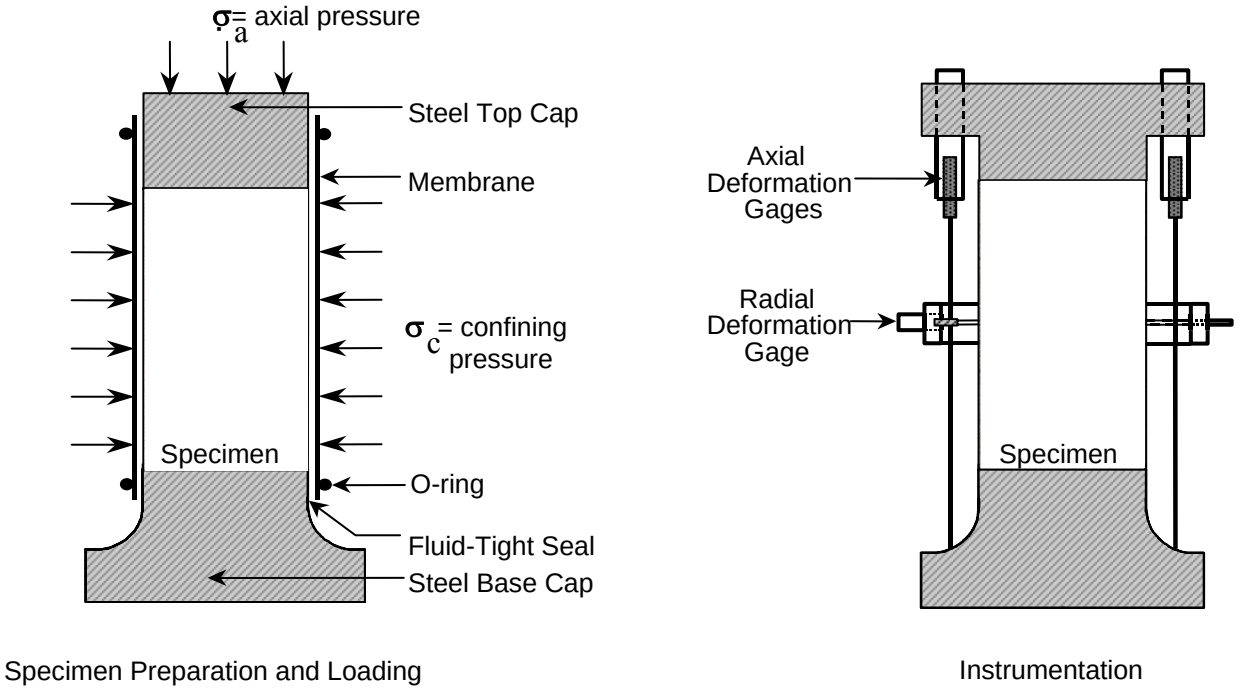

Figure 3-3: Schematic of an instrumented soil specimen.

Figure 3-4: Specimen photo.

Electronic instruments were used to monitor the applied loads and specimen responses during the tests. Three linear variable differential transformer (LVDT) type displacemefnt transducers were installed as illustrated in Figure 3-3 to provide measurements of specimen deformations under load. A pressure transducer was used to monitor the confining pressure, which is equal to the radial stress on the on the specimen, and a load cell measured the axial load. The load cell was located inside the pressure vessel to eliminate errors that would result from seal friction if it were outside the vessel. The necessary corrections were made to eliminate the effects of confining pressure on the load cell output. All of the instruments were calibrated against standards traceable to the National Institute of Standards Technology (NIST) and adjusted to provide the necessary measurement resolution over the expected range of each test. A microcomputer based digital data acquisition system was used to record the transducer output at equally-spaced discrete intervals in time.

3.1.5.3. Deriving constitutive parameters from triaxial test results

In the triaxial compression, or strength test, the specimen is loaded hydrostatically to a pre-selected confining pressure. The confining pressure is then held constant while a compressive axial strain is imposed. The imposed axial strain induces an increment of axial stress above the confining pressure level, and that stress difference results in shear stresses on all planes except the principal directions parallel and perpendicular to the specimen axis. The shear strength of

earth materials is strongly dependent on the normal stress level. By performing strength tests at a range of confining pressure levels, the strength envelope (yield surface) of the material can be defined. The measured specimen deformations provide additional information on the material's volumetric response to shear loading. For this effort, confining pressures of 2, 5, 10, 20, and 50 psi were selected. Each test corresponds to a point on the strength (yield surface) curve, and the maximum shear stresses achieved at these pressures define the strength of the materials over the stress range of interest. The lower confining pressures simulate the near surface soil conditions.

Two components of load are measured in the triaxial compression test. The measured confining pressure is equal to the radial stress on the specimen. Force is also measured in the axial direction, from which the axial stress is determined. The strength data in this report are presented in terms of true axial stress, σ_a. True axial stress is computed at each evenly spaced time interval. It is defined as the total axial load divided by the current cross sectional area of the specimen as derived from the radial deformation measurement. True stress difference, σ_Δ, is the difference between the true axial stress and the confining pressure. Because the confining pressure is always applied to the current area, it is naturally a measure of true radial stress, σ_c. For presentation of strength results, the true stress difference is plotted against true mean stress, $\bar{\sigma}$, which is the average of the stresses in three perpendicular directions. True mean stress is equal to pressure p in LS-DYNA, as explained in the following derivation. The triaxial test outputs are:

$$\sigma_\Delta = \sigma_a - \sigma_c = \text{true stress difference} \qquad \textbf{Equation 3-3}$$

$$\bar{\sigma} = (\sigma_a + 2\sigma_c) / 3 = \text{true mean stress} \qquad \textbf{Equation 3-4}$$

where: σ_a = true axial stress
σ_c = true radial stress = confining pressure
$\bar{\sigma} = p$ = pressure, as explained in the following derivation

To relate the triaxial test data to LS-DYNA's yield surface, one must use Equation 19.5.1 in LS-DYNA's user manual (see Appendix A) to describe the shear failure surface in Material Model 5 format:

$$\frac{1}{2} s_{ij} s_{ij} = a_0 + a_1 p + a_2 p^2 \qquad \textbf{Equation 3-5}$$

LS-DYNA Equation 2.10 specifies s_{ij} as the deviatoric stress tensor defined by:

$$s_{ij} = \sigma_{ij} + (p + q)\delta_{ij} \qquad \textbf{Equation 3-6}$$

Where p is the pressure and q is the bulk viscosity. Because viscosity is not used in Material Model 5, $q = 0$. LS-DYNA Equation 2.11 defines p as:

$$p = -\frac{1}{3}\sigma_{ij}\delta_{ij} = -\frac{1}{3}\sigma_{kk} \qquad \textbf{Equation 3-7}$$

where: σ_{ij} = the stress tensor
δ_{ij} = the Kronecker delta, which is one if the subscripts are the same and zero otherwise

Equation 3-5 and Equation 3-7 are written using indicial notation, in which summation over the repeated subscripts in each term is implied. Thus, *p* is simply the mean (average) of the three diagonal components of the stress tensor, shown in Equation 3-4.

In the special case of the triaxial compression test, the measured stresses are principal stresses and the intermediate principal stress is equal to the minimum principal stress. Specifically, the axial stress, σ_a, is the maximum principal stress and the other two principal stresses are equal to the confining pressure, σ_c. In triaxial testing, one of the most important data outputs is principal stress difference, σ_Δ, given in Equation 3-2. σ_Δ is also referred to as the stress deviator.

Because the stresses measured with respect to the axial and radial directions on the test specimen are principal stresses, the stress tensor expressed relative to those axes has no off-diagonal components, and is given by:

$$\sigma = \begin{bmatrix} \sigma_a & 0 & 0 \\ 0 & \sigma_c & 0 \\ 0 & 0 & \sigma_c \end{bmatrix} \qquad \textbf{Equation 3-8}$$

Returning to Equation 3-6, the expanded version of the stress deviator tensor, *s*, is given by:

$$s = \begin{bmatrix} \sigma_a - p & 0 & 0 \\ 0 & \sigma_c - p & 0 \\ 0 & 0 & \sigma_c - p \end{bmatrix} \qquad \textbf{Equation 3-9}$$

In a triaxial compression test, *p* is given by:

$$p = \frac{\sigma_a + 2\sigma_c}{3} \qquad \textbf{Equation 3-10}$$

and:

$$\sigma_a - p = \frac{3\sigma_a - \sigma_a - 2\sigma_c}{3} = \frac{2(\sigma_a - \sigma_3)}{3} = \frac{2\sigma_\Delta}{3} \qquad \textbf{Equation 3-11}$$

$$\sigma_c - p = \frac{3\sigma_c - \sigma_a - 2\sigma_c}{3} = \frac{\sigma_c - \sigma_a}{3} = \frac{-\sigma_\Delta}{3} \qquad \textbf{Equation 3-12}$$

Thus, Equation 3-9, still for the special case of triaxial compression loading, can be re-written:

$$s = \begin{bmatrix} \frac{2\sigma_\Delta}{3} & 0 & 0 \\ 0 & \frac{-\sigma_\Delta}{3} & 0 \\ 0 & 0 & \frac{-\sigma_\Delta}{3} \end{bmatrix} \qquad \textbf{Equation 3-13}$$

The left hand side (LHS) of Equation 3-5 is the second invariant of the stress deviator tensor, defined as J_2':

$$J_2' = \frac{1}{2} s_{ij} s_{ij} \qquad \textbf{Equation 3-14}$$

When the stress tensor is a diagonal, the indicial notation of Equation 3-14 expands to:

$$J_2' = \frac{1}{2}\left[\left(s_{11}\right)^2 + \left(s_{22}\right)^2 + \left(s_{33}\right)^2 \right] \qquad \textbf{Equation 3-15}$$

Further, for the triaxial compression deviator stress tensor given by Equation 3-13, we have:

$$J_2' = \frac{1}{2}\left(\frac{\sigma_\Delta}{3} \right)^2 \left(2^2 + \left(-1\right)^2 + \left(-1\right)^2 \right) = \frac{\sigma_\Delta^2}{3} \qquad \textbf{Equation 3-16}$$

The foregoing development details the methods for computing J_2' (the LHS of Equation 3-5) and p from the stresses measured in the triaxial compression tests at the strength limit (or elastic limit). Once triaxial data are converted to J_2' and p, one can plot the resulting of values of J_2' against p and perform a quadratic fit to define the required Material Model 5 coefficients, a_0, a_1, and a_2.

An example strength envelope based on triaxial compression tests is presented in terms of mean stress and stress difference in Figure 3-5. Also shown is the linear fit to the triaxial compression test data that corresponds to reasonable values of cohesion and friction angle. To derive the coefficients for input to LS-DYNA, it is necessary to fit the square of the stress difference, as defined by Equation 3-16. The strength data is re-plotted in terms of J_2' vs. pressure p, and is shown in Figure 3-6. Material Model 5 uses a quadratic fit to describe this yield surface, given in Equation 3-17.

$$J_2 = 0.490 + 1.386\,p + 0.979\,p^2 \qquad \textbf{Equation 3-17}$$

Therefore, the Material Model 5 strength coefficients are:

$$A0 = 0.490$$
$$A1 = 1.386$$
$$A2 = 0.979$$

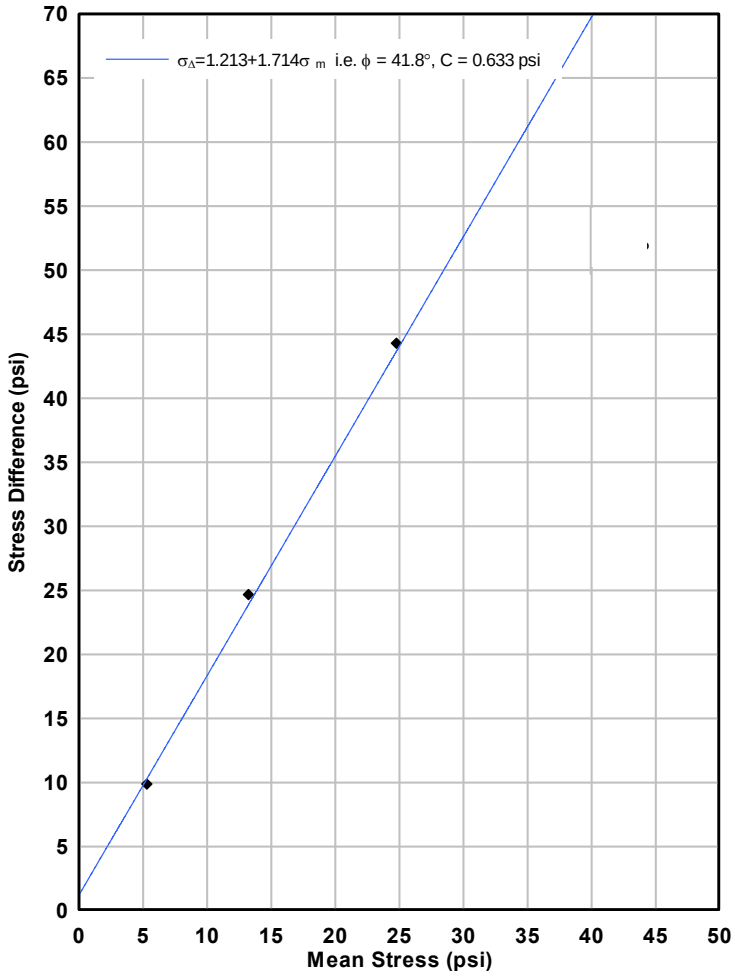

Figure 3-5: Example strength envelope. Black points represent peak strengths from triaxial tests. Blue line is a strength fit.

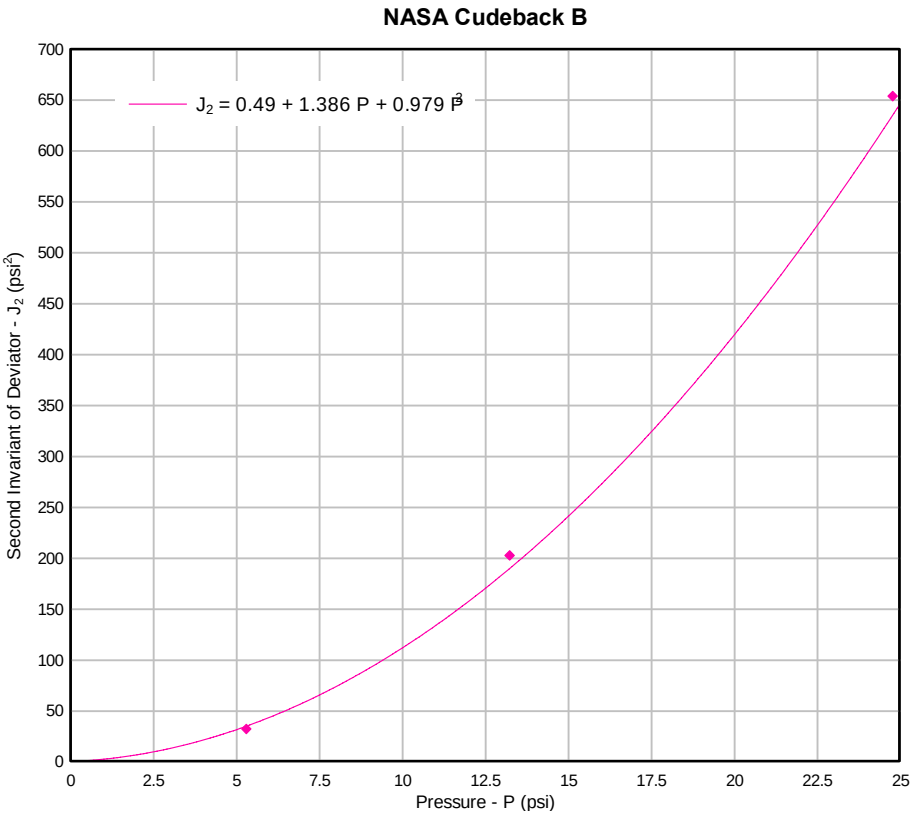

Figure 3-6: Strength envelope in terms of LS-DYNA's yield surface, J_2' vs. *p*. Black points from Figure 3-5 are converted to J_2' and plotted as pink points.

3.1.6 Hydrostatic compression

Hydrostatic compression tests are also conducted using the triaxial device. In the hydrostatic compression test, the cylindrical soil specimens are loaded only by fluid (air) pressure, without any piston loading. The stresses on the specimen are the same in all directions and there is no shear stress on any plane. This is referred to as the hydrostatic state of compression. Material Model 5's pressure *p* is equal to the fluid pressure. The results of these tests are used to define the volumetric deformation behavior of the material for modeling. The stress state is completely defined by the confining pressure. When confining pressure is reduced, the soil expands at a different rate than compression. This expanding rate yields the bulk unload modulus (BULK, see Table 2-1).

In the laboratory, LVDT measurements are used to define axial and radial deformations which, in turn, are used to compute the current volume of the specimen at each time step. The volumetric strain, ε_v, can be computed using the following equation:

$$\varepsilon_v = \frac{V_o - V_d}{V_o}$$ **Equation 3-18**

Where V_d = current (deformed) volume of the specimen
and V_o = initial specimen volume (including grains and void space)

3.1.6.1. Deriving constitutive parameters from hydrostatic compression

The axial and radial specimen strains are recorded as the fluid pressure increases inside the vessel. The recorded data forms a pressure vs. volumetric strain curve. The test typically starts with an initial rate of compression, denoted as I in Figure 3-7.

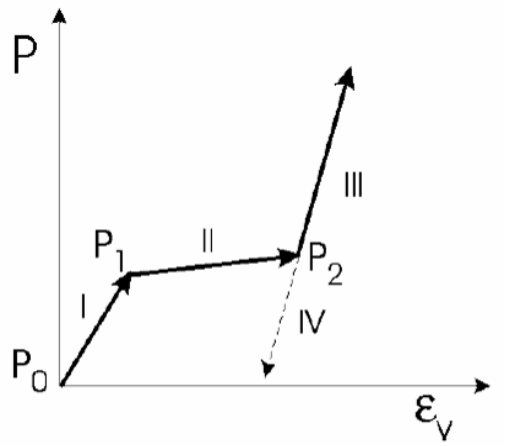

Figure 3-7: Theoretical hydrostatic compression curve. Pressure *p* vs. volumetric strain ε_v. The slope of Segment IV, the unloading portion, corresponds to the bulk unloading modulus.

3.1.7 Uniaxial strain

The uniaxial strain test also utilizes the triaxial device, albeit differently. In a uniaxial strain test, the axial stress and confining pressure are applied in such a way that the specimen undergoes compressive axial strain with no strain in the radial direction. The uniaxial strain loading is accomplished with an automated loading control system using the radial deformation measurement as feedback in the control loop. If the radial strain increases, the confining pressure is increased to return the radial strain to zero. Because no radial strain is allowed in a uniaxial strain test, the axial strain is equal to the volumetric strain in the specimen. There is a difference between axial and radial stress, and hence shear stresses exist in the specimen. However, the uniaxial strain constraint typically prevents the stress state from reaching the strength envelope, and failure of the specimen does not occur. The Material Model 5 shear modulus G and the pressure-volume curve can be derived from uniaxial strain data, as described in the following section.

3.1.7.1. Deriving constitutive parameters from uniaxial strain

The elastic constants to calculate shear modulus G are derived from a uniaxial strain test. First, Poisson's ratio can be obtained from an axial stress vs. confining pressure plot, a uniaxial test output. There are two independent components of loading applied, confining pressure and axial load. Other linear combinations of these two independent components can yield other properties. For example, the mean stress and stress difference are invariants of the stress tensor and deviatoric stress tensor, respectively. To assure consistency, two different derivations of Poisson's ratio are presented below. As an aid, example plots are provided.

The first derivation is based on a relationship between axial stress and confining pressure. The elastic Poisson's ratio value can be derived from the initial portion of the axial stress vs. confining pressure curve. A fitted line is drawn over the initial curve portion. The inverse slope of the fitted line is commonly called lateral earth pressure, k_0. Poisson's ratio, ν, is related to k_0 by:

$$\nu = \frac{k_0}{1 + k_0} \qquad \textbf{Equation 3-19}$$

Figure 3-8 is an example application of the first method of obtaining ν from uniaxial test results. Commonly, there is a very small region at the beginning of the test where the data look somewhat incoherent because the loading piston is just making contact with the specimen. Usually, uniaxial strain control cannot maintained in this region because of sample "seating," when the loading piston closes the tiny gaps between test hardware contact points. Because it occurs at very low stress only, it is ignored for this analysis. The Poisson ratio ν is derived from the initial linear portion of the test. In Figure 3-8, the initial linear portion reaches 35 psi axial stress. By fitting a line to that region, we find that it has a slope of 4.406. So k_0 = 1/4.406. From Equation 3-19, k_0 = 0.227 and ν = 0.185.

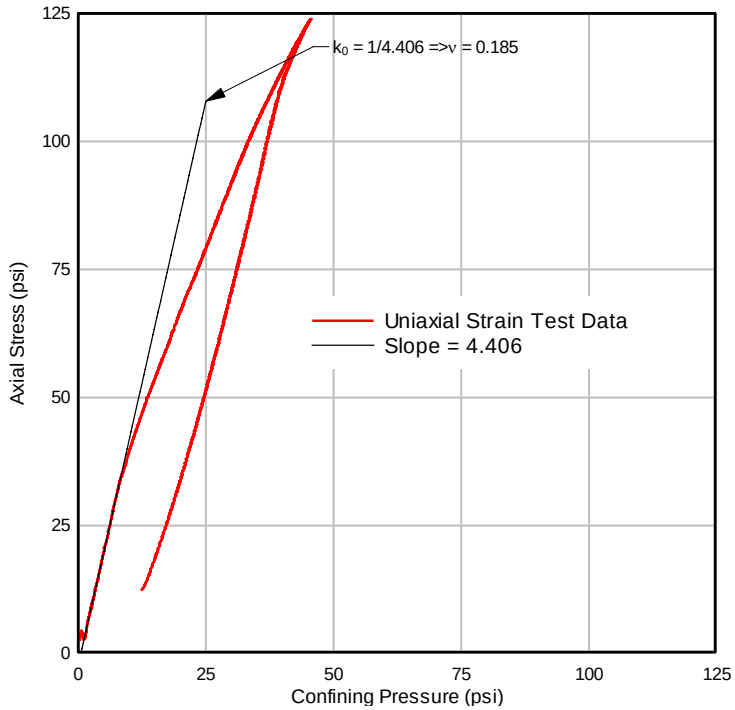

Figure 3-8: Example of axial stress vs. confining pressure plot from uniaxial test.

The second method of deriving ν is to examine the stress path in terms of mean stress and stress difference. Uniaxial test data can be used to plot mean stress vs. stress difference, as shown in Figure 3-9. The definitions of mean stress and stress difference are shown in Equation 3-3 and Equation 3-4. The slope of this different curve can also be used to calculate ν.

In Figure 3-9, the slope does not have a commonly used name or symbol. For convenience, call the slope of the line k^*. It is seen that $k^* = 1.598$. Poisson's ratio is related to k^* by:

$$\nu = \frac{3 - k^*}{6 + k^*} \qquad \textbf{Equation 3-20}$$

Thus, ν = 0.185, which agrees with the first derivation.

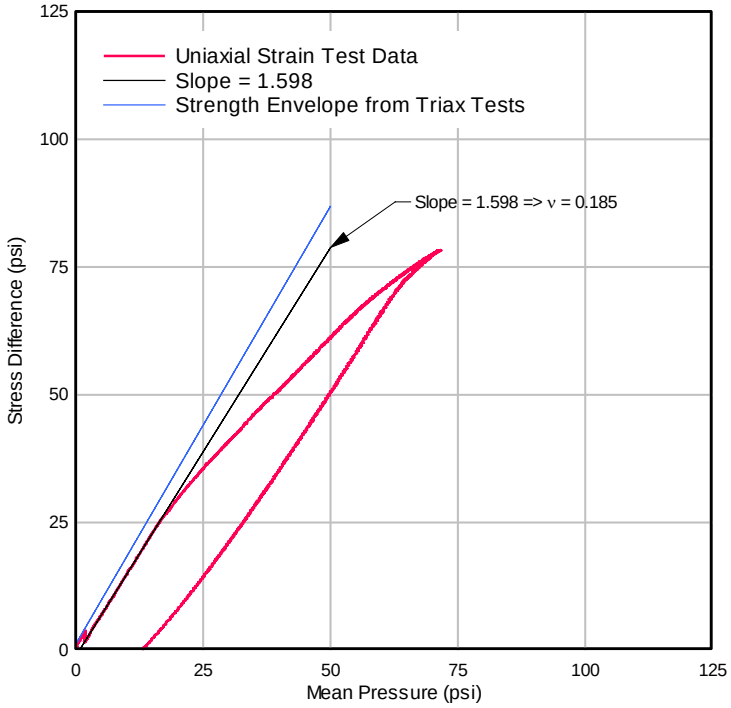

Figure 3-9: Example of stress difference vs. mean stress plot from uniaxial test.

The preceding paragraphs present two approaches to defining Poisson's ratio, which is one elastic constant. It is necessary to have one more elastic constant for a complete set. Consider the stress-strain curves plotted in Figure 3-10. In a uniaxial strain test, the radial strain is constrained to be zero, and the axial strain is the same as the volume strain. In Figure 3-10, axial strain is plotted against both axial stress and mean stress. As with the definition of Poisson's ratio, for the purpose of defining elastic constants, attention is confined to the initial linear regions of the curves. First, consider the axial stress curve in Figure 3-10. The initial slope of the axial stress curve is the constrained modulus, M, of the material. It is defined as the ratio of axial stress to axial strain under uniaxial strain conditions. From Figure 3-10, it is seen that M = 6950 psi.

Similarly, the slope of the mean stress-volume strain curve is defined as the bulk *loading* modulus, K. Actually, bulk modulus is defined as the ratio of pressure to volumetric strain under hydrostatic loading, but as long as the material behaves elastically, this definition is equivalent. From Figure 3-10, K = 3370 psi. It is of interest to know how these values relate to other elastic constants. Recall that Young's modulus, E, is the ratio of axial stress to axial strain under unconfined compression (or tensile) loading. The relations between E and the constrained and bulk moduli are:

$$M = \frac{E(1-\nu)}{(1+\nu)(1-2\nu)} \qquad \textbf{Equation 3-21}$$

$$K = \frac{E}{3(1-2\nu)} \qquad \textbf{Equation 3-22}$$

From those two equations, it is straightforward to find the relationship between M and K:

$$\frac{M}{K} = \frac{3(1-\nu)}{(1+\nu)}$$ **Equation 3-23**

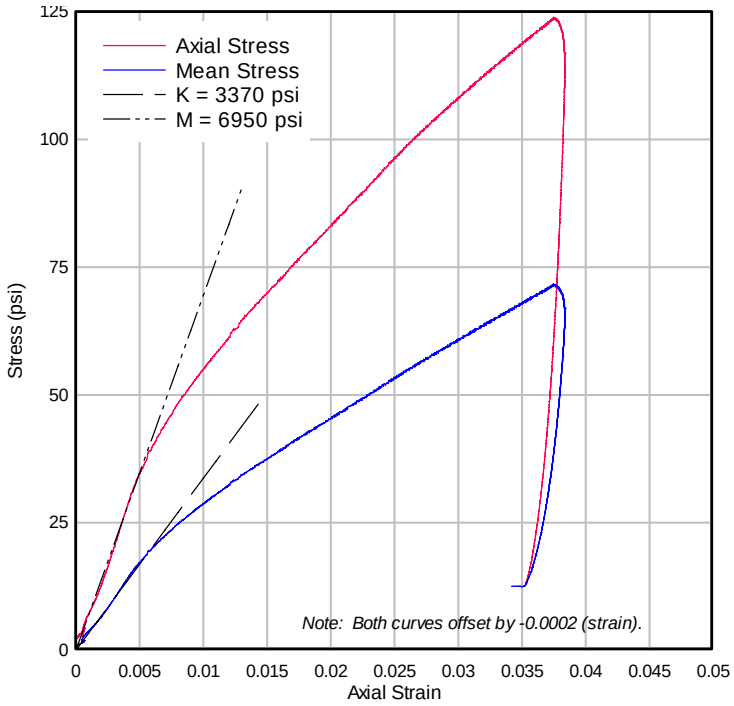

Figure 3-10: Example stress vs. strain curves from uniaxial test.

If the right hand side (RHS) of Equation 3-23 is computed from the values of M and K determined above and the left hand side (LHS) is computed from ν, it is found that both are equal to 2.06. Thus, we have a consistent set of elastic constants. During Material Model 5 input derivation, slight fit adjustments for constrained and bulk moduli were made to ensure Equation 3-23's consistency. The final elastic constant of interest is the shear modulus, G, which is related to E and ν by:

$$G = \frac{E}{2(1+\nu)}$$ **Equation 3-24**

In summary, for the initial linear loading phase, the elastic constants for the example case are:

Table 3-1: Example summary of elastic constants from uniaxial strain testing

Young's Modulus E	6370	psi
Poisson's Ratio ν	0.185	
Shear Modulus G	2690	psi

Bulk Loading Modulus K	3370	psi
Constrained Modulus M	6950	psi

The unload bulk modulus is derived from the same uniaxial strain test data as shown in Figure 3-10. Because bulk modulus is required, attention is restricted to the mean stress vs. volume strain curve. Figure 3-11 is an expanded view of the unload region. As the unloading behavior is not very linear, geotechnical expertise is used to approximate the curve with a single line. The portion shown as a heavy blue line was considered in the linear fit. The resulting value of unload modulus is K_u = 17,000 psi.

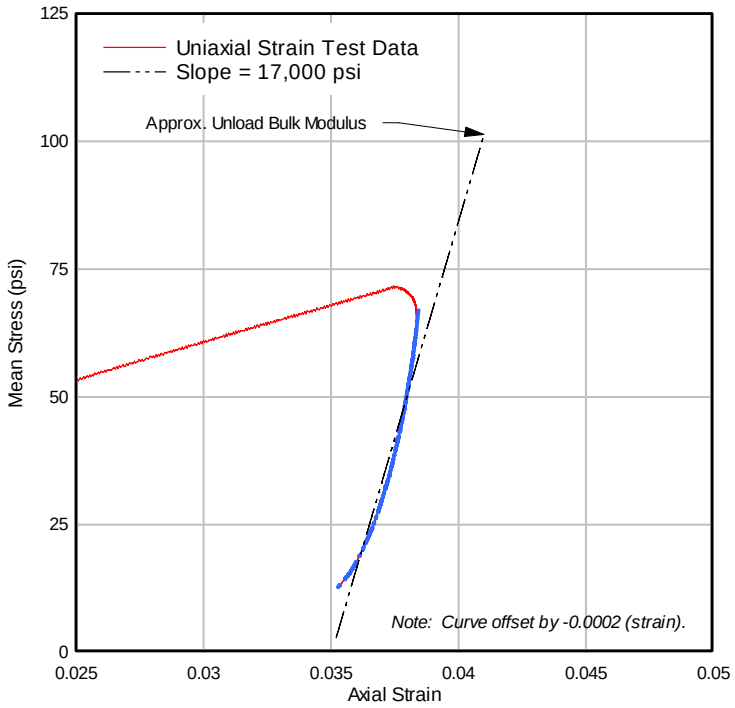

Figure 3-11: Expanded view of the unload region of the uniaxial strain test.

According to the LS-DYNA documentation, the compressibility curve used for Material Mode 5 is defined in terms of logarithmic strain, which is defined as:

$$\varepsilon_{\log} = \ln\left(\frac{V}{V_0}\right) \qquad \textbf{Equation 3-25}$$

where: V = current volume
V_0 = initial unstressed volume

Because there is no radial strain in the uniaxial strain test, the cross sectional area remains constant and the logarithmic strain can be computed from the initial length and change in length of the specimen as:

$$\varepsilon_{\log} = \ln\left(\frac{L_0 - \Delta L}{L_0}\right) \qquad \textbf{Equation 3-26}$$

where: L_0 = initial specimen length
ΔL = change in length (positive in compression)

The logarithmic strain is negative in compression. The pressure-logarithmic strain curve from the uniaxial strain test is presented in Figure 3-12 along with the ten-point idealization for input to LS-DYNA. The tabulated points are:

Table 3-2: Example pressure-volume points from uniaxial strain test.

Pressure (psi)	Logarithmic Strain
0	0.0000
16.39	-0.0050
18.24	-0.0056
20.44	-0.0064
22.48	-0.0072
24.31	-0.0080
28.42	-0.0100
36.81	-0.0149
52.42	-0.0250
70.6	-0.0378

The ten points are chosen in such a way to best characterize the shape of the compressibility curve.

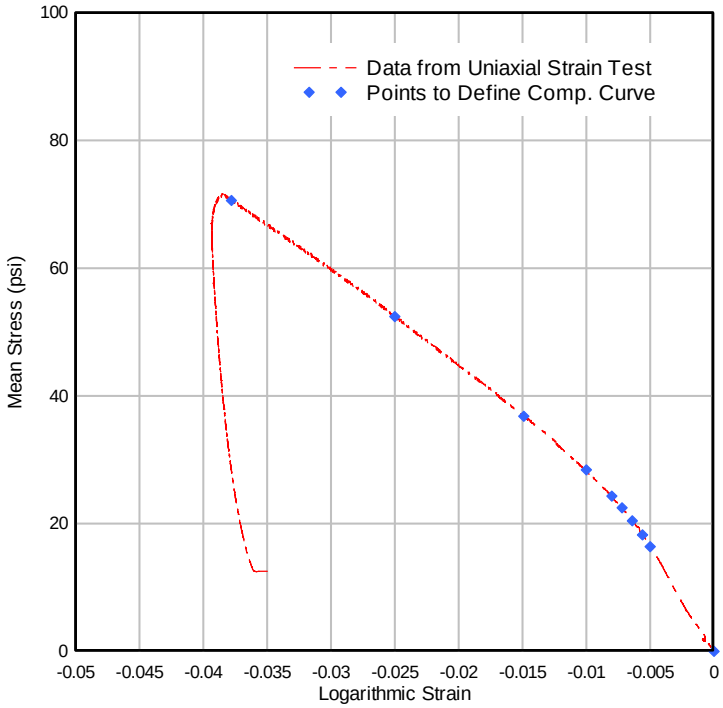

Figure 3-12: Example of ten points on the pressure-volume compressibility curve in terms of logarithmic strain.

4 Unwashed Sand

The general description, field observations, test data, and Material Model 5 inputs for unwashed sand are discussed in this chapter. Unwashed sand is the name given to a particular drop test soil used at LaRC's gantry facility during early stages of CEV landing analysis. The soil was tested at in situ moisture content when collected from the gantry. One constitutive model was developed and is intended to be the closest representative model during test conditions. LaRC recorded drop test dates and conditions and provided the density and moisture data to ARA.

4.1 Location

LaRC is located in Hampton, VA. The LaRC field visit was conducted 4 February 2008. The gantry is located on Bush Road within LaRC grounds. Figure 4-1 displays gantry in relation to the test soil. The embossed bed in the center is unwashed sand. Mock CEVs were swung onto the test bed using the gantry. LaRC acquired the soil from a construction fill distributor and deployed the soil using earth moving equipment. The process of deploying the soil resulted in a high in situ density due to mechanical compaction from equipment driving over it.

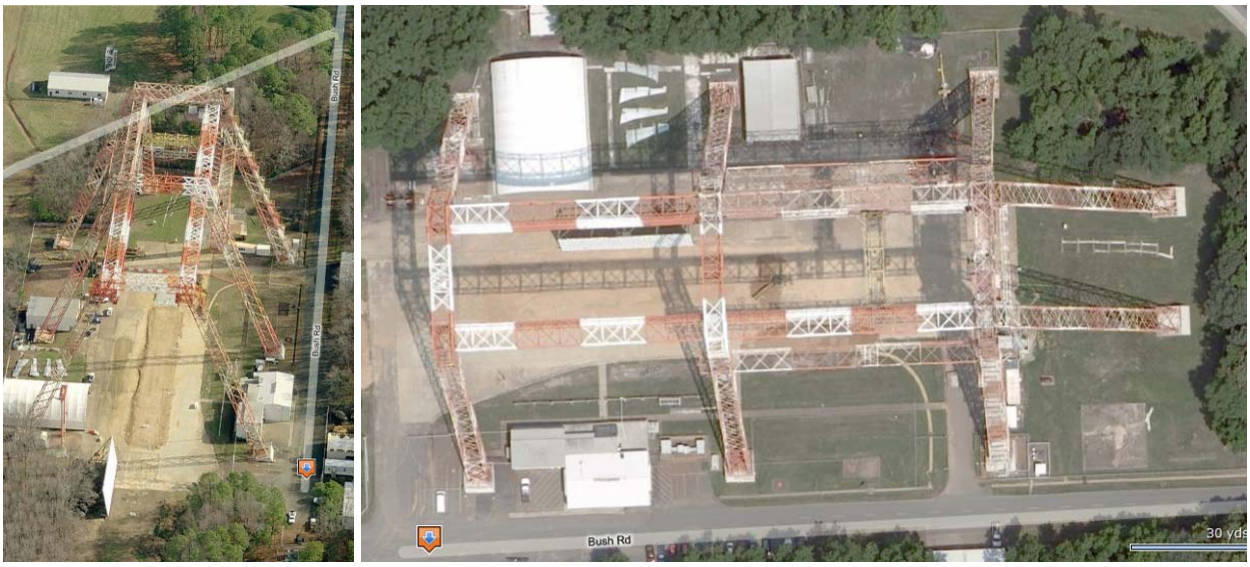

Figure 4-1: Aerial views of LaRC gantry with unwashed sand deployed for testing

4.2 General description

The unwashed sand was exposed to the environment during the entire course of mock CEV drop testing. As a result, the test soil experienced changes in moisture contents with the passing of rain. The density also changed with each deployment. The bed thickness ranged from 2-3 ft and was underlain by a concrete platform. The test bed surface was maintained smooth. The test soil is barren of vegetation and susceptible to hardening under dry conditions. Table 4-1 summarizes the variation in moisture content.

Table 4-1: Moisture content data for unwashed sand, collected by LaRC

Record type	Average w%	Min w%	Max w%	Std Dev
(1) Moisture only	8.4	4.2	14.9	3.0
(2) Moisture & Density	12.2	9.5	14.9	2.2

Unwashed sand can vary from relatively hard when it is dry to sticky and soft when thoroughly wet. On the 4 February 2008 field visit, LaRC gantry personnel noted that it had rained two days prior to the day of sampling. Laboratory testing revealed a moisture content of 12%, consistent with the moisture & density data provided by LaRC.

The unwashed sand was sampled directly from the gantry site. The samples were sealed in impermeable bags and shipped to the laboratory in airtight containers. The samples were reconstituted to the moisture and density average. It is essential for laboratory testing that both moisture and density is recorded. One cannot confidently reconstitute a field representative sample without both. Therefore, the moisture content associated with record type (2) was used. Four wet density measurements were made during drop testing. Wet density reflects the bulk density of the soil, including in situ water. No additional density measurements were possible because the test bed had been cleared and stored in a pile on the day of sampling. The following table summarizes the density data.

Table 4-2: Wet density data for unwashed sand, collected by LaRC

Record type	Average	Min	Max	Std Dev
Wet density (lbs/ft^3)	130.0	125.4	132.8	2.2

4.3 Soil classification

Unwashed sand is classified as SM under the Unified Soil Classification System. SM is a silty sand, a mostly sand material with silty fines that lend some plastic behavior. It is low plasticity and the silt content was approximately 25%. The soil hardens when drying. The table below summarizes the classification by Atterberg limits.

Table 4-3. Unwashed sand Atterberg limits

Liquid Limit	Liquid Limit	Plasticity Index	Soil Classification
20	19	1	SM

4.4 Laboratory test data

This section contains the results of laboratory tests on unwashed sand. The fits to obtain elastic constants for Material Model 5 are included with the test result figures. The test log in Table 4-4 summarizes the tests conducted. After each specimen was tested, a portion of the sample was used for moisture content testing. The specimen density is calculated from total reconstitution mass in a known mold volume.

Table 4-4: Test log for unwashed sand tests

Test ID	Sample ID	Type	Confining Pressure (psi)	Moisture content	Wet Density (lbs/ft^3)	Dry Density (lbs/ft^3)	Grain Density G_s (g/cm^3)	Porosity n
F19B08	Unwashed sand	Triax	2	13.49%	130.8	115.2	2.67	30.9%
F20B08	Unwashed sand	Triax	5	11.72%	130.8	117.0	2.67	29.8%
F21B08	Unwashed sand	Triax	10	11.91%	130.8	116.8	2.67	29.9%
F28B08	Unwashed sand	Triax	20	11.36%	130.8	117.4	2.67	29.6%
F29B08	Unwashed sand	Triax	50	11.40%	130.8	117.4	2.67	29.6%
M3A08	Unwashed sand	Uniax	50	11.56%	130.8	117.2	2.67	29.7%

4.4.1 Grain size distribution

Figure 4-2 displays the wet sieve results for unwashed sand. The thick line represents the unwashed sand's grain size distribution. The Carson Sink and Cuddeback soils are shown as thin lines for comparison.

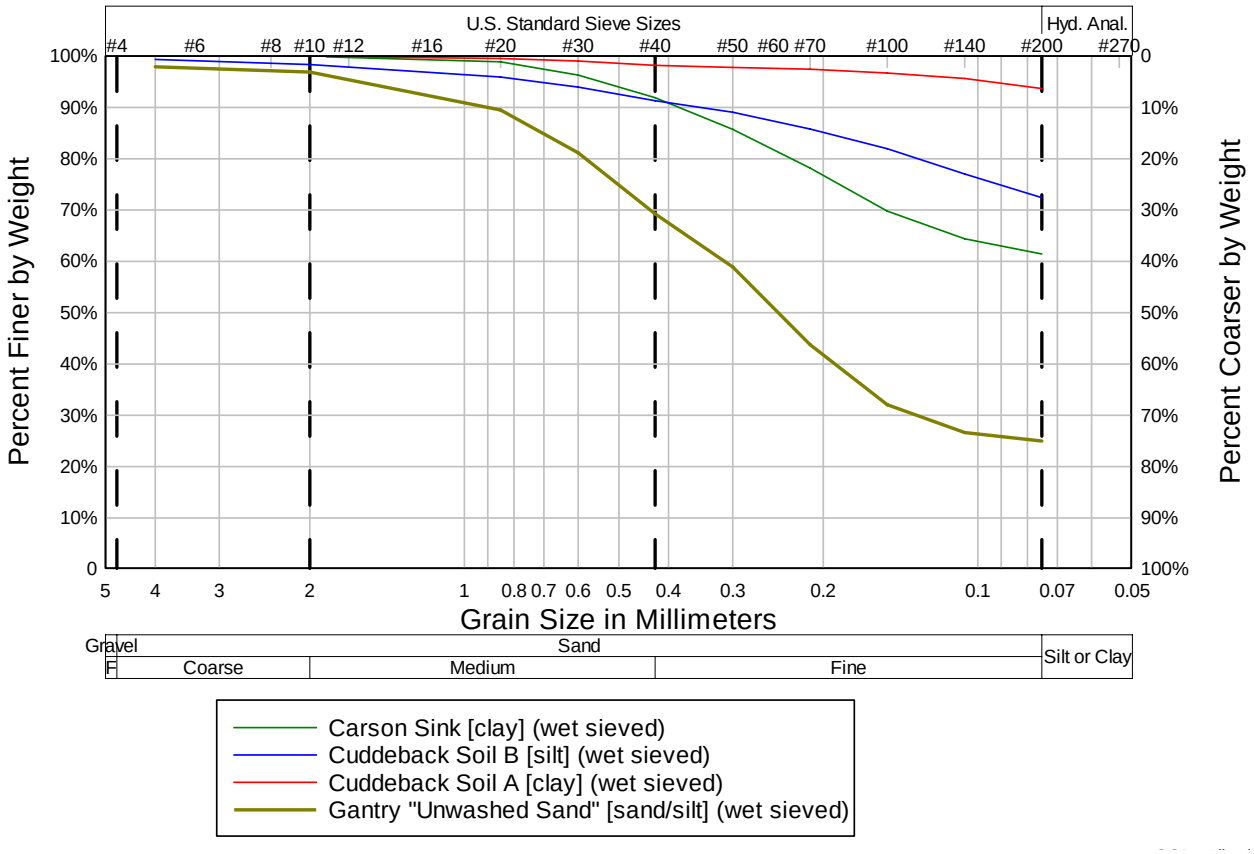

Figure 4-2: Unwashed sand grain size distribution.

4.4.2 Triaxial compression

A suite of five triaxial compression tests were run on each of the soils. In a triaxial compression test, a confining pressure is maintained on the specimen's sides while axial load is applied. The confining pressure is held constant throughout the test. The five confining pressures used for this study were 2, 5, 10, 20, and 50 psi, which should cover the range of modeling interest. The bias toward low confining pressures reflects the low stress design of the airbag landing systems. LaRC Landing Systems ADP presented two airbag designs with design pressures between 2 and 6 psi.

Figure 4-3 shows the results of all five triaxial compression tests in terms of stress different vs. strain. Both radial and axial strain are shown. Radial strain, the lateral expansion of the cylindrical specimen, is on the left. Axial strain, the vertical compression, is shown on the right. Throughout this report, 2 psi tests are shown in red, 5 psi in blue, 10 psi in green, 20 psi in purple, and 50 psi in orange. Stress difference is defined in Equation 3-3. The layout of the plot allows one to track both radial and axial strain at the same loading. A point on the stress difference axis represents a single load on the specimen. The strain axis represents the two separate strains associated with that loading. The peak of the curve represents the strength of the specimen. The peak stress difference value for each test is then used to derive the constitutive material properties as described in Chapter 3.

In Figure 4-4, the peaks from Figure 4-3 are plotted as a strength envelope. The strength envelope space is stress difference vs. mean stress. Mean stress is equivalent to pressure *p* in Material Model 5. It is defined in Equation 3-4. The five triaxial tests generate five points on the strength envelope plot. A fitted line is drawn through the five points, and is referred to as the failure envelope. An element of soil whose stress path encounters this line would experience shear failure.

The slope of the line is correlated to φ, the internal angle of friction, which is 32.9°. The angle φ describes the friction between the grains of the soil. The physical meaning is the maximum angle at which the soil can support itself. To aid in understanding, imagine the granular soil falling from the top of an hourglass into the bottom. The soil forms a conical accumulation shape, and the slope of the cone is the angle of internal friction. If subjected to a greater slope, the soil collapses and returns to the internal friction slope. The angle φ is a shear strength property of the soil commonly used in geotechnical engineering. The cohesion *c* is correlated to the intersection of the failure envelope and the stress difference axis. Cohesion represents the tensile strength of the soil, which is 1.7 psi. Most soils have some small amount of cohesion, influenced by water, and clays have the highest amount. Dry sands have zero cohesion.

Figure 4-5 shows the laboratory test derived LS-DYNA's Material Model 5 yield surface. The points from Figure 4-4 are equated to J_2' and plotted as a function of pressure *p*. The method of equating stress difference to the second invariant J_2' is described in Chapter 3.1.5.3. A quadratic fit to the five triaxial strength points is made, and the fit coefficients are the a_0, a_1, and a_2 inputs for Material Model 5.

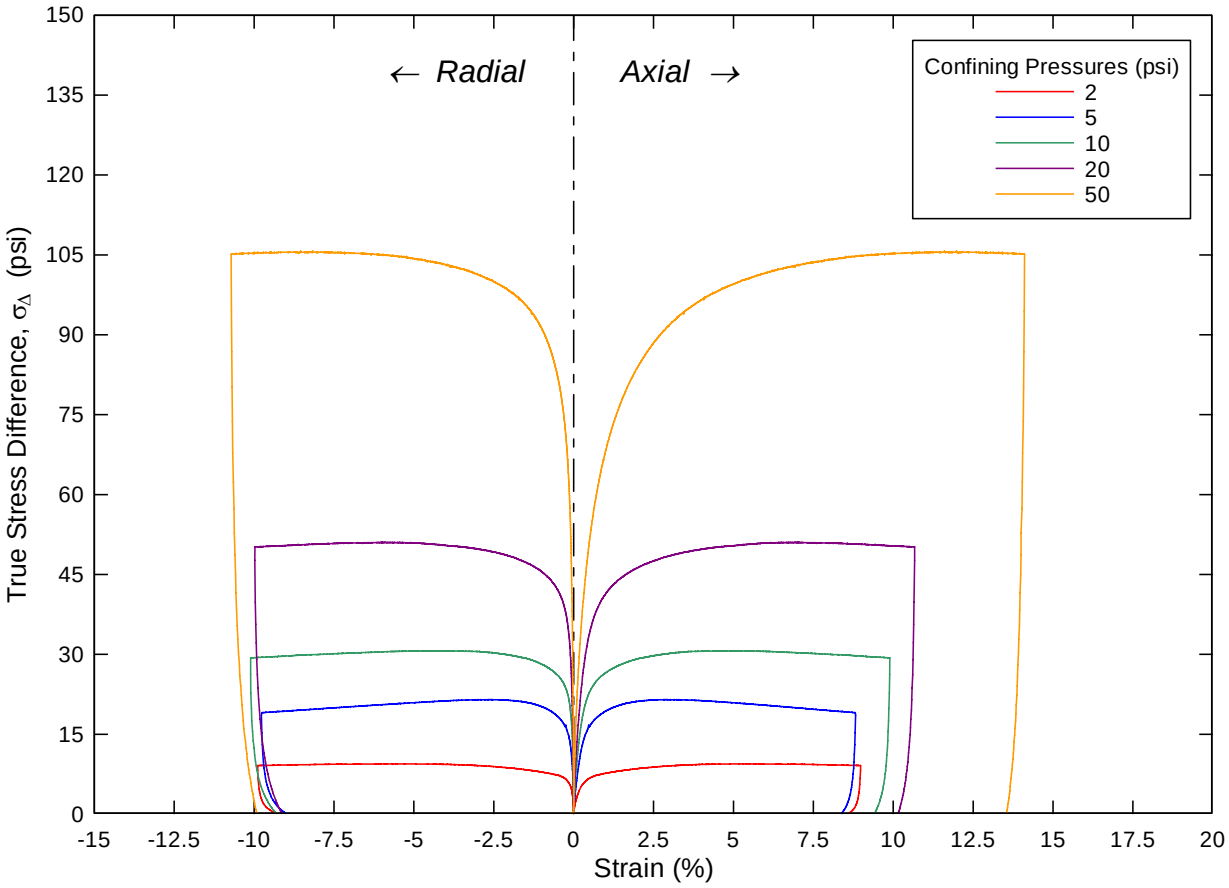

Figure 4-3: Unwashed sand triaxial test results for 2, 5, 10, 20, and 50 psi confining pressures.

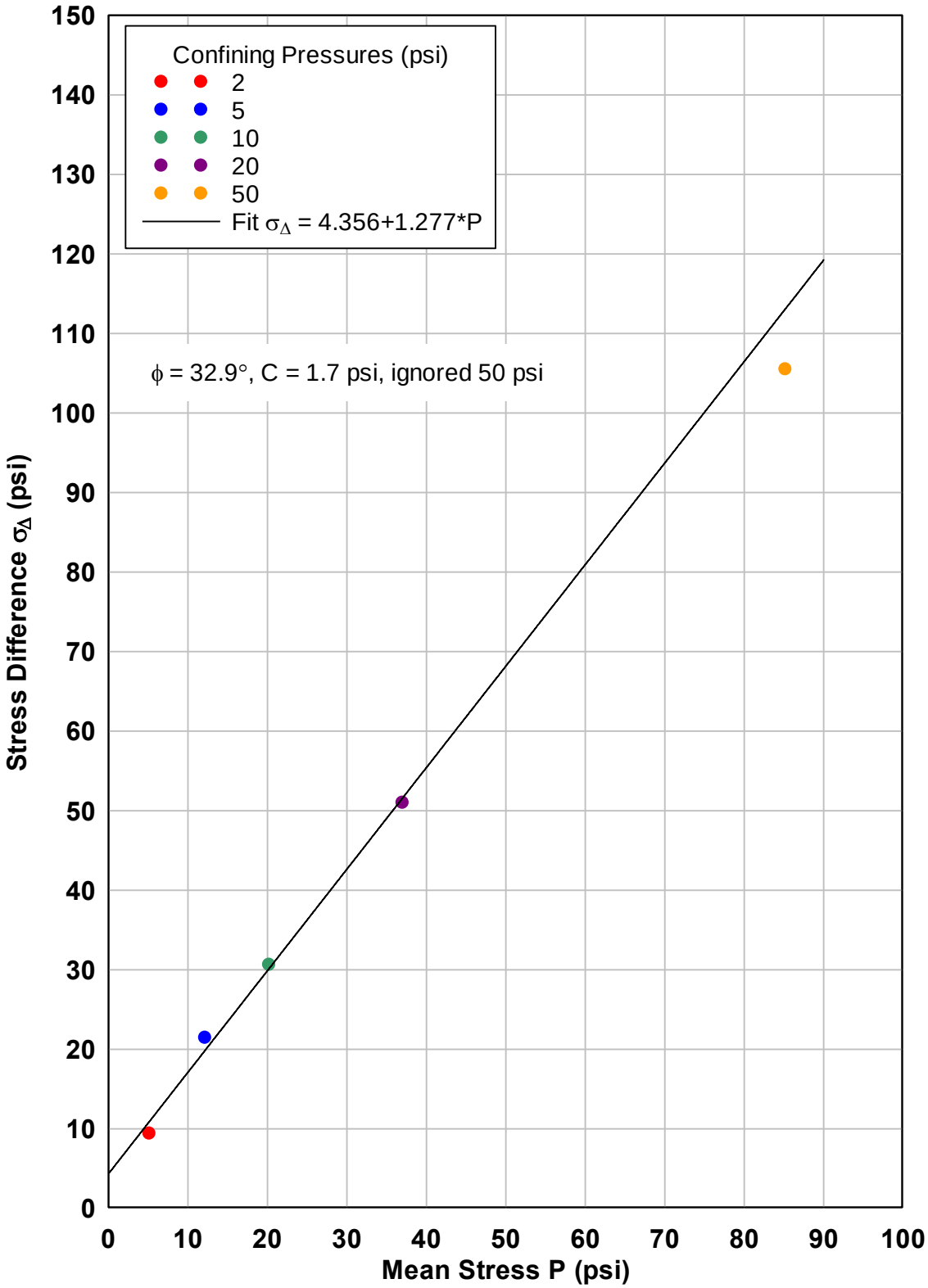

Figure 4-4: Unwashed sand strength envelope results.

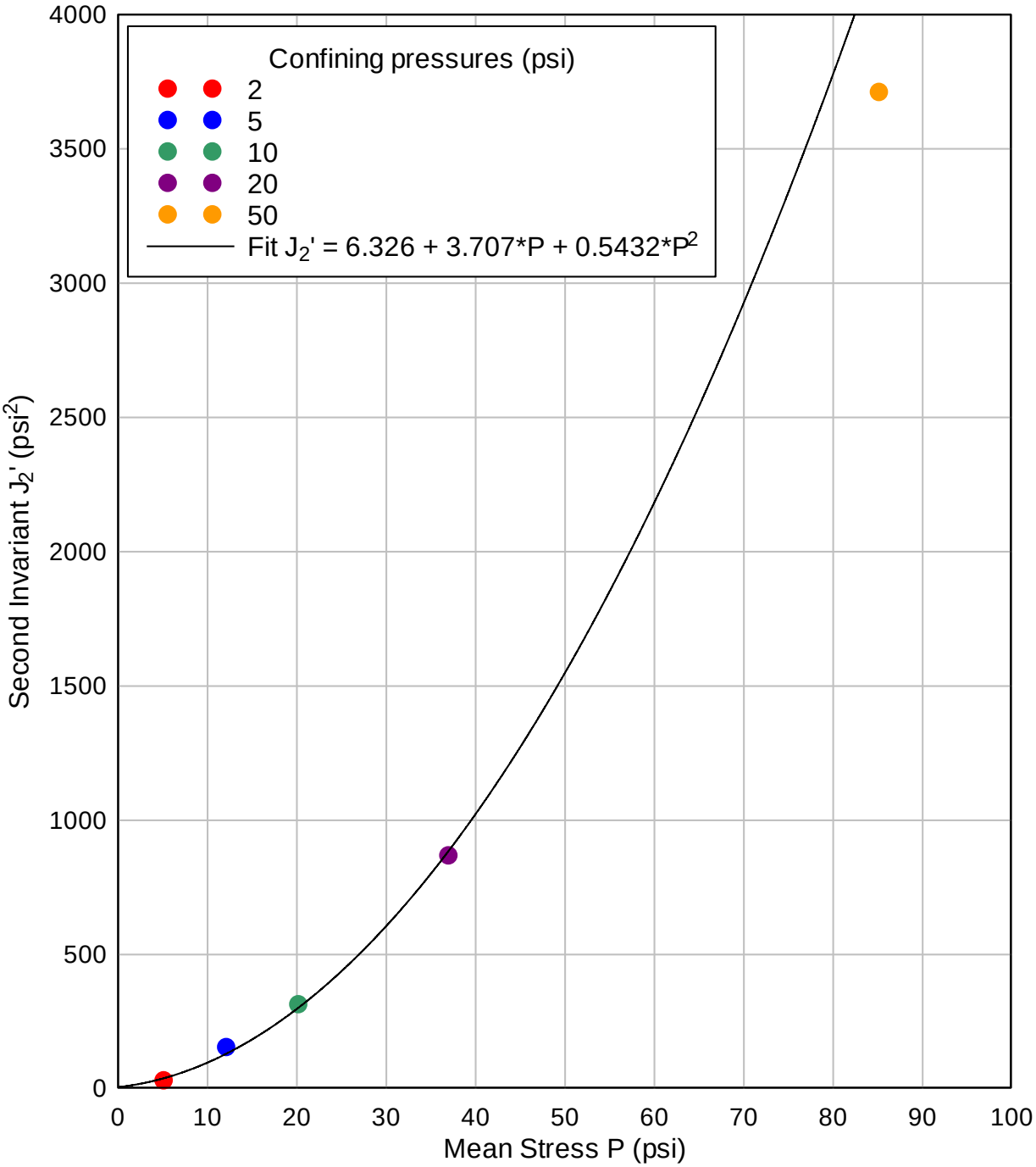

Figure 4-5: Unwashed sand Material Model 5 yield surface fit from triaxial test data.

4.4.3 Uniaxial strain

One uniaxial strain test was run on unwashed sand. The uniaxial strain test prevents radial strain from occurring by means of a radial confining pressure control algorithm. As load is applied, a radial LVDT measures the strain, and the data feed is used to control the amount of confining pressure applied to the specimen. As a result, the uniaxial confining pressure is always increasing to maintain zero radial strain during the test.

The uniaxial strain tests typically have three segments: an initial loading portion, a stiffer closed void portion, and an unload portion. The three segments can be idealized by three slopes. The initial loading portion represents the constrained modulus used in constitutive model construction. The second portion always has a lower slope (lower modulus) than the first because the soil is stiffening up as the voids close. The third portion represents the expansion of the soil when unloaded, similar to the hydrostatic compression.

Figure 4-6 shows the three segments of the uniaxial test in terms of stress difference vs. mean stress. Figure 4-8 is a plot of only the unloading portion of the test in terms of mean stress vs. volumetric strain. The unloading portion can also be used to compute the bulk unloading modulus (BULK) input for Material Model 5. It provides an additional method to confirm the bulk unloading rate.

The shear modulus *G* can be obtained from either the slopes drawn in Figure 4-7, or the Poisson ratio calculation in Figure 4-9. The method for calculation *G* from uniaxial strain is outlined in Chapter 3. Figure 4-10 is the uniaxial test data plotted in terms of mean stress vs. logarithmic strain. Because mean stress is equal to pressure *p* and logarithmic strain is the logarithmic change in axial strain (no radial strain allowed, $\varepsilon_c = 0$), Figure 4-10 represents the pressure-volume behavior of unwashed sand in the axial direction. Because the soil is assumed to be isotropic, the same curve also represents pressure-volume deformation in the radial direction.

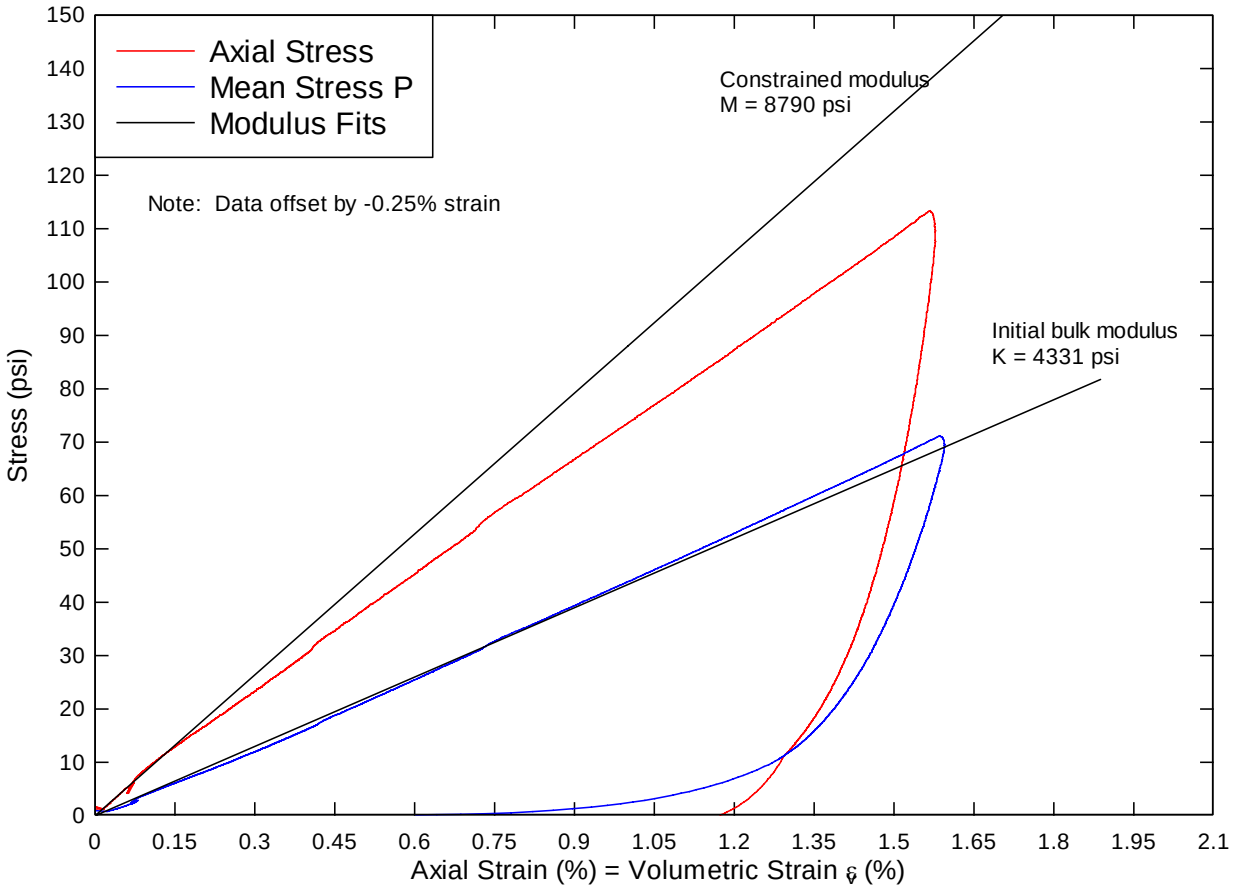

Figure 4-6: Unwashed sand uniaxial strain test results. Constrained and bulk moduli fits shown.

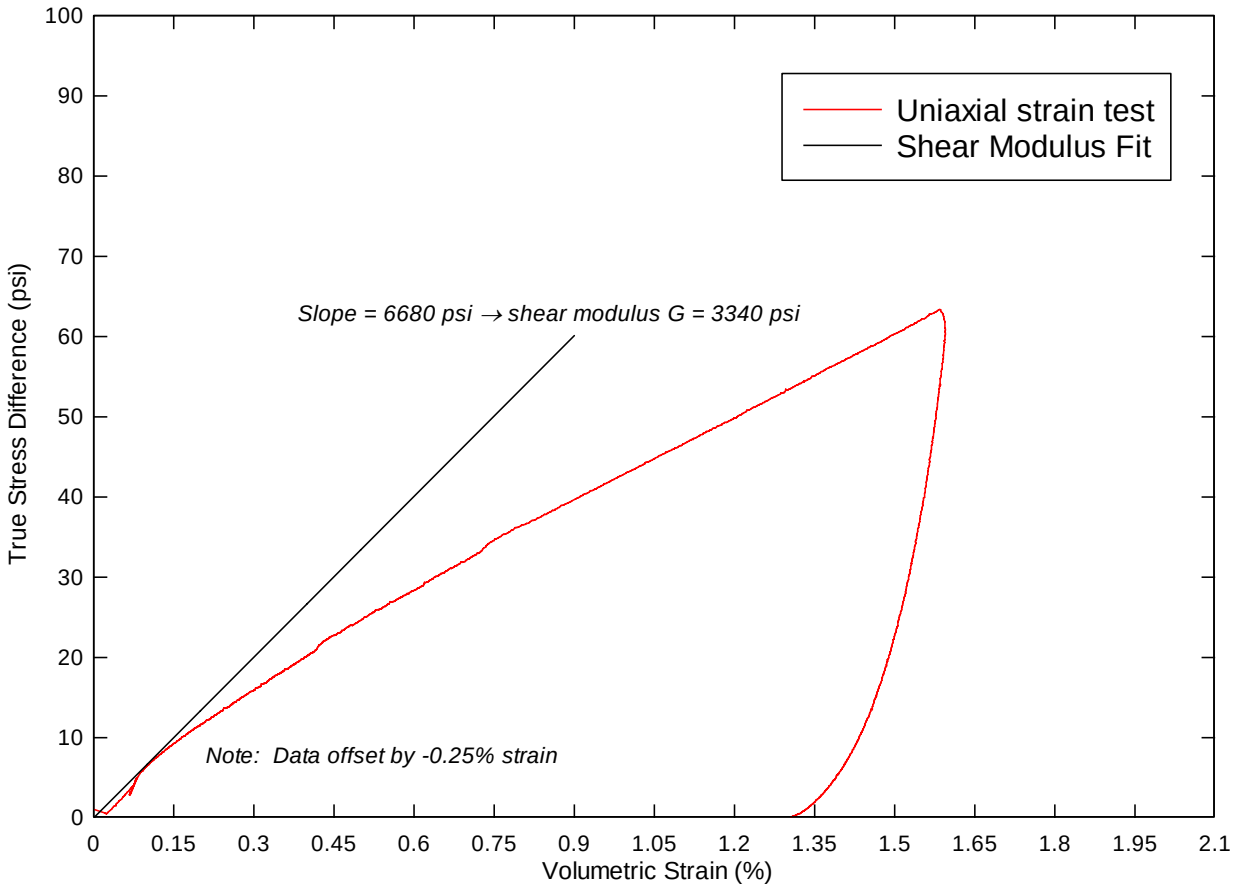

Figure 4-7: Unwashed sand uniaxial strain test results plotted as stress difference vs. strain. Shear modulus G fit shown. Shear stress is half of stress difference. Uniaxial strain is equal to shear strain.

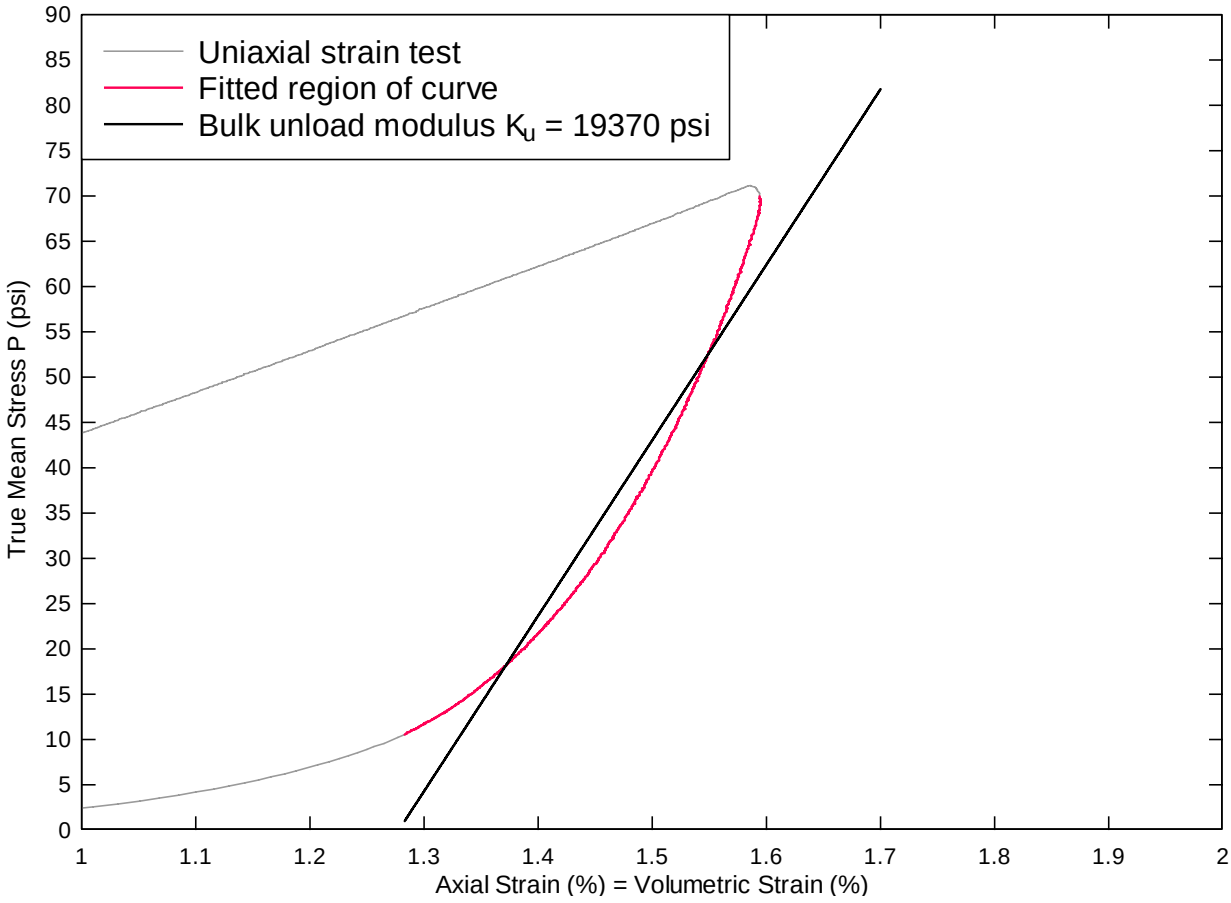

Figure 4-8: Unwashed sand uniaxial strain unloading portion. Determination of bulk unloading modulus K_u (BULK) by linear fit.

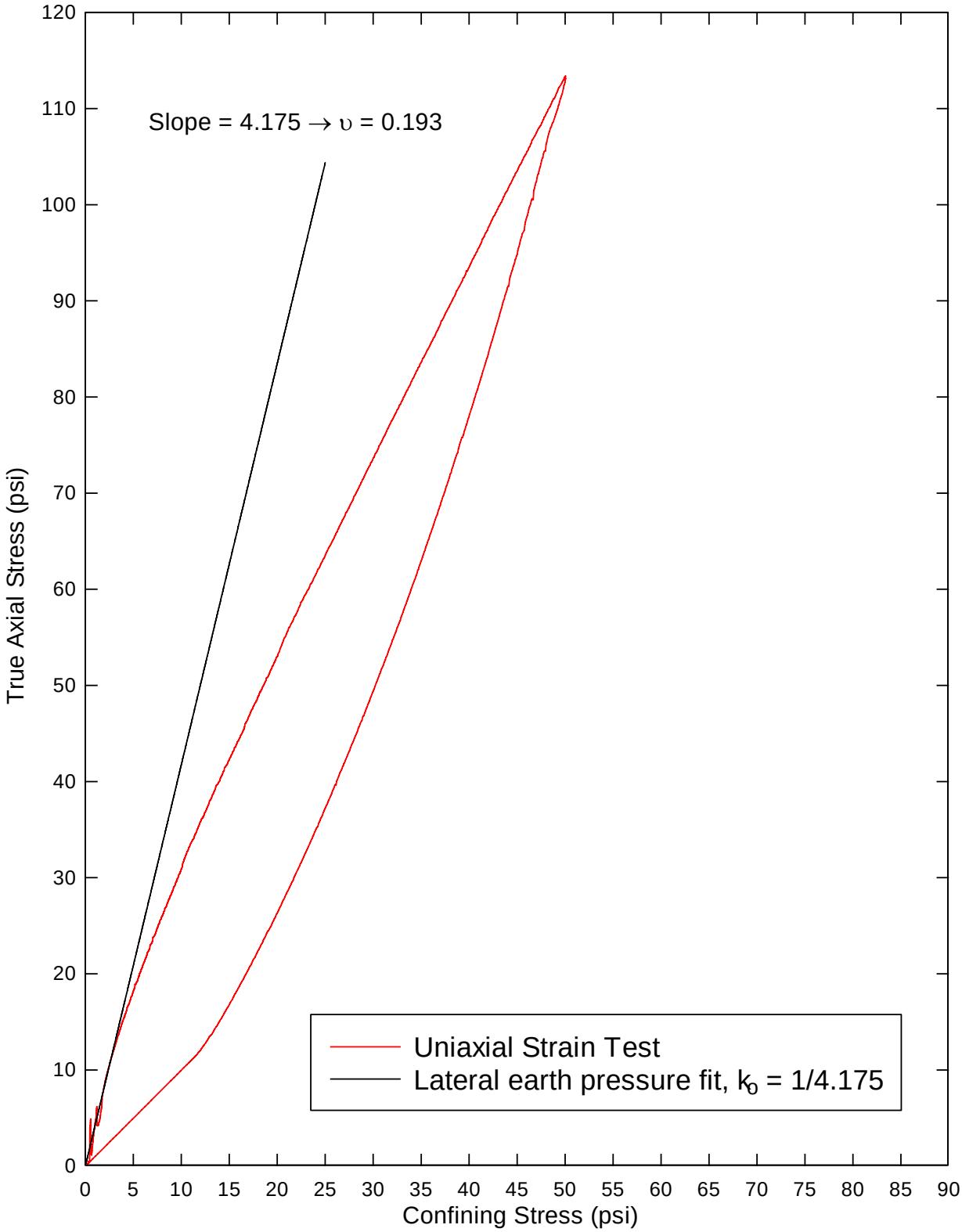

Figure 4-9: Unwashed sand uniaxial strain test. Determination of Poisson's ratio.

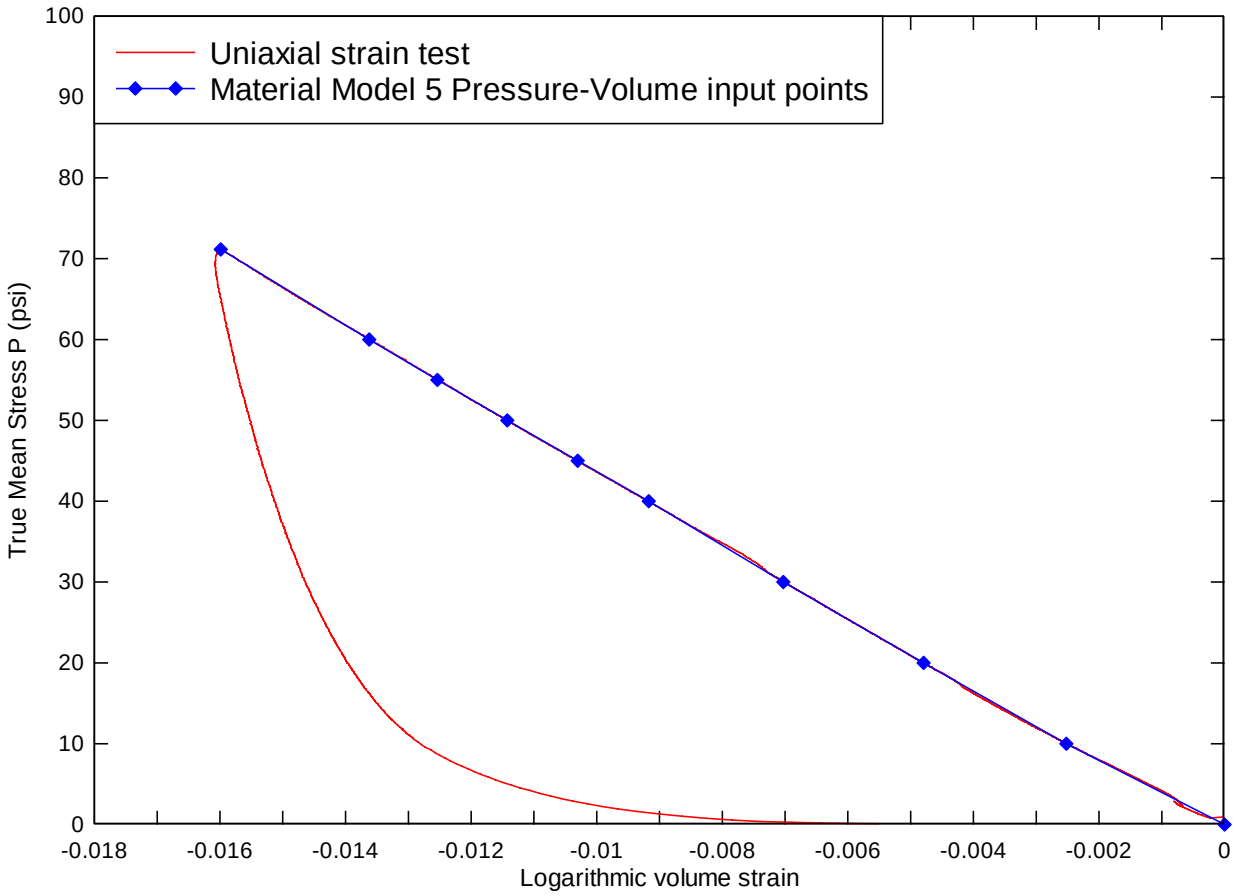

Figure 4-10: Unwashed sand Material Model 5 pressure-logarithmic volume curve with 10 input points. Obtained from uniaxial strain test.

4.5 LS-DYNA Material Model 5 inputs

The recommended set of inputs for modeling unwashed sand in LS-DYNA Material Model 5: Soil and Foam is shown in the table below.

Table 4-5: Material Model 5 inputs for unwashed sand

	Input	Value	Units
Mass density	**RO**	0.000196	lb s^2/in^4
Shear modulus	**G**	3340	psi
Bulk unloading modulus	**K**	19370	psi
Yield surface coefficient	**A0**	6.326	psi^2
Yield surface coefficient	**A1**	3.707	psi
Yield surface coefficient	**A2**	0.5432	-
Pressure cutoff	**PC**	-1	psi

	Input	Value	Input	Value	Units
Pressure-volume point	**EPS1**	0.0000	**P1**	0	psi
Pressure-volume point	**EPS2**	-0.00252	**P2**	10	psi
Pressure-volume point	**EPS3**	-0.00479	**P3**	20	psi
Pressure-volume point	**EPS4**	-0.00703	**P4**	30	psi
Pressure-volume point	**EPS5**	-0.00917	**P5**	40	psi
Pressure-volume point	**EPS6**	-0.0103	**P6**	45	psi
Pressure-volume point	**EPS7**	-0.01143	**P7**	50	psi
Pressure-volume point	**EPS8**	-0.01254	**P8**	55	psi
Pressure-volume point	**EPS9**	-0.01362	**P9**	60	psi
Pressure-volume point	**EPS10**	-0.01599	**P10**	71.15	psi

Table 4-6: Summary of elastic constants

Young's Modulus E	7969	psi
Poisson's Ratio ν	0.193	
Shear Modulus G	3340	psi
Initial Bulk Modulus K	8970	psi
Constrained Modulus M	4331	psi

4.6 Recommended range of model application

The unwashed sand material model is recommended for simulating conditions near 12% water content and 130 lbs/ft^3 density. The farther away the actual conditions are, the less applicable the model. Reducing moisture content will increase stiffness and strength. Increasing moisture will have the opposite effect.

5 KSC Low Density Dry Sand

The general description, field observations, test data, and Material Model 5 inputs for KSC Low Density Dry (LDD) Sand is discussed in this chapter. KSC LDD Sand comprises the soft shoreline near the beach dunes. It is above the waterline and almost completely dry. It is a fine sand deposited under low density conditions, making it the weakest and most compressible KSC sand.

5.1 Location

KSC lies on a sand bar deposit from the Eocene era. Most of the surface sands were deposited within the last 7000 years, making all sands closely related in terms of origin. All sands near the KSC Pads have common parent material constituents and similar grain size distributions. Figure 5-1 is an aerial view of the planned launch pads (39A and 39B) for the CEV.

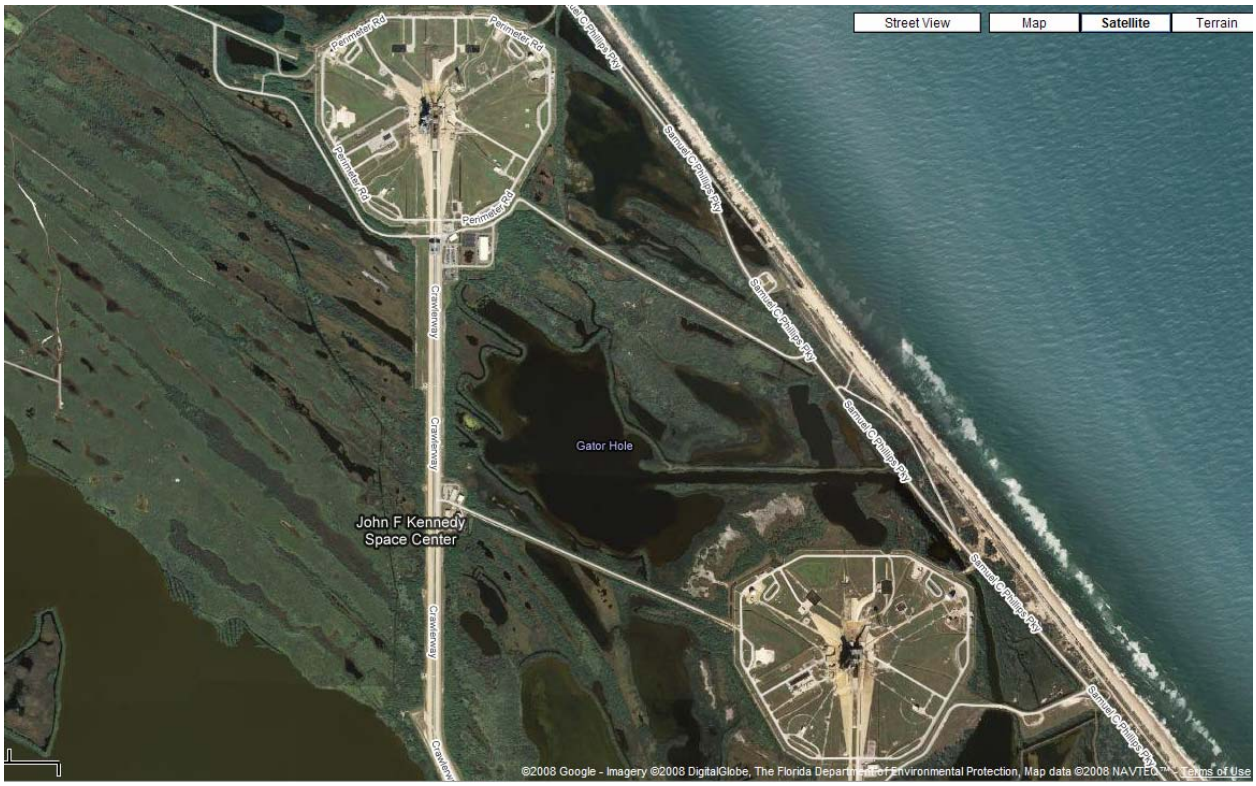

Figure 5-1: Aerial view of Kennedy Space Center. Pad A is the southernmost. Pad B is the northernmost.

KSC LDD Sand lies along the coastal dunes. It also reasonably represents any KSC sand deposits that are fall under these conditions: fine sand, <80 lbs/ft^3 density within the first 8 inches of depth, and an air dried state of <5% moisture content. Figure 5-2 displays a soil map and sands under similar conditions.

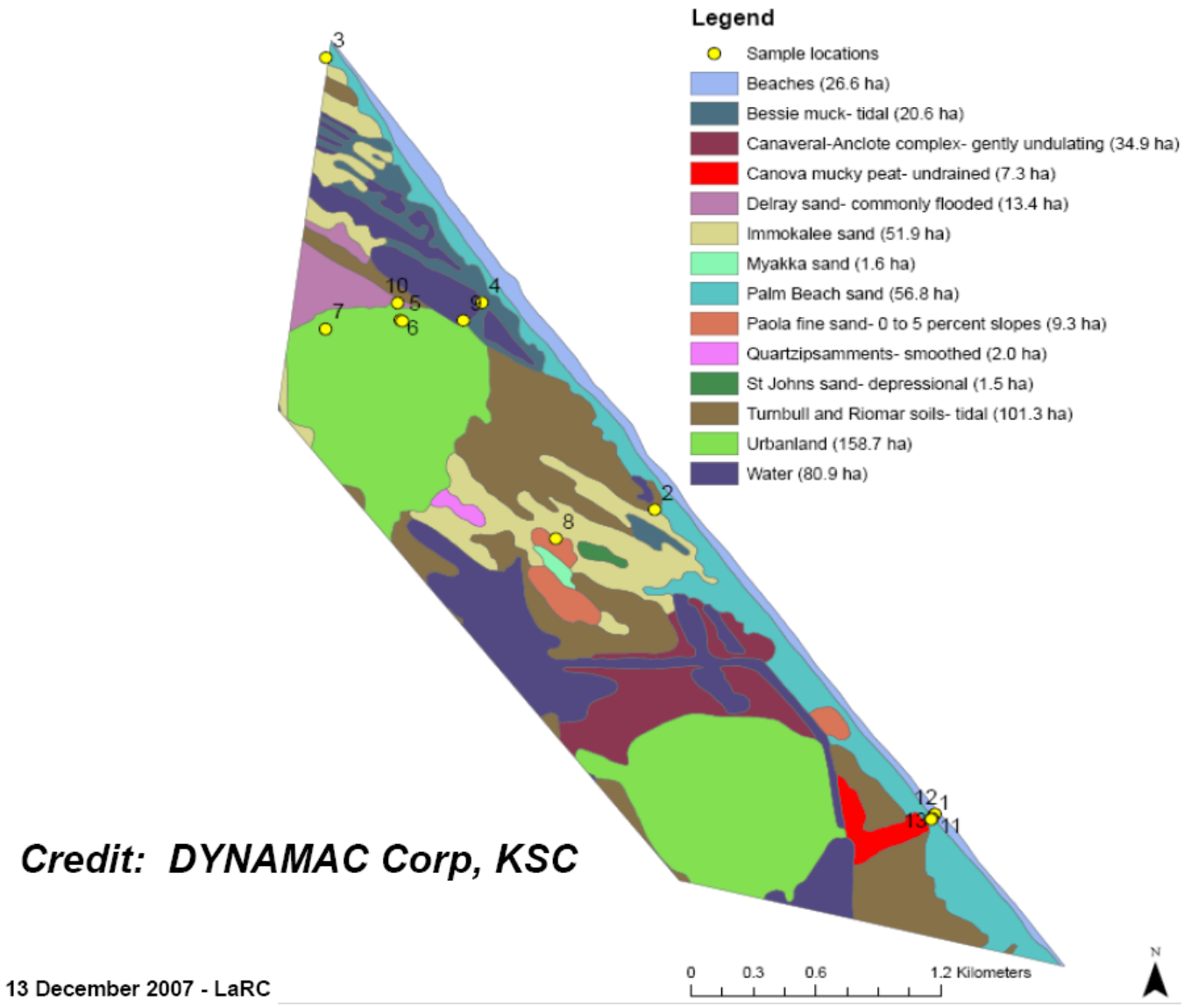

Figure 5-2: KSC soil map, sourced from Dynamac (Reference 9). "Palm Beach Sand" was the sampling source for KSC Low Density Dry Sand. Immokalee and Paola sand also fall under similar conditions. The areas labeled urbanland are Pads 39 A and B.

5.2 General description

KSC LDD Sand was the softest soil observed at KSC. It is a fine sand deposited by wind and ocean movements thousands of years. The sand type was observed to remain consistent to a depth of 30 inches. It is highly likely that the sand is uniform with depth across the entire KSC coastline. A small portion of the sand attributes its source to organic particle accumulation. The

surf zone sand, KSC High Density Flooded Sand, contains higher organic particle content, such as finely broken shell fragments. The natural methods of deposition add very little compactive effort to the soil. As a result, the soil surface deforms several percent strain when loaded with even small pressures. This is because LDD sand is cohesionless and very dependent upon confining pressure for strength. The sand's ability to highly compress is due to the granular nature of sand when it is very dry. In the lack of moisture, there is no cohesive force to resist shear stress, and without significant confining pressure, the low density soil responds by compressing to a stronger density to support load.

Most coastal terrain had less than a 5% slope except for the dunes. LDD sand's surface is essentially barren of vegetation except for the dunes. Table 5-1 shows the field density measurements conducted by Dynamac using a pipe typically sampling up to 3 inches depth. A steel ring is driven to a shallow depth and the soil mass is recovered from inside the ring. Notice the very low field minimum density. This is due to the shallow sampling from 3 inch depths. ARA's specimen mold is 8 inches tall, and therefore it is impossible to maintain 56 lbs/ft^3 because gravity compacts the bottom layers. It is also extremely difficult to handle a specimen below 80 lbs/ft^3. All KSC LDD Sand tests were conducted at the minimum feasible density (Table 5-2).

Table 5-1: Field density measurements from Dynamac 2000 report

KSC coastal sand	Samples N	Field Min	Field Max	Mean
Wet Density (lbs/ft^3)	23	56.2	87.4	74.3

Table 5-2: Absolute density minimum and maximum from ARA laboratory's 4"x8" specimen cylinder mold

	Absolute Lab Min	Absolute Lab Max	Min Feasible for Testing
Wet Density (lbs/ft^3)	64	99	80

Figure 5-3: KSC LDD Sand sampling site (left). Uniformity with depth apparent (right).

5.2.1 Soil classification

KSC Low Density Dry Sand is classified as SP in the Unified Soil Classification System, a poorly graded fine sand. The poor gradation indicates that most particle sizes are about the same. Classification was based on standard sieve analysis.

Table 5-3: KSC Low Density Dry Sand soil classification. Source – Dynamac 2000.

Soil Class	Mean Grain Size (mm)	USCS Class
Coastal (includes KSC Low Density Dry Sand and High Density In Situ w% Sand)	0.31	SP, fine sand

5.3 Laboratory test data

Laboratory tests conducted on KSC LDD Sand are presented in this section. The test log summarizes the tests using the triaxial apparatus.

Table 5-4: Test log for KSC LDD Sand

Test ID	Sample ID	Type	Confining Pressure (psi)	Moisture content	Wet Density (lbs/ft^3)	Dry Density (lbs/ft^3)	Grain Density G_s (g/cm^3)	Porosity n
M10B08	Pad A	Triax	2	3.05%	80.00	77.51	2.67	53.4%
M10D08	Pad A	Triax	5	3.04%	80.00	77.49	2.67	53.4%
M11E08	Pad A	Triax	10	2.78%	80.00	77.83	2.67	53.3%
M11H08	Pad A	Triax	20	2.78%	80.00	77.83	2.67	53.3%
M12B08	Pad A	Triax	50	2.89%	80.00	77.74	2.67	53.4%
M12I08	Pad A	Uniax	50	2.70%	80.00	77.84	2.67	53.3%

5.3.1 Grain density and grain size analysis

Figure 5-4 displays the dry sieve results for KSC LDD Sand. Dry sieve analysis was provided from the Dynamac report (Reference 9).

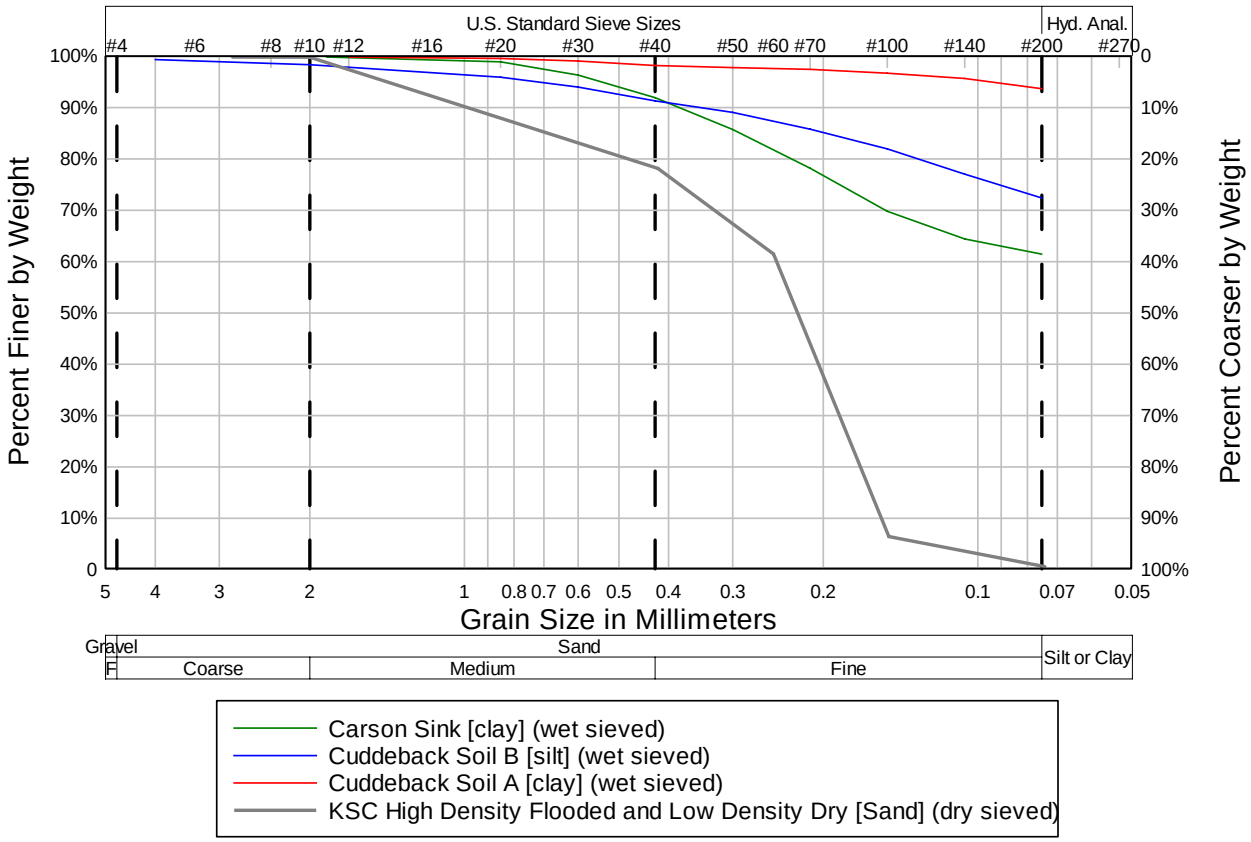

Figure 5-4: KSC Low Density Dry Sand grain size distribution.

5.3.2 Triaxial compression

The triaxial compression test results for KSC LDD Sand are shown on the next few pages.

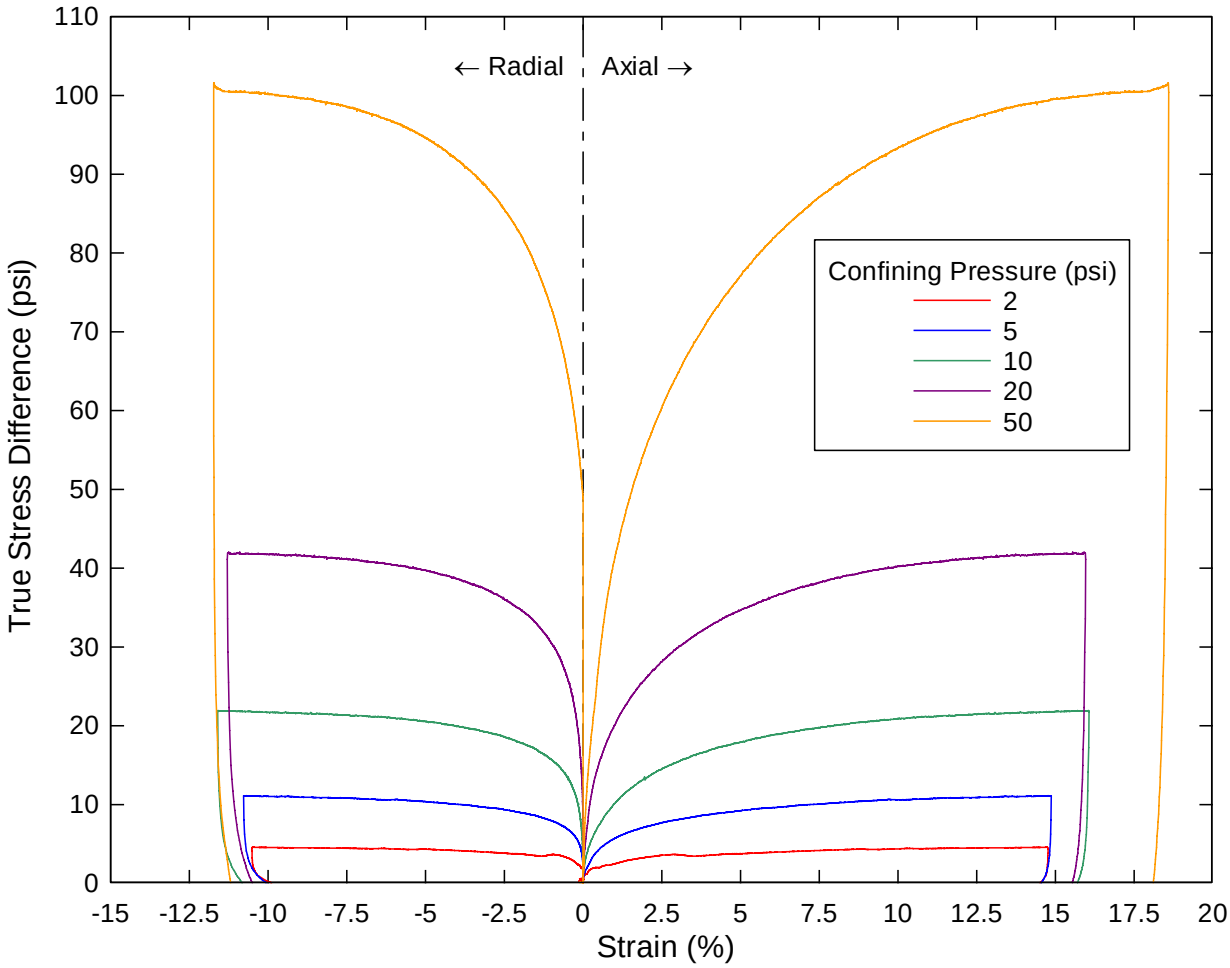

Figure 5-5: KSC LDD Sand triaxial test results.

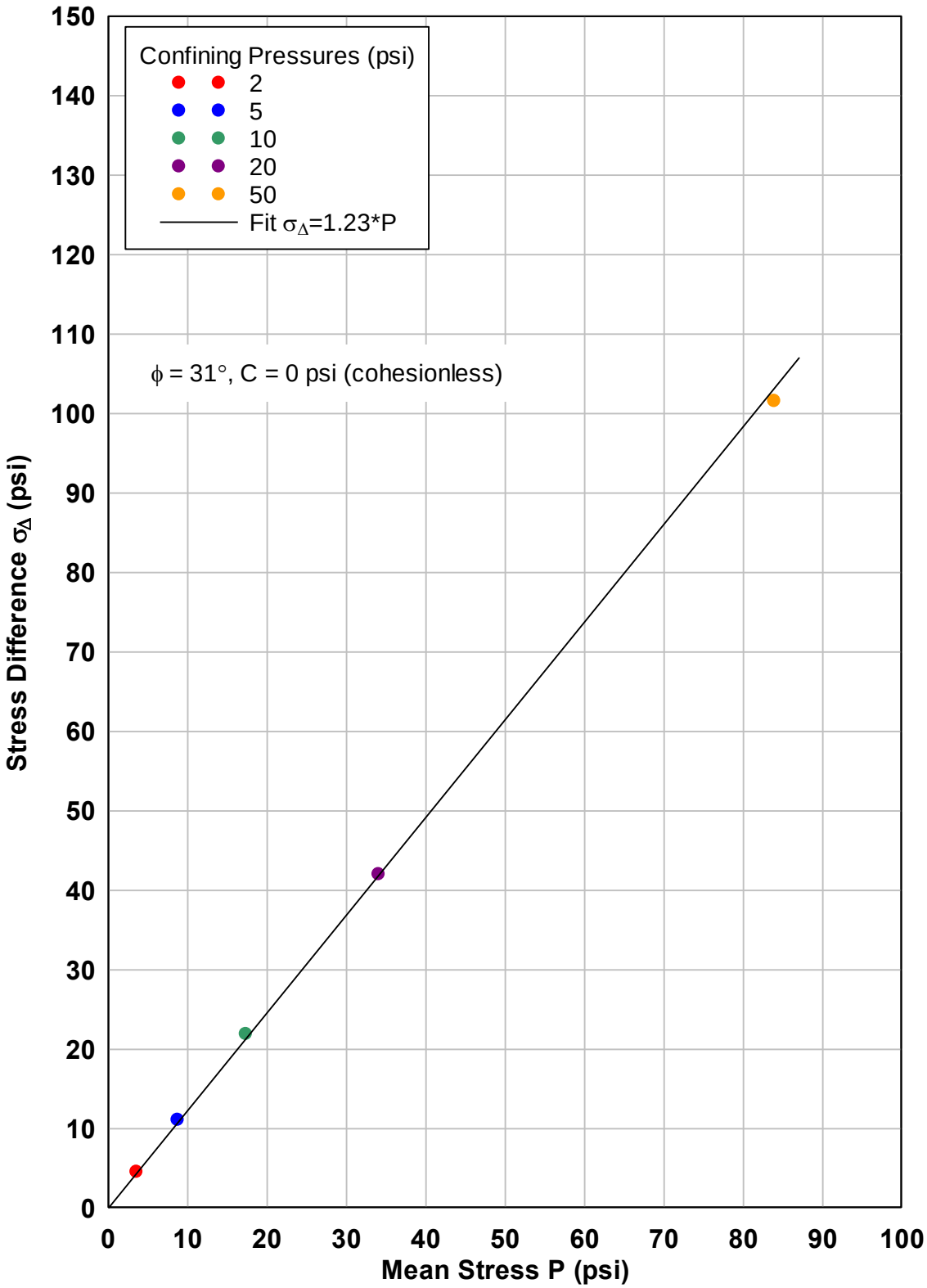

Figure 5-6: KSC LDD Sand's strength envelope from triaxial data.

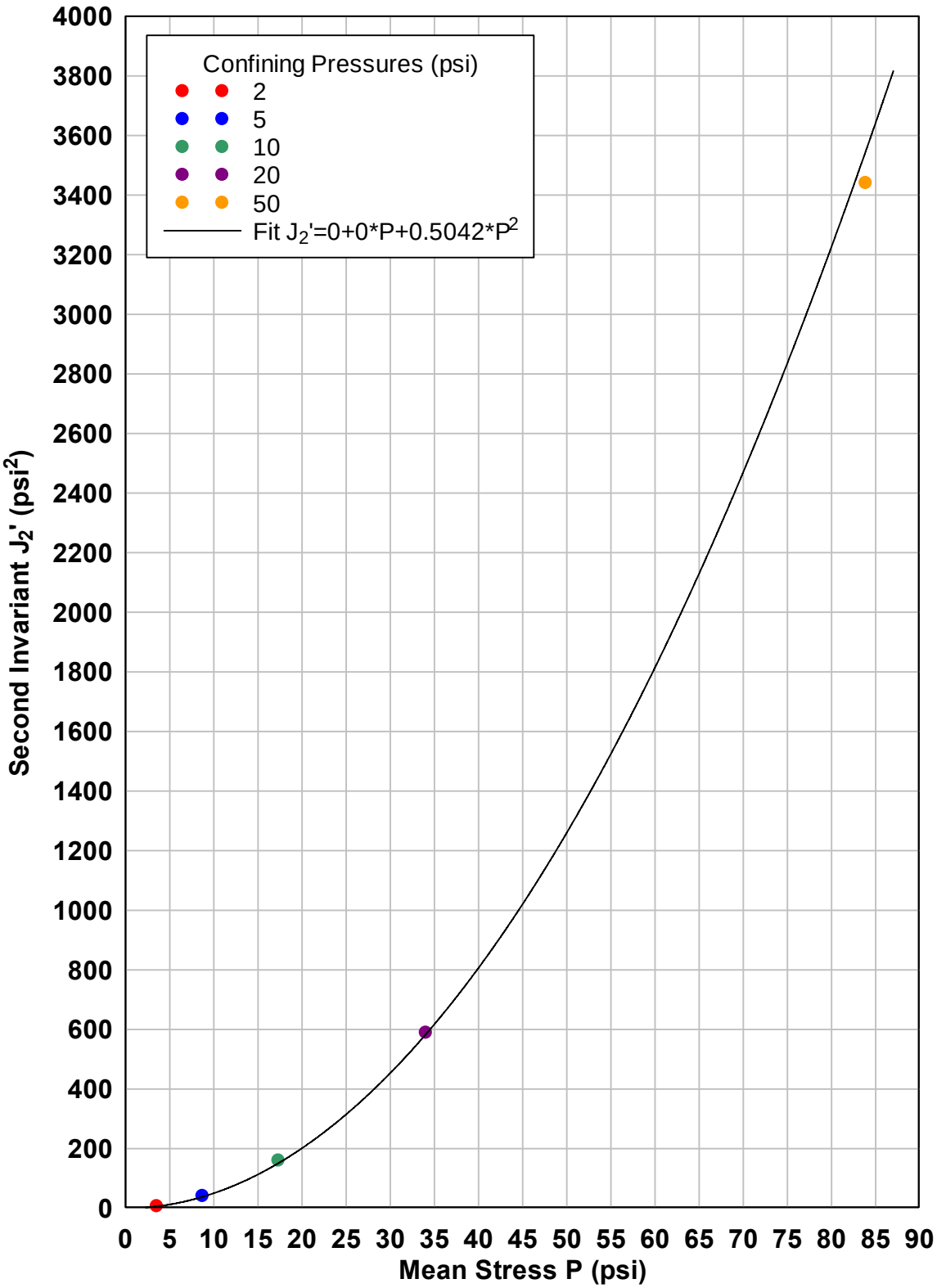

Figure 5-7: KSC LDD Sand, Material Model 5 yield surface fit from triaxial test data.

5.3.3 Uniaxial strain

The uniaxial strain data for KSC LDD Sand is shown on the next few pages. Is it important to note the flat portion of the test between 1.2% - 2.7% strain in Figure 5-8. ARA ran multiple uniaxial strain tests to confirm this behavior. The best uniaxial strain test was used for this report, and is shown in the next figure. The flat portion physically represents the loading piston pressing into the specimen, but no additional load is seen by the load cell at the bottom of the specimen. This means the downward movement of the piston is compressing the sand, but the sand is collapsing without taking additional load. Void space within the sand is essentially being closed, but without the soil skeleton transmitting additional load to the load cell at the bottom.

This phenomenon is attributed to testing at such low densities. It is extremely difficult to perform measurements on cohesionless sands at very low loading and low confining pressures. However, we believe the behavior between 0% - 1.2% strain is reliable, as well as the behavior beyond >3% strain. The multiple uniaxial tests confirmed these regions of behavior. Because The effect of the flat portion between 1.2% - 2.7% is unknown on LS-DYNA modeling, two compressibility options are presented here. The first is 10 pressure-volume points that define the data as measured. The second option includes is an artificially smoothed curve to bridge the flat gap between 1.2% and 3% strain, which presents a more expected and typical test response. It also eliminates a large-strain-small-load sensitivity that may cause LS-DYNA problems. The shear modulus is not affected by smoothing because it is based on early behavior below 1.2% strain.

The flat portion is also confirmed by hydrostatic tests. We believe what is physically happening is the compaction energy from loading is being absorbed by the sand skeleton itself. The beginning of the flat portion marks a breakdown in the sand skeleton, and grains continue to reorganize until the skeleton can sustain load again, which terminates shortly after 2.7% strain. Energy from compaction is being dissipated through sand skeleton breakdown.

Large deformations, such as the behavior under 3% strain, make sense for loose dry sands on the surface. This behavior is expected within the first few inches of the surface. The latter portion of the test, after 3% strain, are more representative of the deeper depths of sand. With depth, the specimen is denser, confining pressure is higher, and the sand will respond increasingly stiffer.

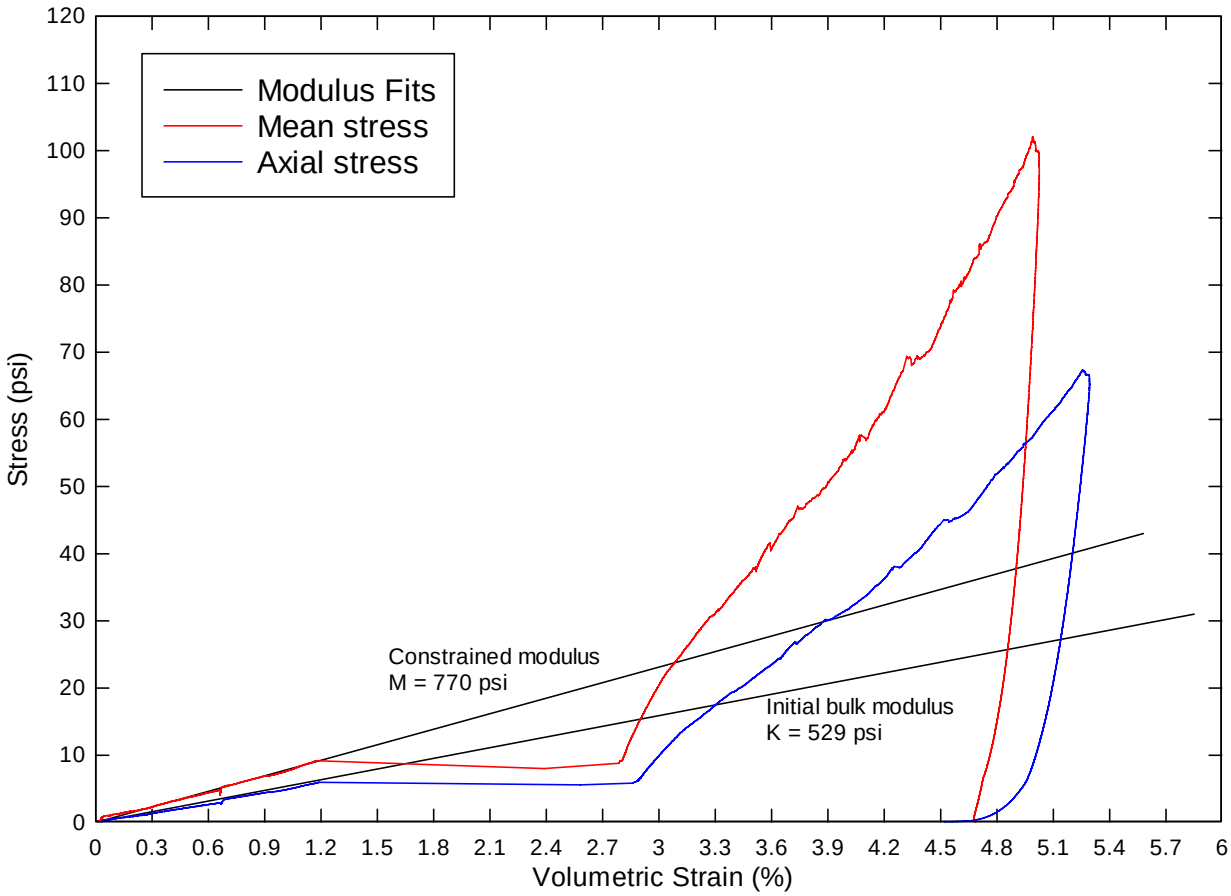

Figure 5-8: KSC LDD Sand uniaxial strain test with constrained modulus M and bulk loading modulus K fitted from initial loading slopes.

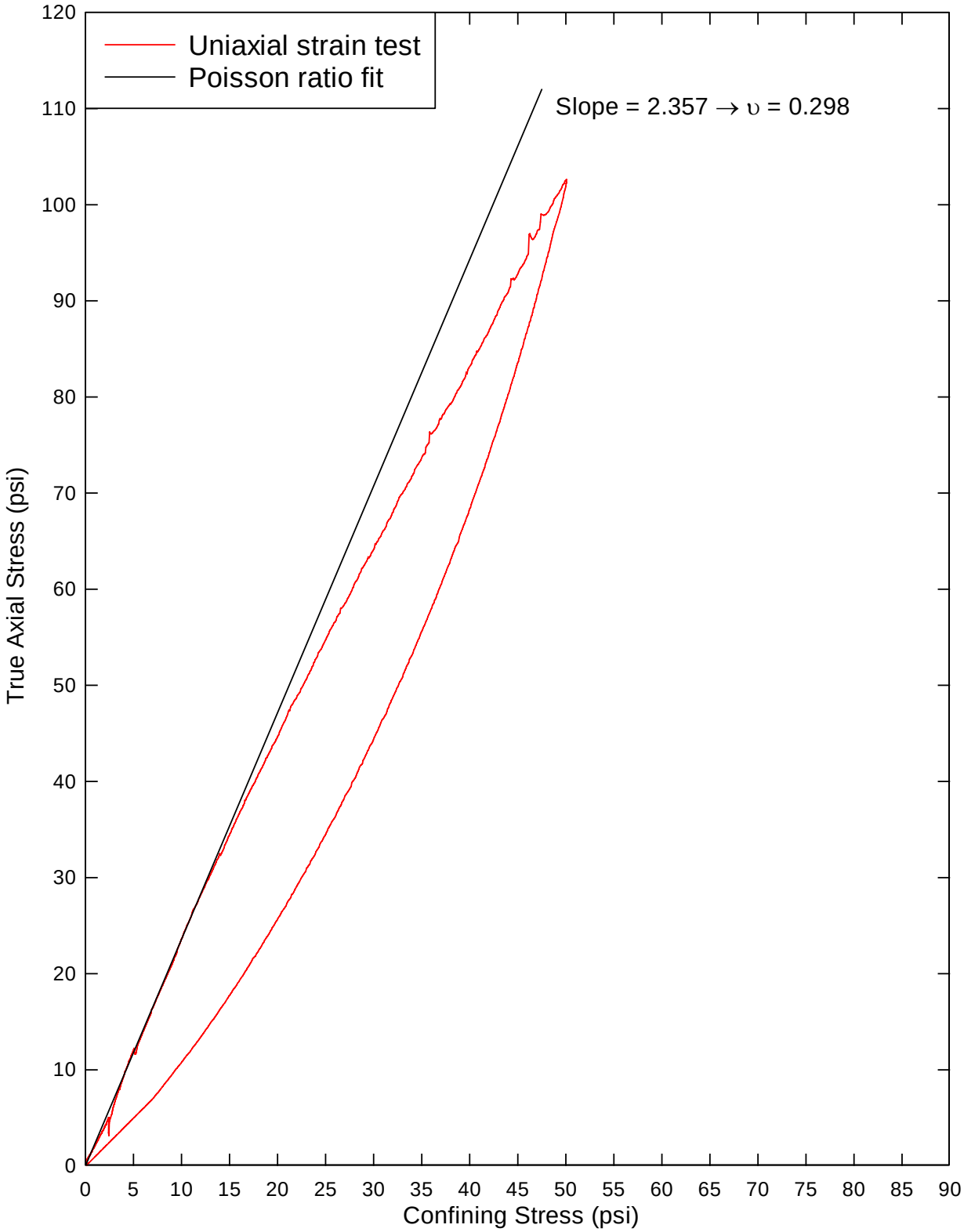

Figure 5-9: KSC LDD Sand uniaxial strain test with Poisson's ratio calculated from confining pressure vs. axial stress slope.

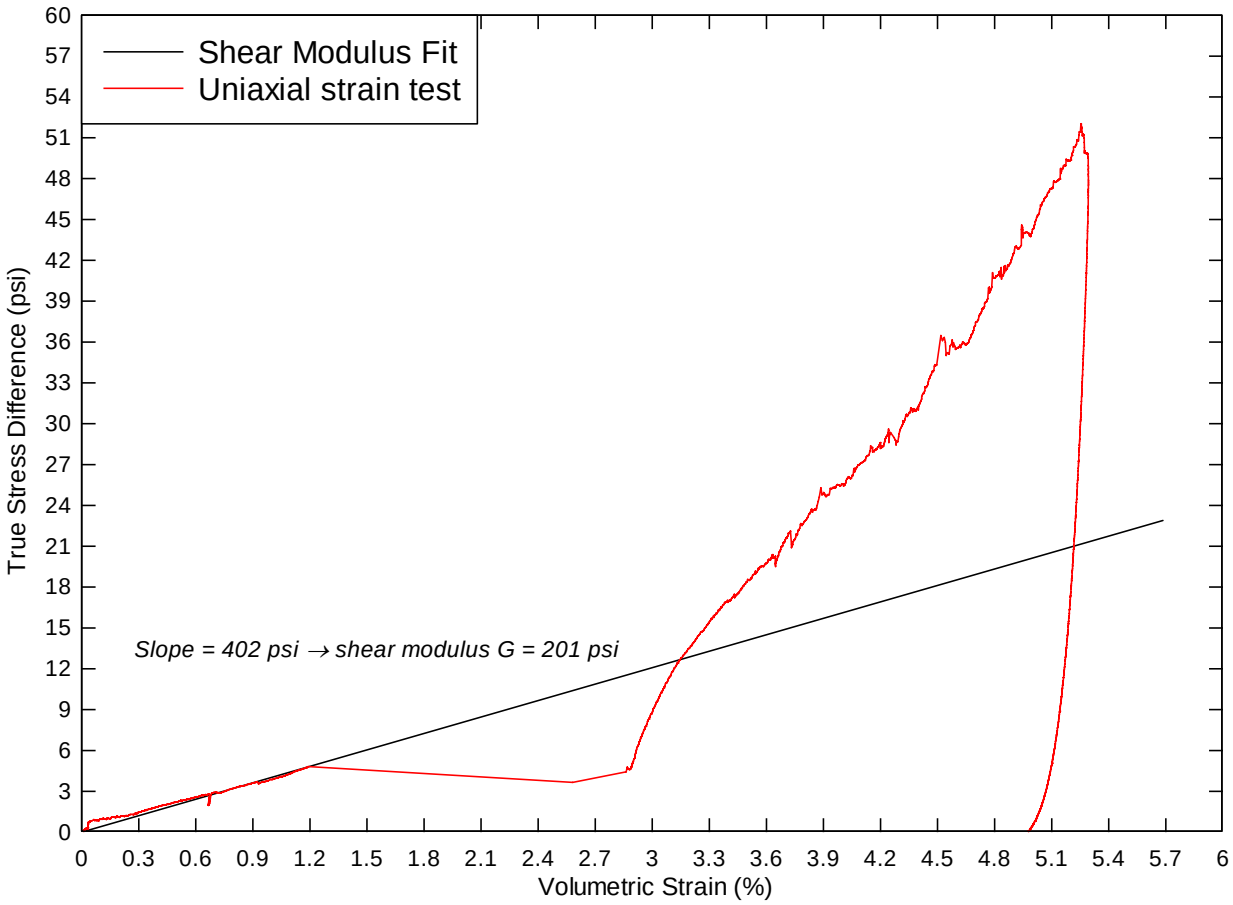

Figure 5-10: KSC LDD Sand uniaxial strain test with shear modulus G calculated from shear strain slope.

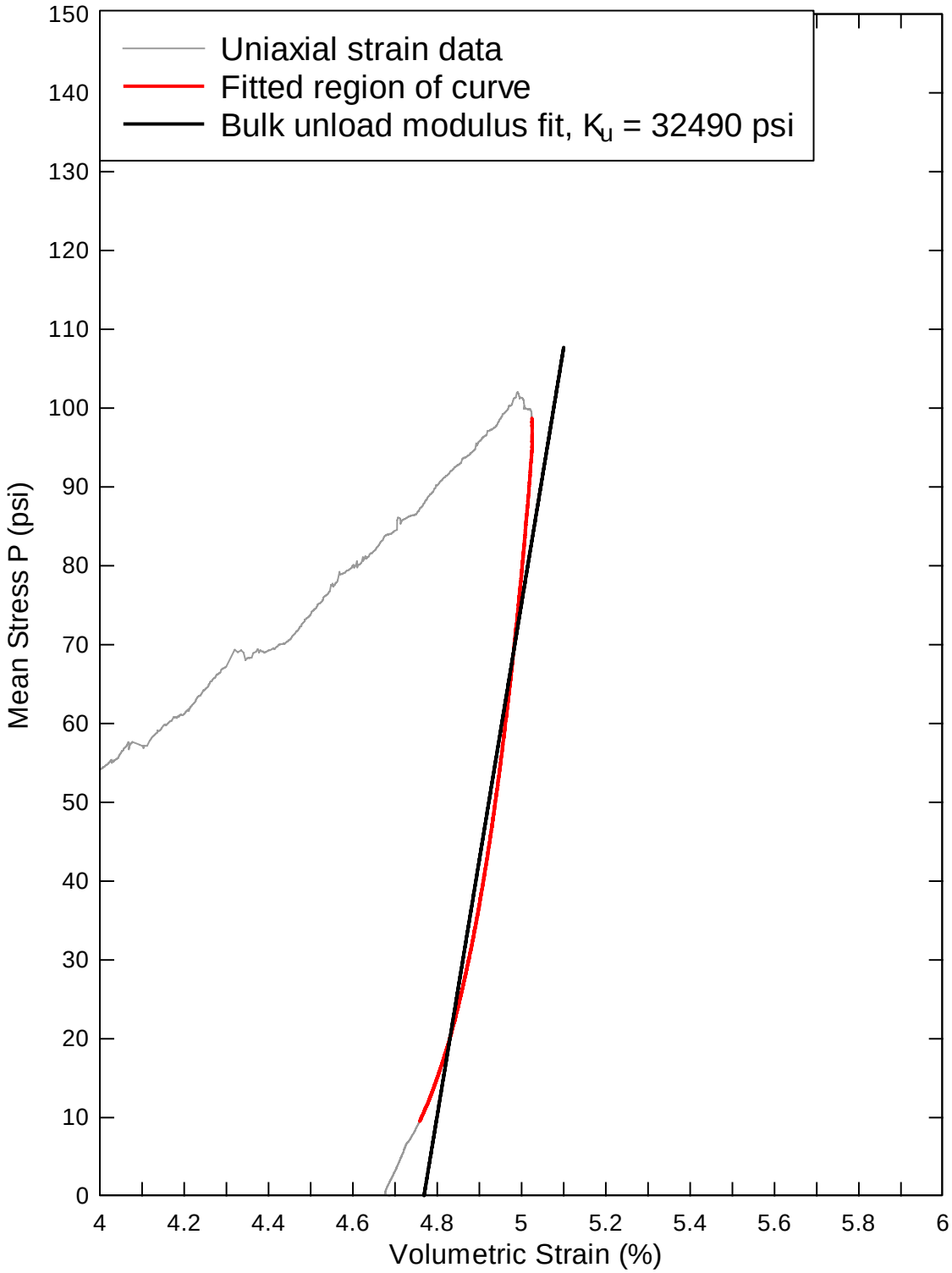

Figure 5-11: KSC LDD Sand uniaxial strain test with bulk unloading modulus calculated from unloading portion of test

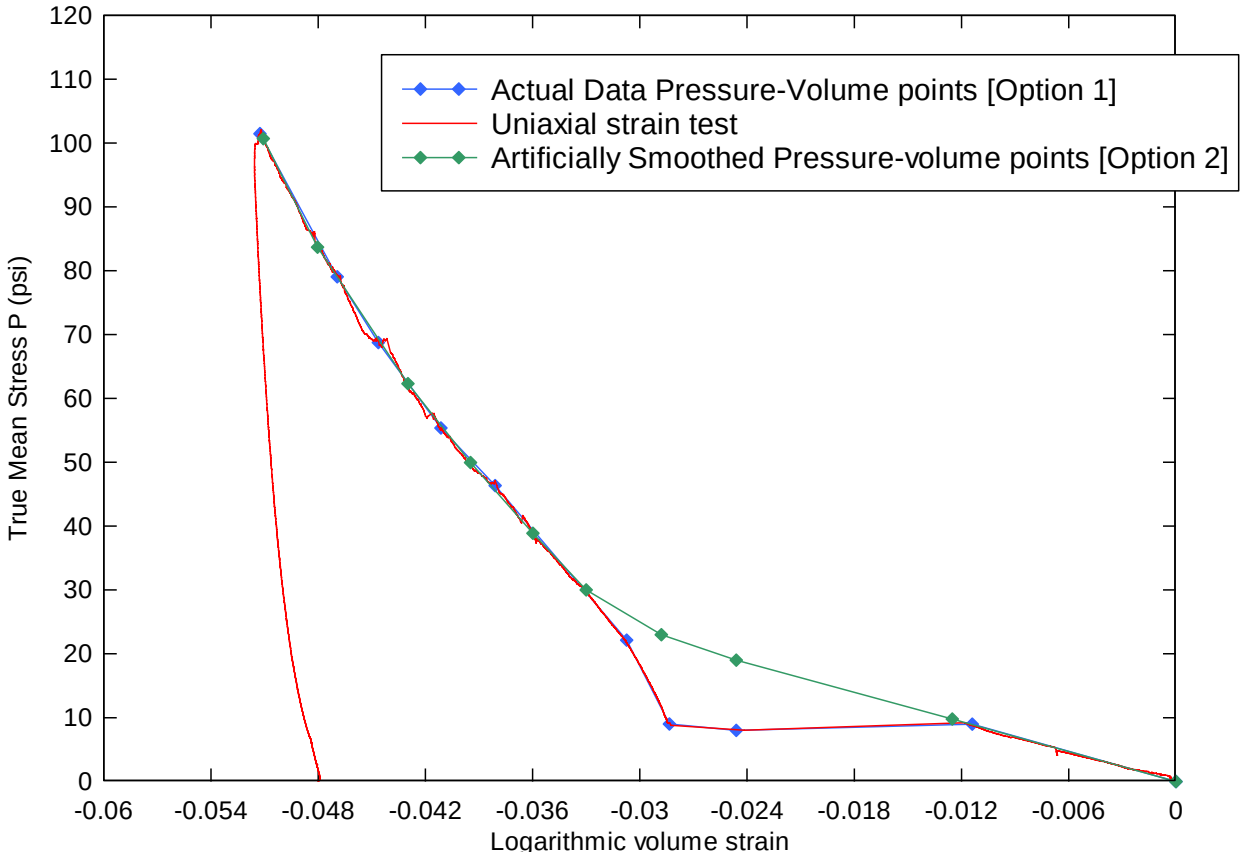

Figure 5-12: KSC LDD Material Model 5 pressure-logarithmic volume curve with 10 input points shown. Option 1 is based on actual data from testing. Option 2 is artificially smoothing the data. Option 1 is recommended unless the large deformations under small load increments cause complications in the LS-DYNA modeling.

5.4 LS-DYNA Material Model 5 inputs

The recommended set of inputs for modeling KSC Low Density Dry Sand in LS-DYNA Material Model 5: Soil and Foam is shown in Table 5-6 as Option 1. Option 1 includes the effect of large deformation with little increase in load between 1.2% and 2.7% strain. If the pressure-volume curve from Option 1 causes deformation complications in LS–DYNA modeling, then Option 2 is suggested. Option 2 assumes the initial loading modulus continues and there is a smooth transition to the higher modulus beginning at 3% strain. Option 2 follows a typical soil deformation response.

Table 5-5: Summary of KSC LDD Sand elastic constants

Constrained Modulus - M	770	psi
Poisson's Ratio - ν	0.298	
Young's Modulus - E	1114	psi
Initial Bulk Modulus - K	529	psi
Shear Modulus - G	201	psi

Table 5-6: Material Model 5 inputs for KSC Low Density Dry Sand [OPTION 1]

	Input	Value	Units
Density	**RO**	0.000120	lb s^2/in^4
Shear modulus	**G**	201	psi
Bulk unloading modulus	**K**	32490	psi
Yield surface coefficient	**A0**	0	psi^2
Yield surface coefficient	**A1**	0	psi
Yield surface coefficient	**A2**	0.5042	-
Pressure cutoff	**PC**	0	psi

	Input	Value	Input	Value	Units
Pressure-volume point	**EPS1**	0.0000	**P1**	0.00	psi
Pressure-volume point	**EPS2**	-0.0114	**P2**	9.00	psi
Pressure-volume point	**EPS3**	-0.0246	**P3**	8.00	psi
Pressure-volume point	**EPS4**	-0.0283	**P4**	9.01	psi
Pressure-volume point	**EPS5**	-0.0307	**P5**	22.15	psi
Pressure-volume point	**EPS6**	-0.0381	**P6**	46.35	psi
Pressure-volume point	**EPS7**	-0.0411	**P7**	55.36	psi
Pressure-volume point	**EPS8**	-0.0446	**P8**	68.76	psi
Pressure-volume point	**EPS9**	-0.0469	**P9**	79.06	psi
Pressure-volume point	**EPS10**	-0.0513	**P10**	101.46	psi

Table 5-7: Material Model 5 inputs for KSC Low Density Dry Sand [OPTION 2]

	Input	Value	Units
Density	**RO**	0.000120	lb s^2/in^4
Shear modulus	**G**	201	psi
Bulk unloading modulus	**K**	32490	psi
Yield surface coefficient	**A0**	0	psi^2
Yield surface coefficient	**A1**	0	psi
Yield surface coefficient	**A2**	0.5042	-
Pressure cutoff	**PC**	0	psi

	Input	Value	Input	Value	Units
Pressure-volume point	**EPS1**	0.0000	**P1**	0.00	psi
Pressure-volume point	**EPS2**	-0.0125	**P2**	9.79	psi
Pressure-volume point	**EPS3**	-0.0246	**P3**	19.00	psi
Pressure-volume point	**EPS4**	-0.0288	**P4**	23.00	psi
Pressure-volume point	**EPS5**	-0.0330	**P5**	30.00	psi
Pressure-volume point	**EPS6**	-0.0360	**P6**	38.88	psi
Pressure-volume point	**EPS7**	-0.0395	**P7**	49.96	psi
Pressure-volume point	**EPS8**	-0.0430	**P8**	62.32	psi
Pressure-volume point	**EPS9**	-0.0480	**P9**	83.69	psi
Pressure-volume point	**EPS10**	-0.0511	**P10**	100.69	psi

6 KSC High Density In Situ Moisture Sand

This chapter describes the KSC High Density In situ moisture (HDI) Sand model. High density means the tested density reflects the more compacted areas around KSC. These include launch pads, road embankments, and other man-made areas. In situ moisture means that the sand was tested as sampled from the site. No changes in moisture content were made. The KSC DHI Sand model's purpose is to simulate the denser, stiffer areas around Pads 39 A and B. These areas are denser than any naturally deposited sand.

6.1 Location

The KSC HDI Sand was sampled from man-made areas. Most notable was within the ring road of Pad 39 B. It represents the "Urbanland" zones marked in Figure 5-2. According to local KSC experts, the fill material was taken from nearby sources. The sands from man made areas are very similar to sands from other areas. It is not uncommon for coastal areas to have uniform sand deposits.

6.2 General description

Nearly all man-made areas are topped with grass-like vegetation. A sandy topsoil layer 1-2 inches thick covers the surface. The topsoil can be described as a sandy organic mix. This thin layer was ignored for modeling purposes in favor of the underlying sand. The underlying sand was the sample source for the KSC HDI Sand model.

The sands underlying man-made areas were also consistent with depth. The sand remained uniform to a depth of at least 30 inches. This is indicative of the geologically uniform sand deposits that created Merritt Island. The sand was also damp due to moisture being trapped underneath the topsoil. Topsoil prevents the sand from drying out. No bodies of water were nearby, and the pads are elevated above the waterline. Because no recent rains occurred, the moisture content obtained from samples is believed to be representative of most man-made areas. Figure 6-1 illustrates the topsoil layer.

Table 6-1: Field density measurements of surface sands from Dynamac 2000 report

KSC disturbed sand (man-made areas)	Samples N	Field Min	Field Max	Mean
Wet Density (lbs/ft^3)	22	37.4	87.4	69.3

Table 6-2: KSC HDI Sand soil classification. Source – Dynamac 2000.

Soil Class	Mean Grain Size (mm)	USCS Class
Disturbed (man-made areas)	0.18	SP, fine sand

Figure 6-1: Excavation at Pad 39 B, inside ring road. Topsoil is brown. Underlying sand is tan.

6.3 Laboratory data

The KSC HDI Sand is classified as poorly graded fine sand (USCS - SP). The grain size distribution indicates that it is 75% fine sand, 10% medium sand, 5% coarse sand, and 10% organic fines. Figure 6-2 shows the KSC DHI Sand's grain size distribution relative to Cuddeback and Carson Sink soils. The test log is shown in Table 6-3.

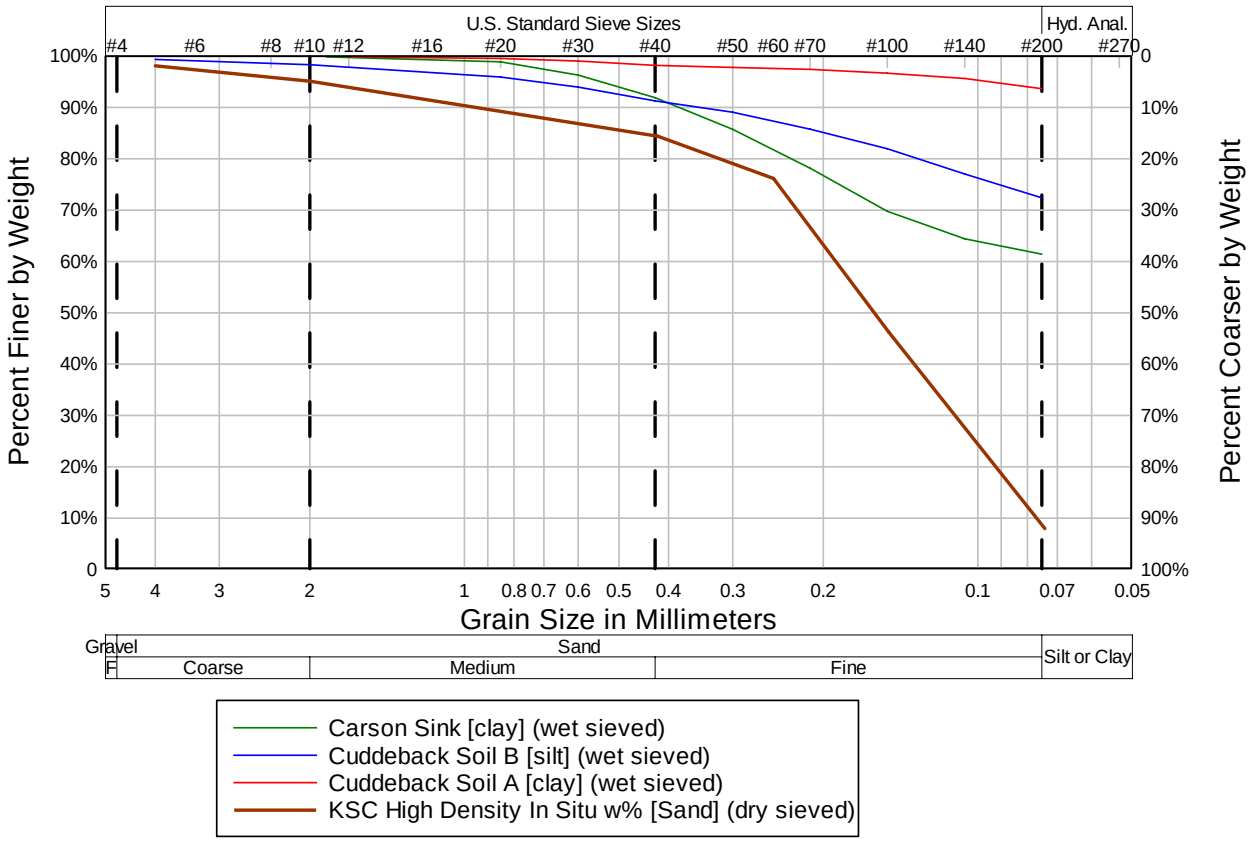

Figure 6-2: Grain size distribution for KSC High Density In Situ Moisture Sand. Taken from "man disturbed" soil category in Dynamac report.

Table 6-3: Test log for KSC HDI Sand

Test ID	Sample ID	Type	Confining Pressure (psi)	Moisture content	Wet Density (lbs/ft^3)	Dry Density (lbs/ft^3)	Grain Density G_s (g/cm^3)	Porosity n
A3A08	Pad B	Triax	20	16.31%	100.3	85.94	2.67	48.3%
A4A08	Pad B	Triax	50	16.27%	100.3	85.98	2.67	48.3%
A7C08	Pad B	Triax	10	17.65%	100.3	84.93	2.67	48.9%
A7E08	Pad B	Triax	5	18.37%	100.3	84.43	2.67	49.2%
A8B08	Pad B	Triax	2	15.69%	100.3	86.42	2.67	48.0%
A10B08	Pad B	Uniax	50	15.76%	100.3	86.41	2.67	48.0%

6.3.1 Triaxial compression

A series of 5 triaxial tests were carried out on KSC HDI Sand at 2, 5, 10, 20, and 50 psi confining pressures. The results are shown Figure 6-3. Strength envelope analysis and LS-DYNA yield surface fits are shown in Figure 6-4 and Figure 6-5.

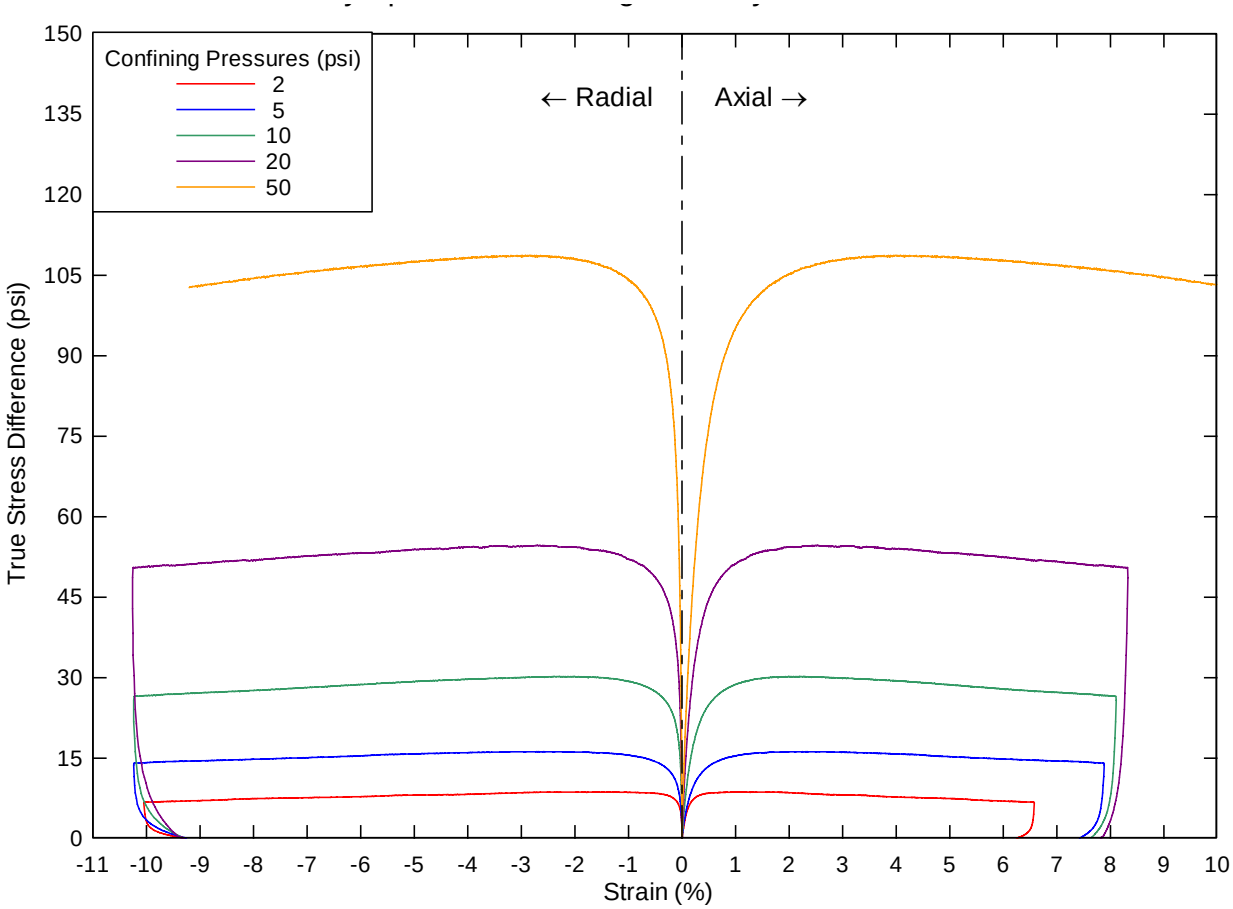

Figure 6-3: KSC HDI Sand model's triaxial compression test results. 50 psi truncated at 10% axial strain post peak.

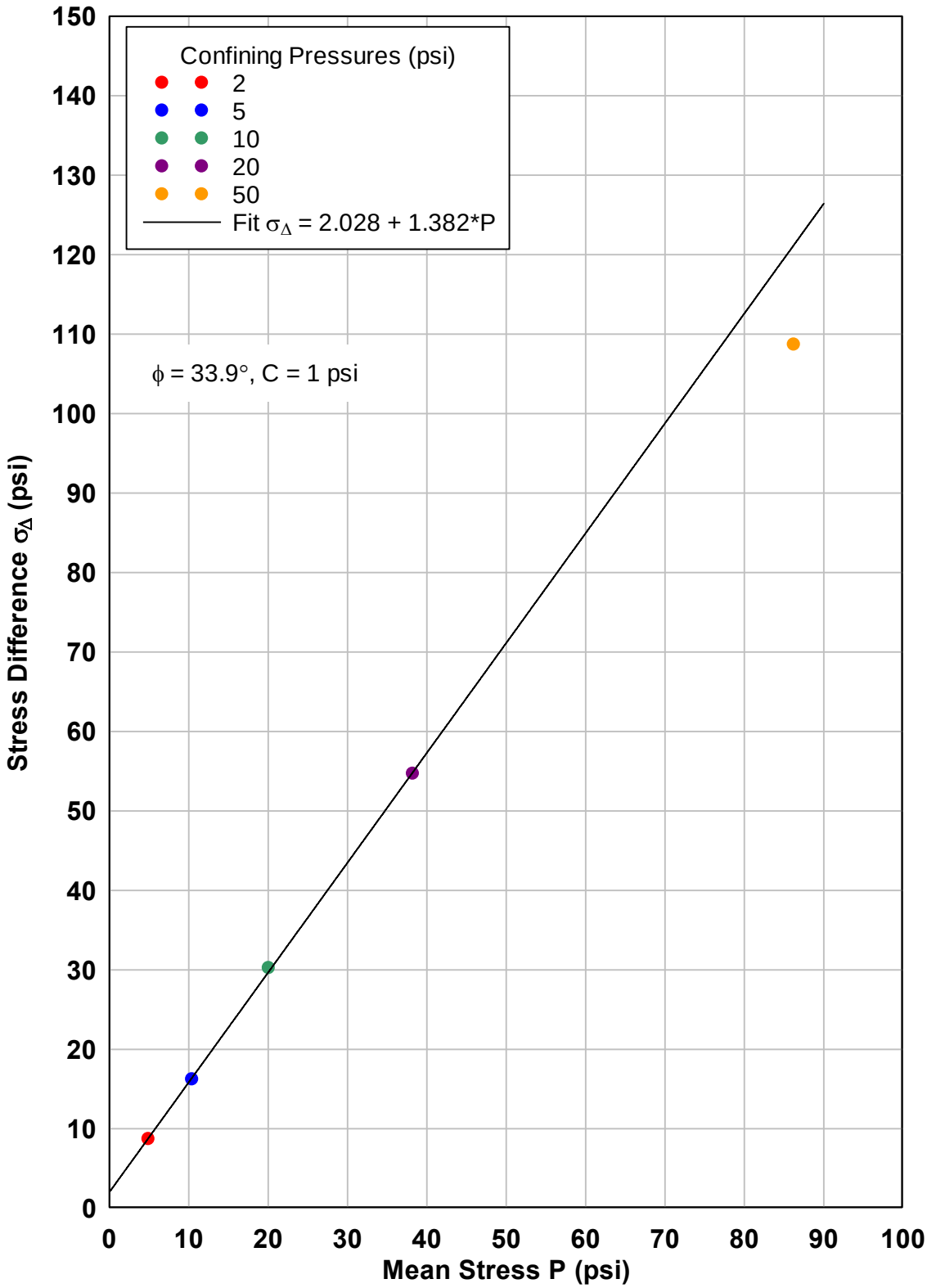

Figure 6-4: KSC HDI Sand model's strength envelope.

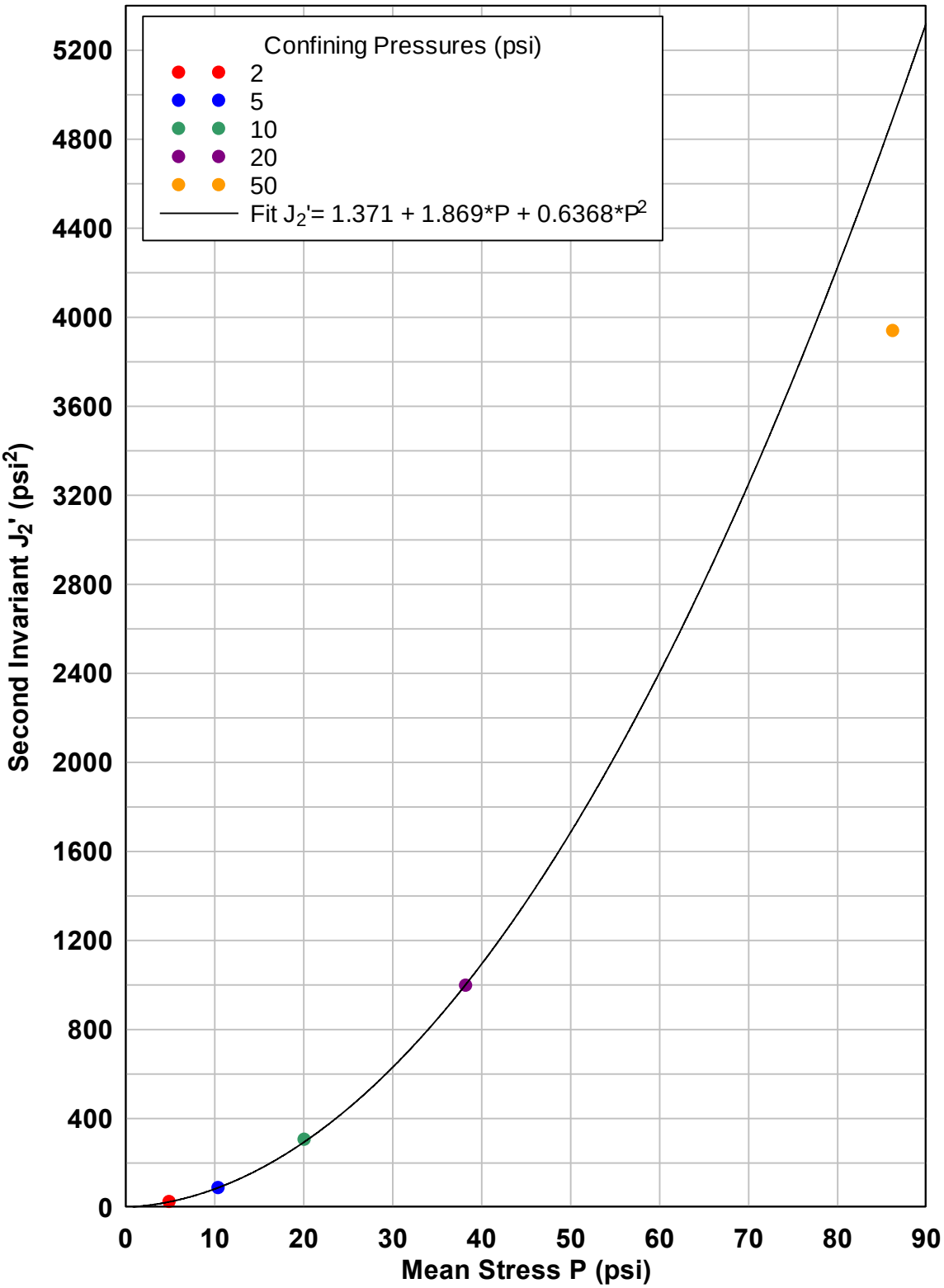

Figure 6-5: KSC HDI Sand Material Model 5 yield surface fit from triaxial data.

6.3.2 Uniaxial strain

KSC HDI Sand model's uniaxial strain test results follow on the next few pages.

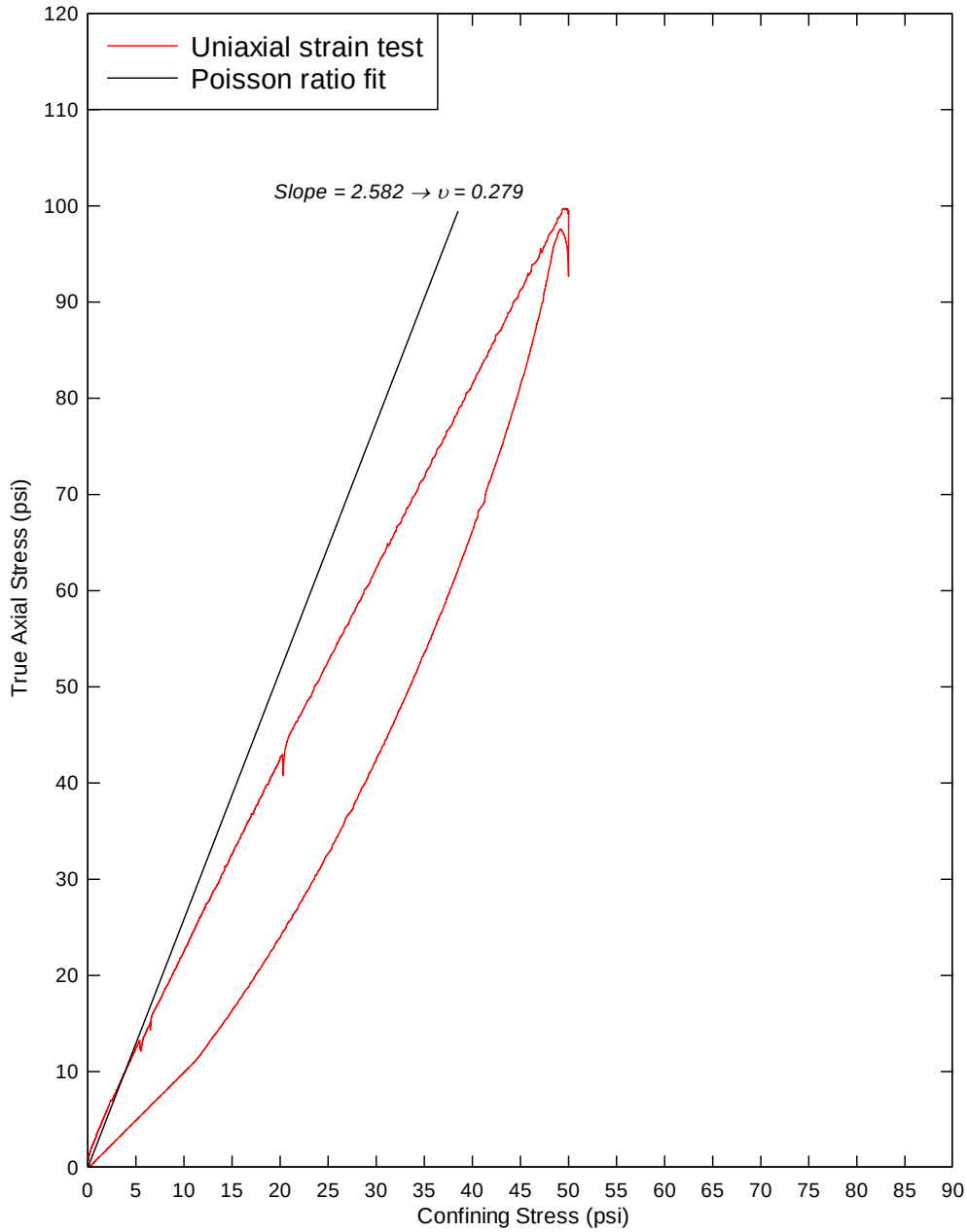

Figure 6-6: KSC HDI Sand model's uniaxial strain test. Axial stress vs. confining stress plotted to calculate Poissons ratio from slopes.

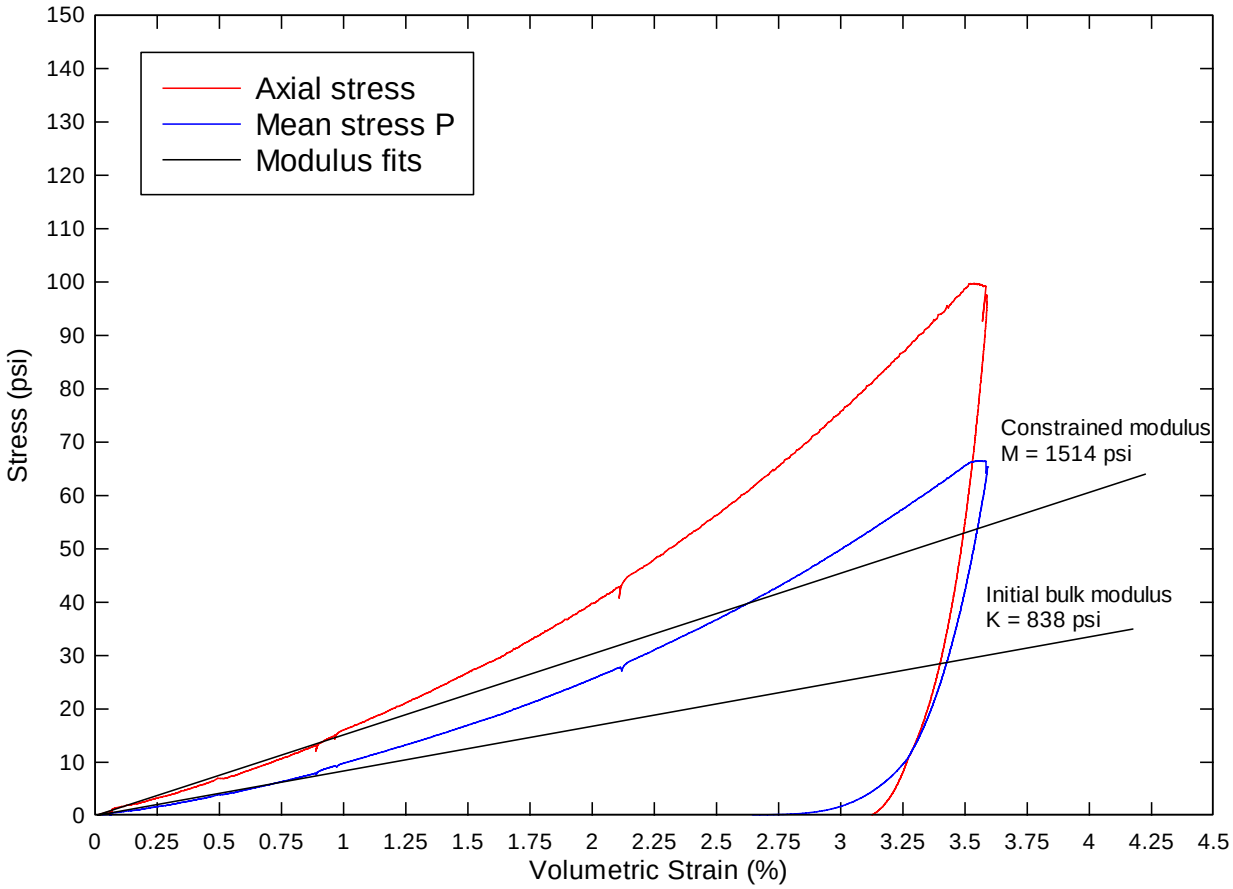

Figure 6-7: KSC HDI Sand model's uniaxial strain test. Stress vs. axial strain plotted to obtain constrained modulus from axial stress and Initial Bulk Modulus from mean stress.

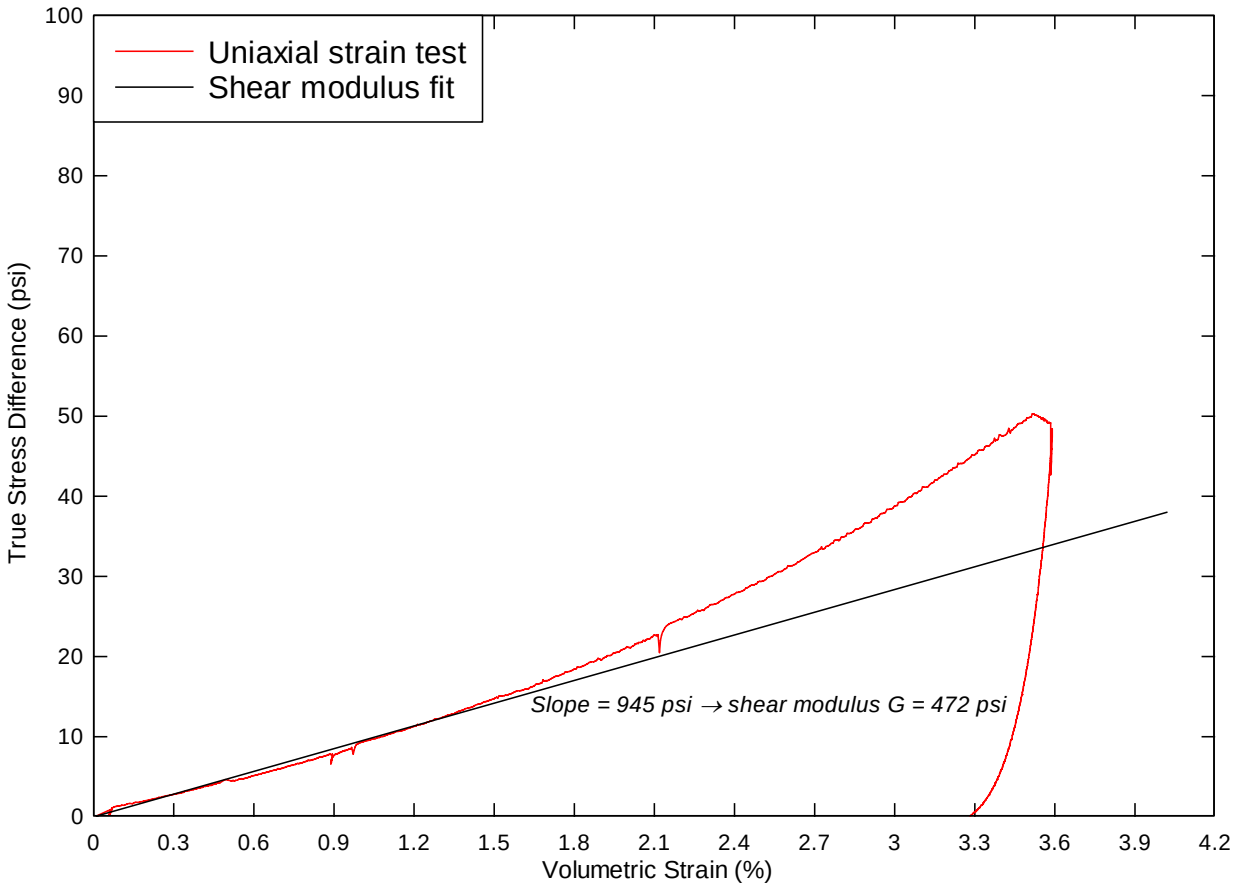

Figure 6-8: KSC HDI Sand model's uniaxial strain test. Stress difference vs. strain difference plotted to obtain shear modulus G.

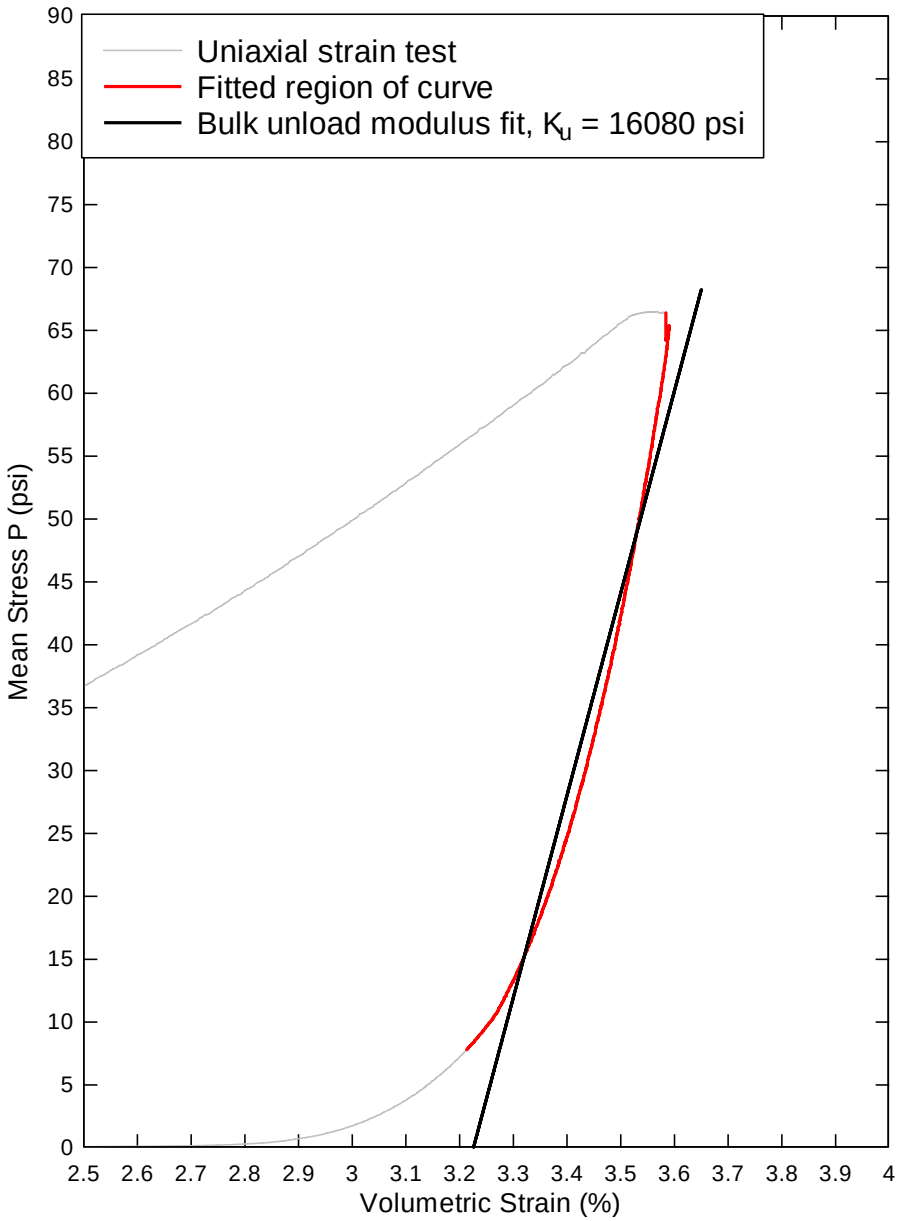

Figure 6-9: KSC HDI Sand model's uniaxial strain test, unloading portion. Mean stress vs. volumetric strain plotted to obtain bulk unloading modulus K_u (BULK). Black line represents slope of K_u. Red line represents fitted portion of test curve.

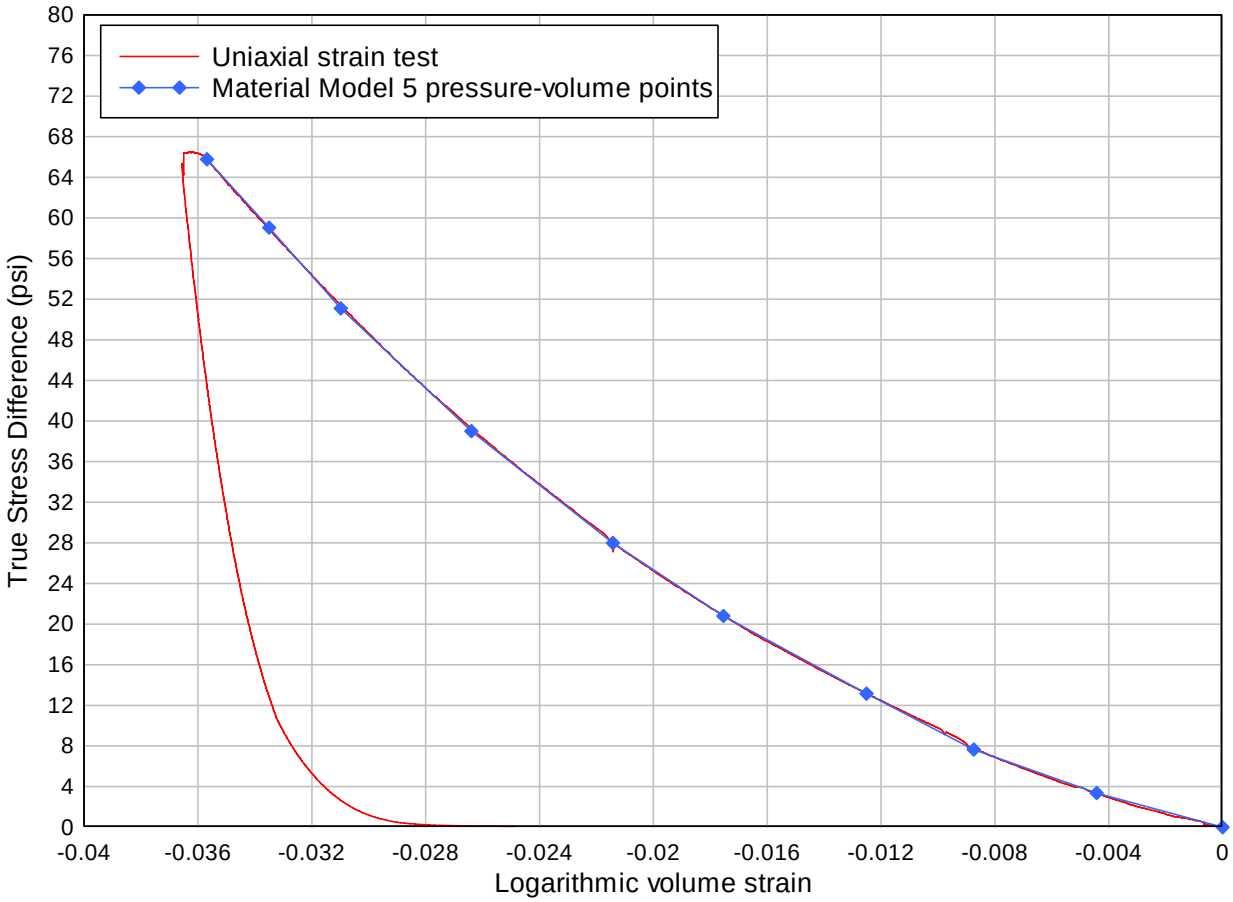

Figure 6-10: KSC HDI Sand model's uniaxial strain test. Mean stress vs. logarithmic volume strain plotted to obtain 10 pressure-volume points for Material Model 5 compressibility curve.

6.4 LS-DYNA Material Model 5 inputs

The recommended set of inputs for modeling KSC High Density In Situ Moisture Sand in LS-DYNA Material Model 5: Soil and Foam is shown in Table 6-4.

Table 6-4: Material Model 5 inputs for KSC HDI Sand.

	Input	Value	Units
Mass density	**RO**	0.000150	lb s^2/in^4
Shear modulus	**G**	472	psi
Bulk unloading modulus	**K**	16080	psi
Yield surface coefficient	**A0**	1.371	psi^2
Yield surface coefficient	**A1**	1.869	psi
Yield surface coefficient	**A2**	0.6368	-
Pressure cutoff	**PC**	0	psi

	Input	Value	Input	Value	Units
Pressure-volume point	**EPS1**	0.0000	**P1**	0.00	psi
Pressure-volume point	**EPS2**	-0.0044	**P2**	3.37	psi
Pressure-volume point	**EPS3**	-0.0087	**P3**	7.65	psi
Pressure-volume point	**EPS4**	-0.0125	**P4**	13.15	psi
Pressure-volume point	**EPS5**	-0.0175	**P5**	20.80	psi
Pressure-volume point	**EPS6**	-0.0214	**P6**	27.99	psi
Pressure-volume point	**EPS7**	-0.0264	**P7**	39.01	psi
Pressure-volume point	**EPS8**	-0.0310	**P8**	51.09	psi
Pressure-volume point	**EPS9**	-0.0335	**P9**	59.04	psi
Pressure-volume point	**EPS10**	-0.0357	**P10**	65.77	psi

Table 6-5: Summary of elastic constants for KSC HDI Sand.

Constrained Modulus - M	1514	psi
Poisson's Ratio - ν	0.279	
Young's Modulus - E	1812	psi
Initial Bulk Modulus - K	838	psi
Shear Modulus - G	472	psi

7 KSC High Density Flooded Sand

The KSC High Density Flooded (HDF) Sand is the wettest model in this report. Test specimens were flooded with water prior to testing. Specimens were allowed to drain during testing. The model's purpose is to simulate the surf zone sands on the coastal beach. It is also a close representation of submerged sands, although underwater modeling is beyond the scope of this report. When flooded, the saturation level is near 100%, but not 100%. This is because sand's permeability properties make the sample drain too quickly to maintain 100% saturation.

7.1 General description

The sample source for KSC HDF Sand was directly from the surf zone at various locations along the coast. The costal sand is slightly coarser than its KSC HDI Sand counterpart. This is because repetitive ocean and wind erosion tend to carry away fines.

The KSC HDF Sand exhibits a weak but stiff response to loading, in the same sense that styrofoam is both weak and stiff. The surf zone area can significantly increase during low tide.

The grain size distribution and average particle size for KSC HDF Sand are the same as KSC LDD Sand. Test specimens for both models were sampled on the coastline, east of the dunes. The KSC HDF sample sites were no more than 50 feet from the KSC LDD sample sites. Sampling is shown in Figure 7-1.

Figure 7-1: KSC High Density Flooded sampling from surf zone (left). Water table encountered at 1 inch depth. Surf zone expanse (right).

7.2 Laboratory test data

This section covers the laboratory tests conducted on KSC HDF Sand. The test log in Table 7-1 summarizes the tests using the triaxial apparatus. The pre-test moisture content is estimated assuming 95% saturation. Full saturation requires the sand to be continuously submerged.

Table 7-1: Test log for KSC HDF Sand

Test ID	Sample ID	Type	Confining Pressure (psi)	*Estim. Pre-test w% (S=95%)	Measured Post-test w%	Wet Density (lbs/ft^3)	Dry Density (lbs/ft^3)	Grain Density G_s (g/cm^3)	Porosity n
A15A08	Surf Zone (flooded/drained)	Uniax	50	31%*	16.59%	99.23	84.90	2.67	48.9%
A16C08	Surf Zone (flooded/drained)	Triax	2	31%*	15.91%	97.33	84.96	2.67	49.6%
A16F08	Surf Zone (flooded/drained)	Triax	5	31%*	12.95%	102.9	85.91	2.67	45.4%
A16H08	Surf Zone (flooded/drained)	Triax	10	31%*	16.21%	98.54	84.46	2.67	49.1%
A17B08	Surf Zone (flooded/drained)	Triax	20	31%*	12.20%	104.4	85.97	2.67	44.2%
A17D08	Surf Zone (flooded/drained)	Triax	50	31%*	11.12%	102.7	85.45	2.67	44.6%

7.2.1 Triaxial compression

Triaxial compression data for KSC HDF Sand is shown on the next few pages.

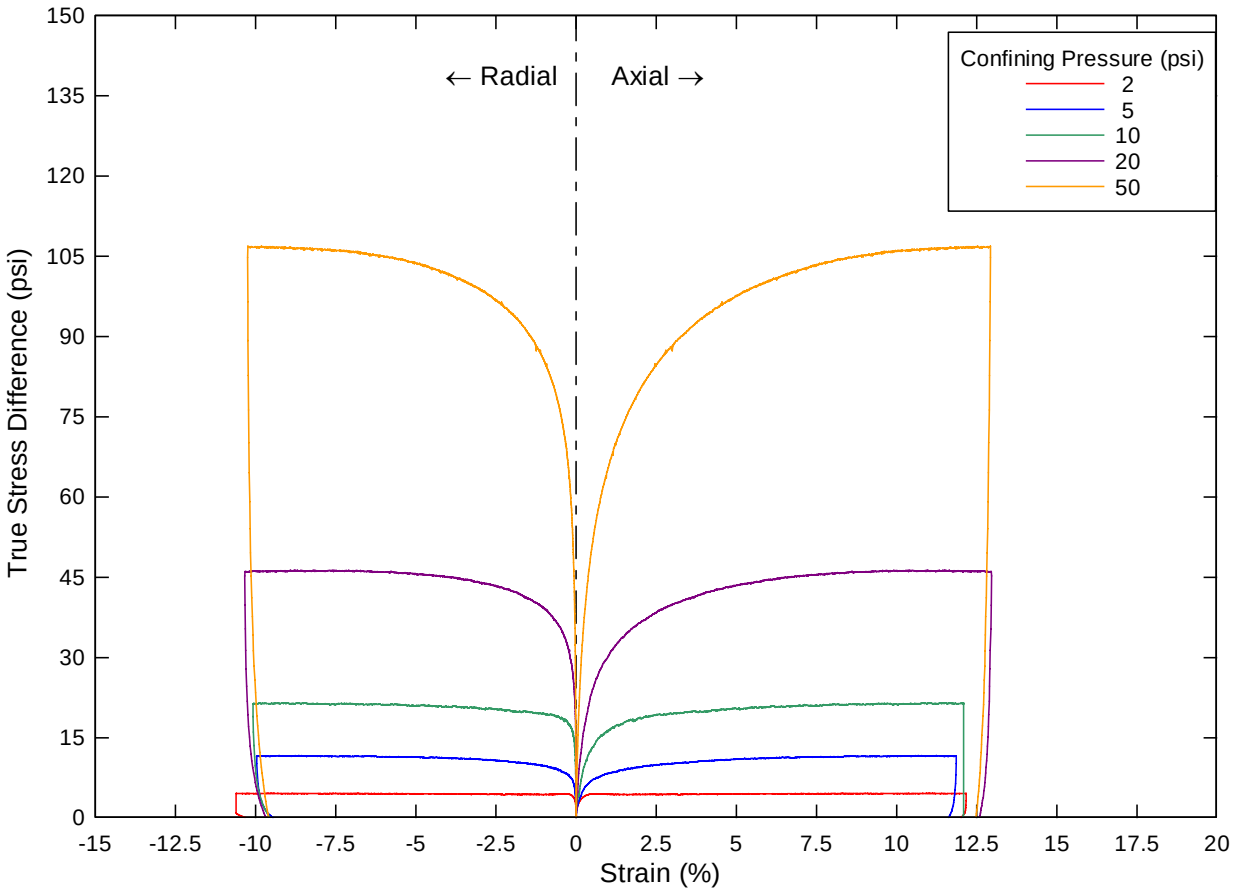

Figure 7-2: KSC HDF Sand model's triaxial test results.

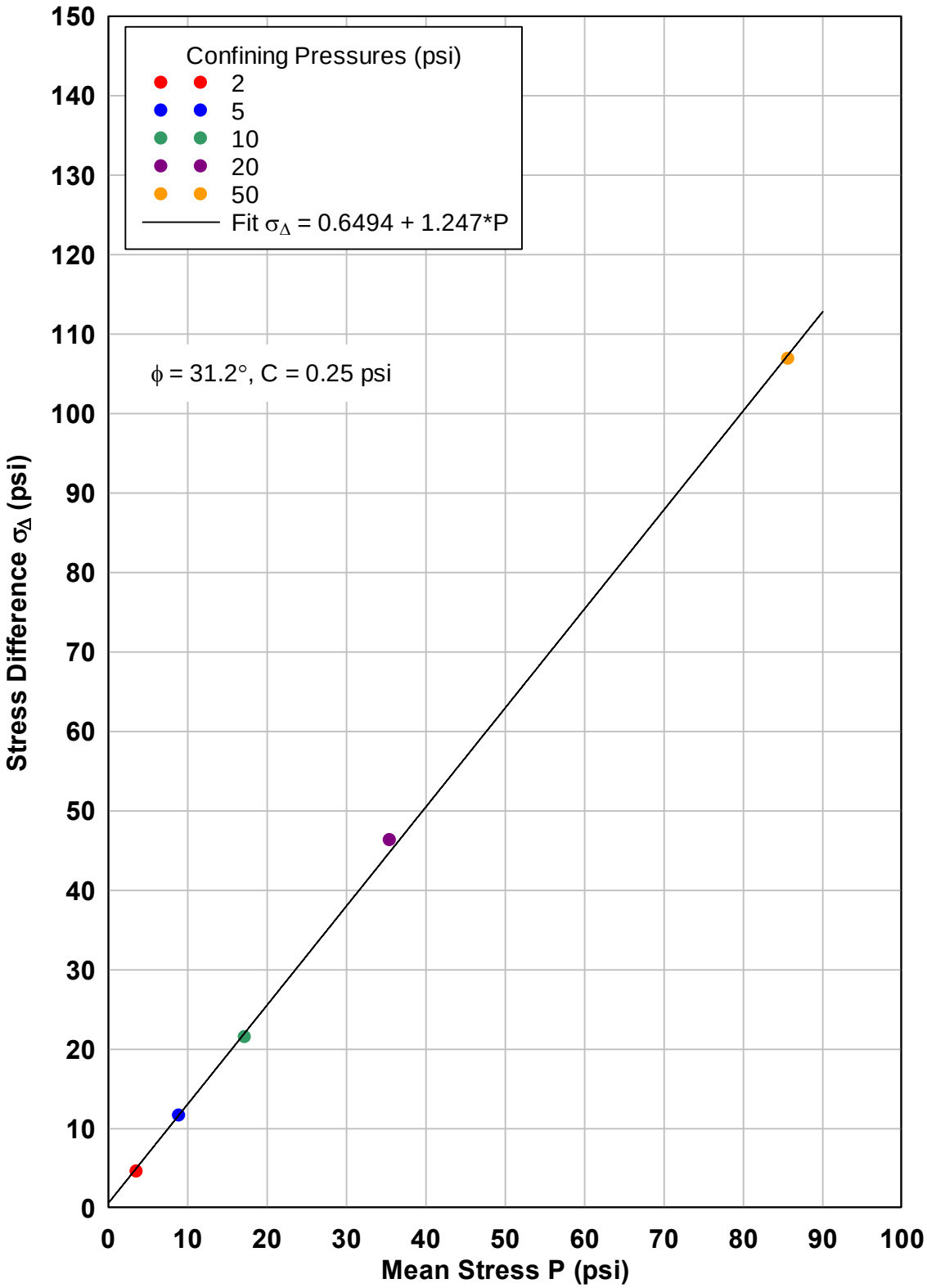

Figure 7-3: KSC HDF Sand model's strength envelope from triaxial tests.

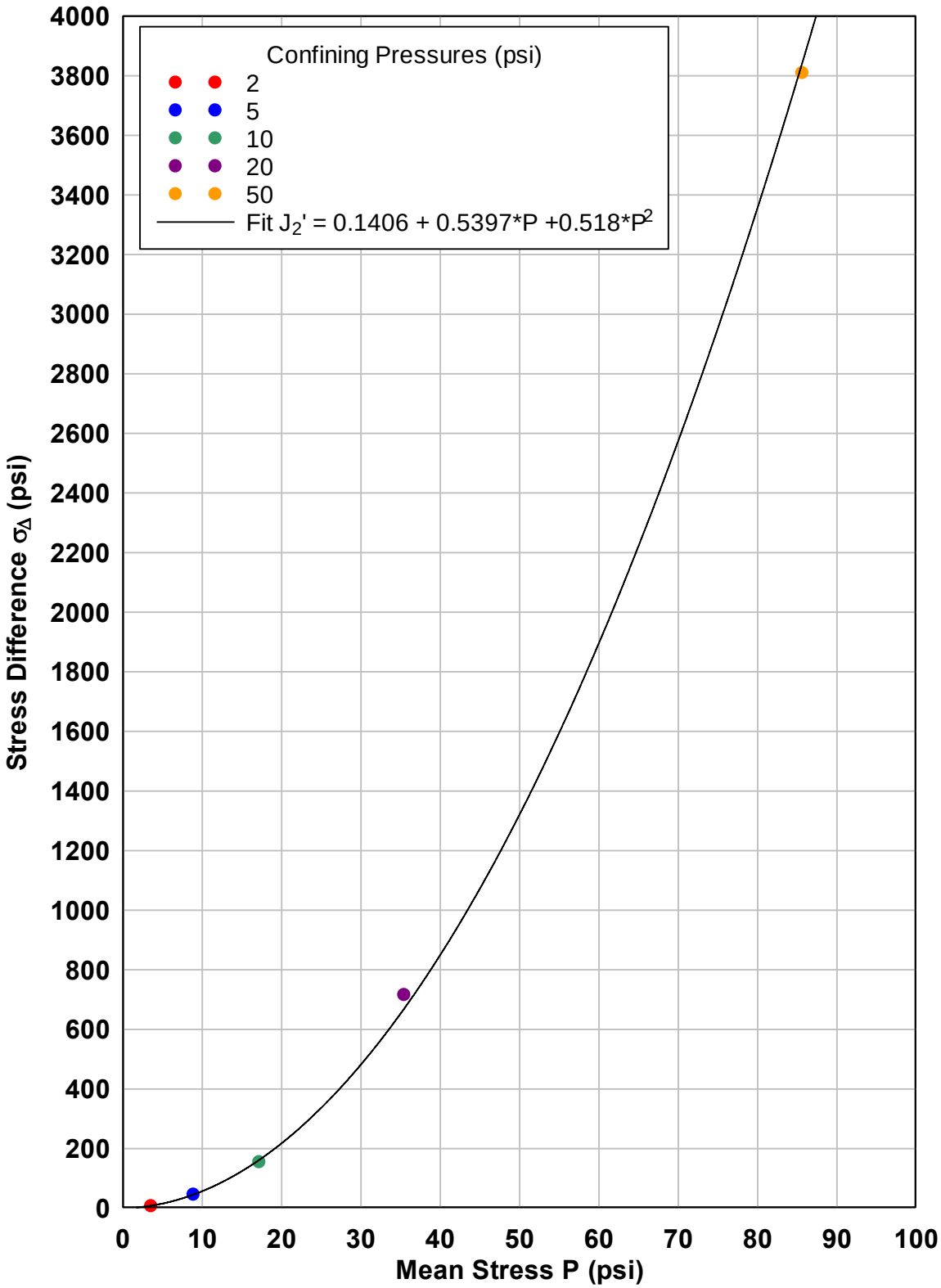

Figure 7-4: KSC HDF Sand Material Model 5 yield surface fit from strength envelope data.

7.2.2 Uniaxial strain

Uniaxial strain tests for KSC HDF Sand model are shown in the following five figures.

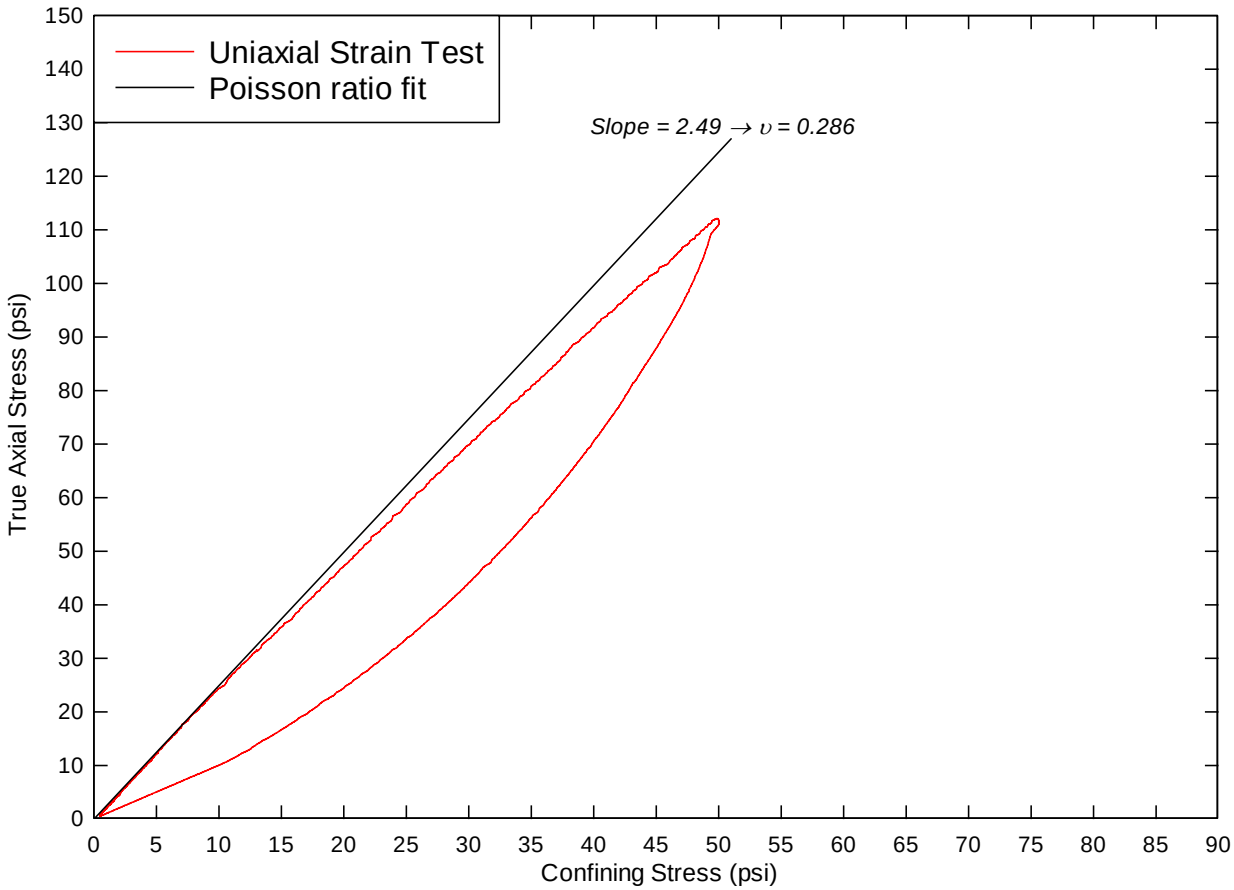

Figure 7-5: KSC HDF Sand model's uniaxial strain test. Axial stress vs. confining stress plotted to obtain Poisson's ratio from slopes.

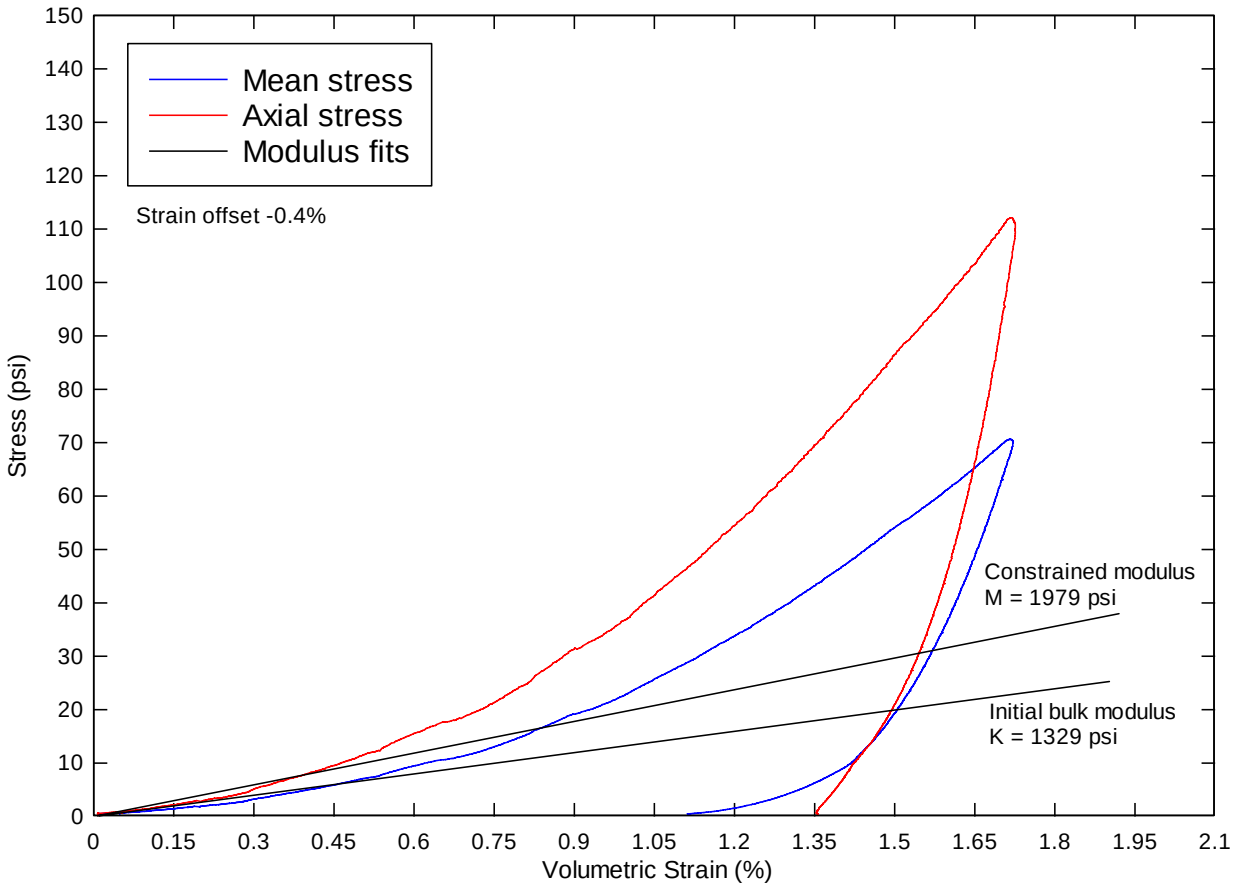

Figure 7-6: KSC HDF Sand's uniaxial strain test. Stress vs. strain plotted to obtain constrained modulus M and Initial Bulk Modulus K.

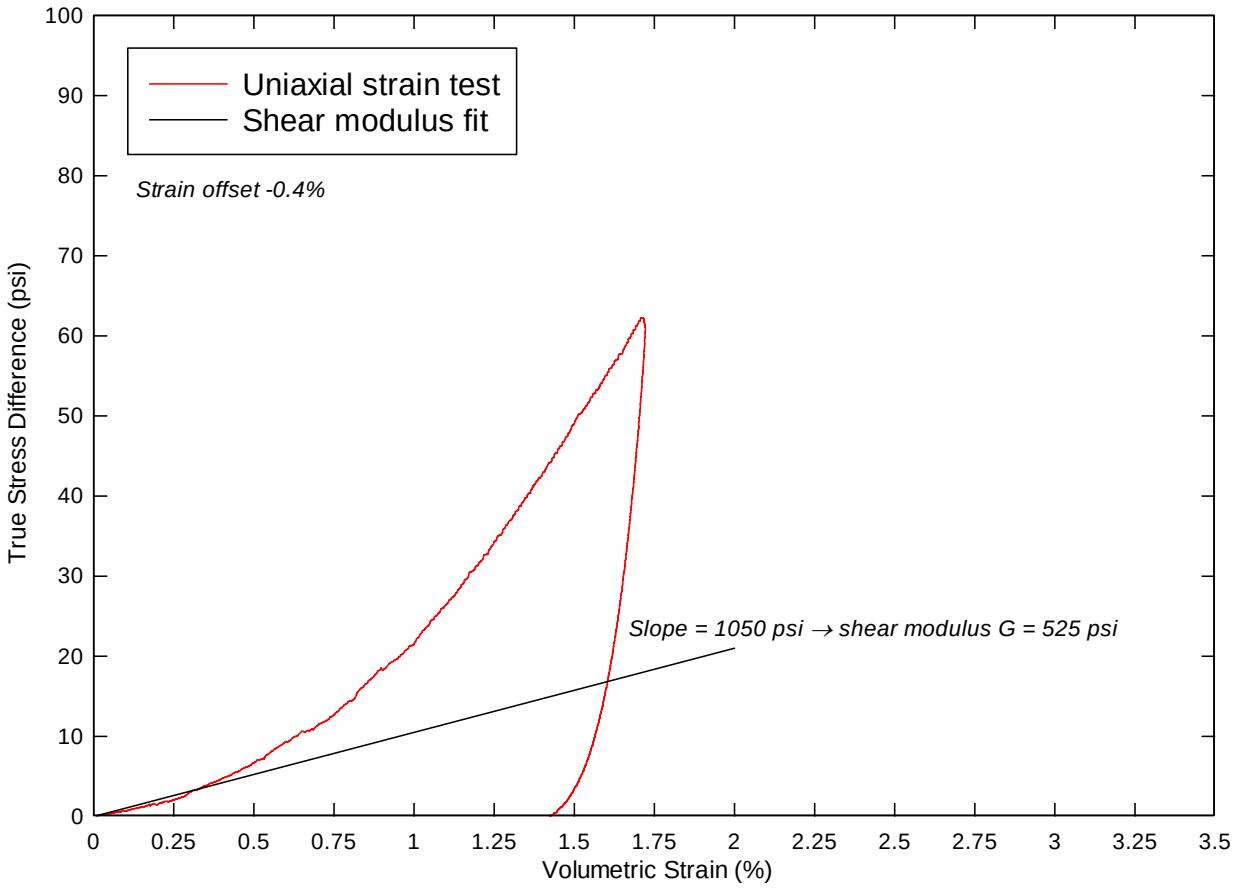

Figure 7-7: KSC HDF Sand model's uniaxial strain test. Stress difference vs. strain difference plotted to obtain shear modulus G from initial slope.

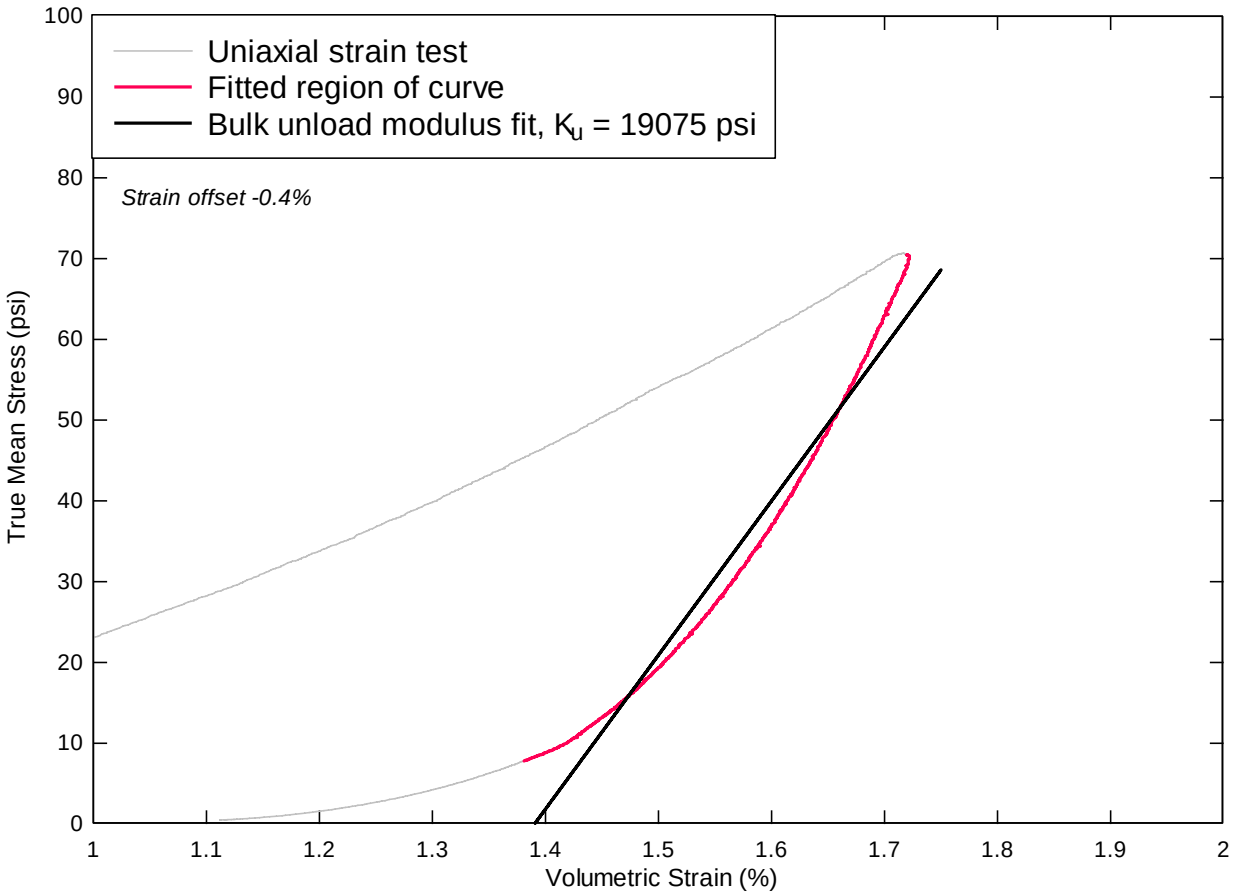

Figure 7-8: KSC HDF Sand model's uniaxial strain test. Mean stress vs. volumetric strain plotted to obtain bulk unload modulus K_u (BULK). Black line is linear fit to the red portion of the test data curve.

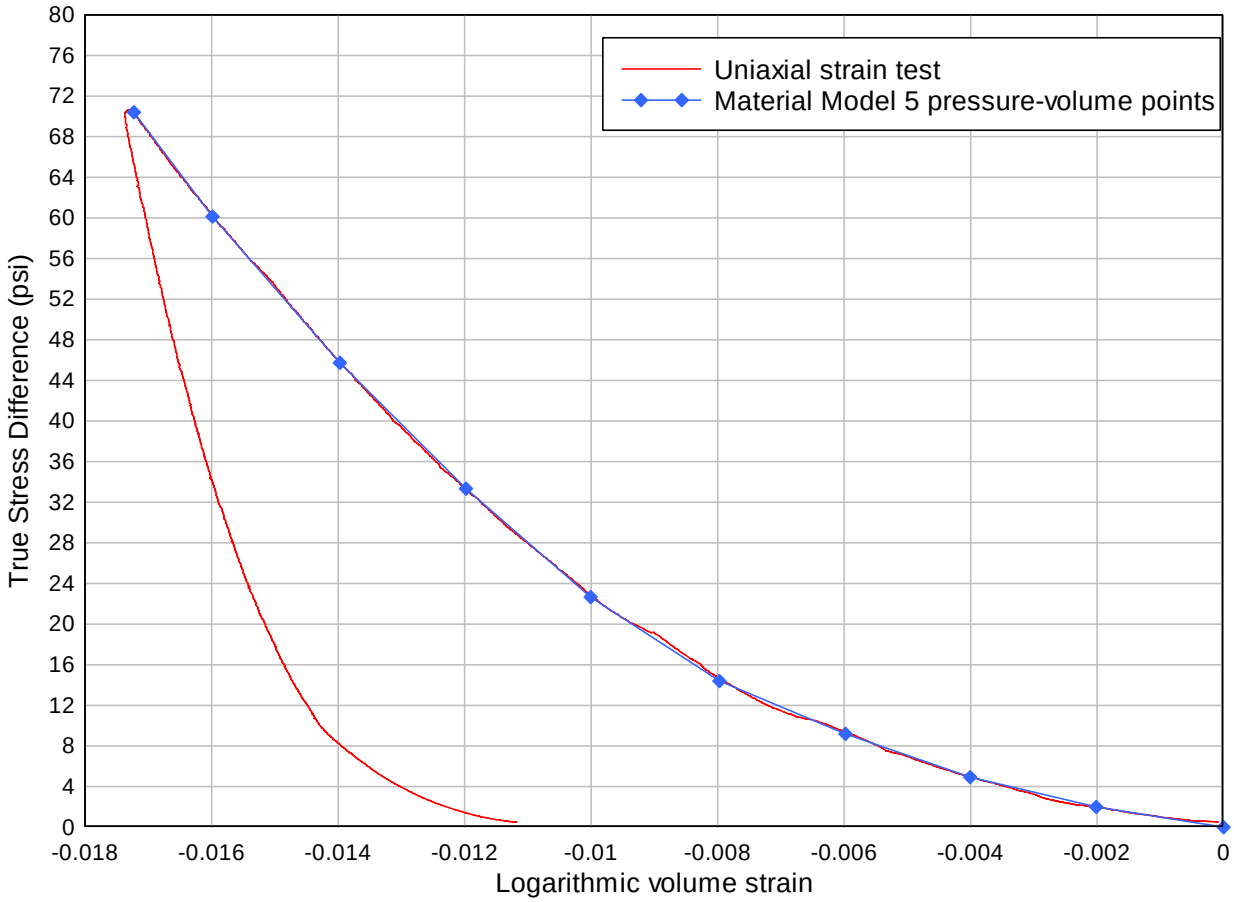

Figure 7-9: KSC HDF Sand model's uniaxial strain test. Mean stress vs. logarithmic volume strain plotted to obtain 10 points on Material Model 5's pressure-volume curve.

7.3 LS-DYNA Material Model 5 inputs

The recommended set of inputs for modeling KSC HDF Sand in LS-DYNA Material Model 5: Soil and Foam is shown in the Table 7-2. Table 7-3 is a summary of elastic constants.

Table 7-2: Material Model 5 inputs for KSC HDF Sand.

	Input	Value	Units
Mass density	**RO**	0.000135	lb s^2/in^4
Shear modulus	**G**	525	psi
Bulk unloading modulus	**K**	19075	psi
Yield surface coefficient	**A0**	0.1406	psi^2
Yield surface coefficient	**A1**	0.5397	psi
Yield surface coefficient	**A2**	0.5180	-
Pressure cutoff	**PC**	0	psi

	Input	Value	Input	Value	Units
Pressure-volume point	**EPS1**	0.0000	**P1**	0.00	psi
Pressure-volume point	**EPS2**	-0.0020	**P2**	2.00	psi
Pressure-volume point	**EPS3**	-0.0040	**P3**	4.93	psi
Pressure-volume point	**EPS4**	-0.0060	**P4**	9.20	psi
Pressure-volume point	**EPS5**	-0.0080	**P5**	14.40	psi
Pressure-volume point	**EPS6**	-0.0100	**P6**	22.67	psi
Pressure-volume point	**EPS7**	-0.0120	**P7**	33.33	psi
Pressure-volume point	**EPS8**	-0.0140	**P8**	45.73	psi
Pressure-volume point	**EPS9**	-0.0160	**P9**	60.13	psi
Pressure-volume point	**EPS10**	-0.0172	**P10**	70.40	psi

Table 7-3: Summary of elastic constants for KSC HDF Sand.

Constrained Modulus - M	1979	psi
Poisson's Ratio - n	0.286	
Young's Modulus - E	1220	psi
Initial Bulk Modulus - K	1329	psi
Shear Modulus - G	525	psi

8 Soil to Soil Comparisons

Plots of model to model comparisons for all LaRC soils tested by ARA are included as Figure 8-1 and Figure 8-2 to demonstrate the relative strengths and softness of each soil model. Ranked from strongest to weakest in terms of strength envelopes, the order is: KSC LDD Sand, KSC HDF Sand, Unwashed Sand, and KSC HDI Sand.

Ranked in terms of softest to stiffest, the order is: KSC LDD Sand, KSC HDI Sand, KSC HDF Sand, and Unwashed Sand. Both Option 1 and 2 for KSC LDD Sand are shown in Figure 8-2. The actual data is the dotted line, while the effect of smoothing is shown as a solid line.

The grain size distribution shown in Figure 8-3 clearly illustrates the difference between sands and silts/clays.

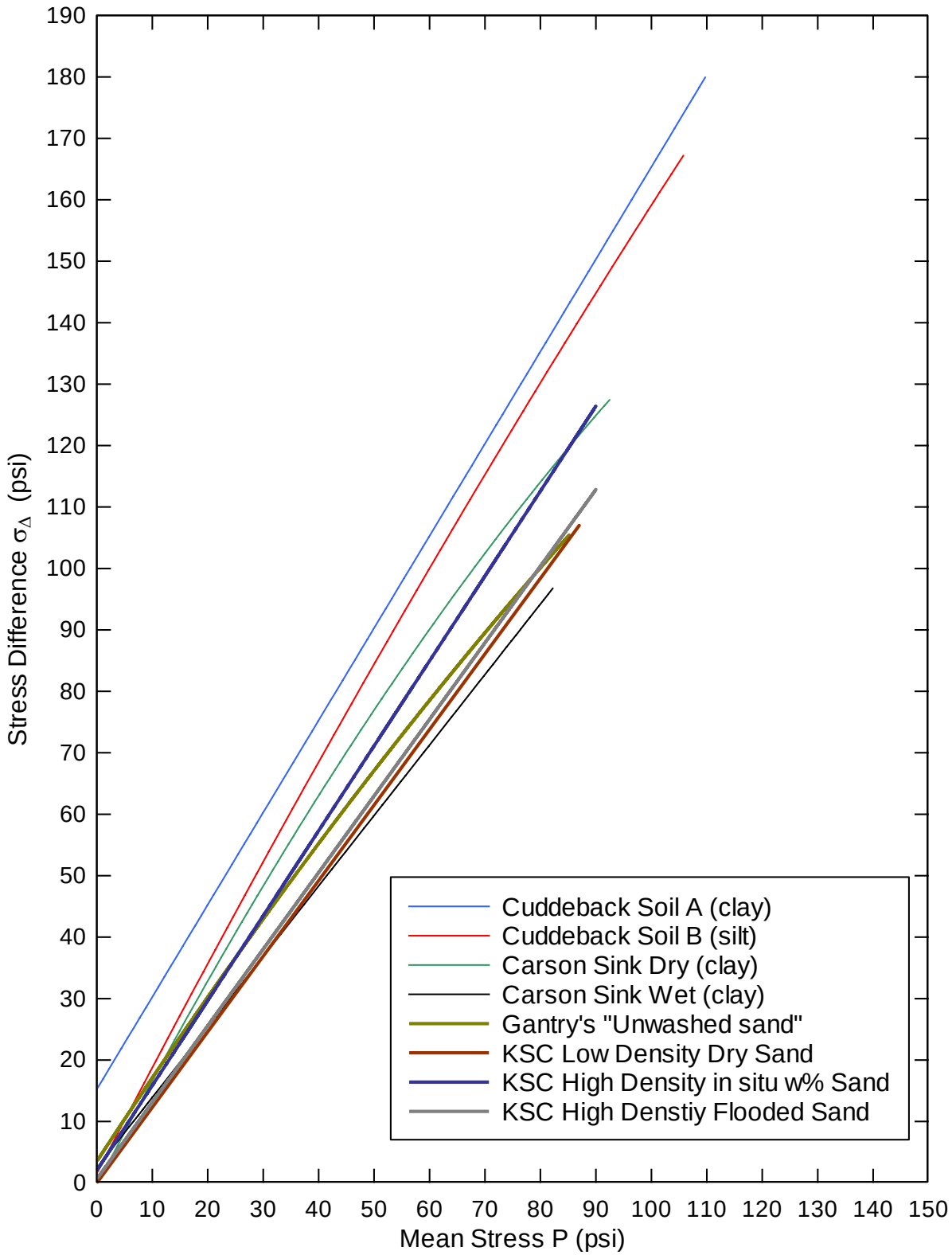

Figure 8-1: Comparison of soil strengths between models.

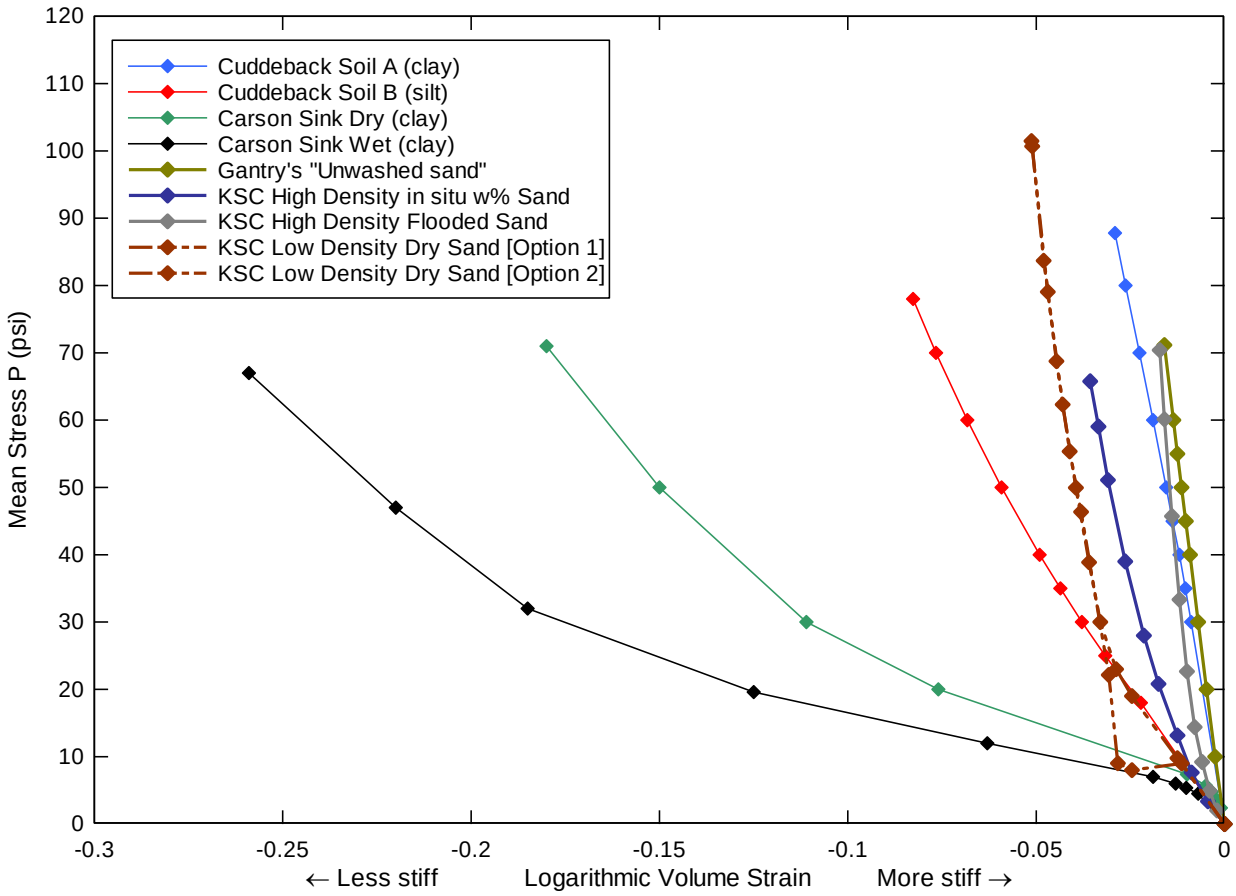

Figure 8-2: Comparison of soil stiffness between models.

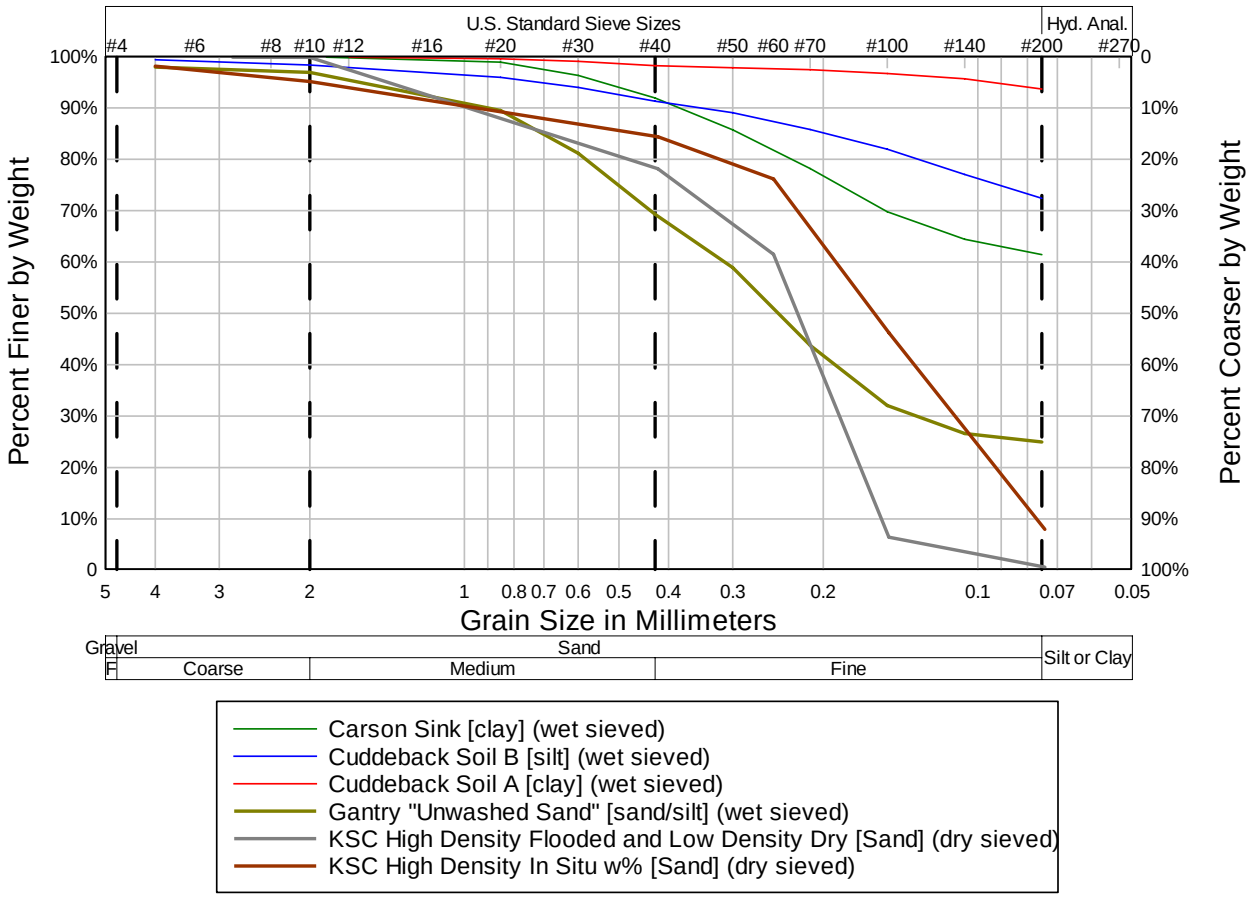

Figure 8-3: Comparison of grain size distribution for all soils.

9 Closing Remarks

The soil models presented here are based on static strength and compressibility tests. No attempt was made at impact loading the soil, nor accounting for strain rate effects. All test specimens were reconstituted from field dug samples.

LS-DYNA *Material Model 5: Soil and Foam* is a basic model well suited for preliminary design purposes. However, this is not the only soil model available. There have been many pressure-dependent material strength models developed for LS-DYNA, one of which is Material Model 25, the *Geological Cap* model. It is more complex than Material Model 5 because it uses kinematic hardening parameters. It uses two surfaces, an initial yield surface and a failure surface. The kinematic hardening parameters alter the behavior of the soil when moving from the initial yield to failure. This feature makes Material Model 25 a higher fidelity soil model because it accounts for more dynamic effects. The laboratory tests required to construct Material Model 25 are the same as Material Model 5. Using the test data for presented here with an additional calibration effort, it is possible to construct a *Geological Cap* model.

10 References

1. "LS-DYNA Theory Manual," 2006, Livermore Software Technology Corporation, Livermore, California.

2. ASTM D2850-03a(2007) Standard Test Method for Unconsolidated-Undrained Triaxial Compression Test on Cohesive Soils.

3. ASTM D6938-08 Standard Test Method for In-Place Density and Water Content of Soil and Soil-Aggregate by Nuclear Methods (Shallow Depth).

4. ASTM D6913-04e1 Standard Test Methods for Particle-Size Distribution (Gradation) of Soils Using Sieve Analysis.

5. ASTM D2216-05 Standard Test Methods for Laboratory Determination of Water (Moisture) Content of Soil and Rock by Mass.

6. ASTM D854-06 Standard Test Methods for Specific Gravity of Soil Solids by Water Pycnometer.

7. ASTM D6951-03 Standard Test Method for Use of the Dynamic Cone Penetrometer in Shallow Pavement Applications.

8. ASTM D4318-05 Standard Test Methods for Liquid Limit, Plastic Limit, and Plasticity Index of Soils (Atterberg Limits).

9. "Soil, Groundwater, Surface Water, and Sediments of Kennedy Space Center, Florida: Background Chemical and Physical Characteristics," 2000, Dynamac Corporation, NASA Environmental Program Office, KSC, FL.

10. "Constitutive Soil Properties for Cuddeback Lake, CA and Carson Sink, NV," 2008, Applied Research Associates, NASA Langley Research Center, Hampton, VA.

11. "Geology, Geohydrology And Soils Of Kennedy Space Center: A Review", 1990, Bionetics Corporation, Kennedy Space Center, FL.

Appendix A: LS-DYNA Theory Manual for Material Model 5

Appendix A is taken from the "LS-DYNA Theory Manual," 2006, Livermore Software Technology Corporation, Livermore, California. The excerpts shown below are from the Material Model 5 description starting on Page 19.21 of the LS-DYNA Theory Manual.

LS-DYNA is a registered trademark of the Livermore Software Technology Corporation.

The following boxed figures are copied from the LS-DYNA Theory Manual. The copied pages refer to the equations used in deriving constitutive parameters in Chapter 3.

Material Model 5: Soil and Crushable Foam

This model, due to Krieg [1972], provides a simple model for foam and soils whose material properties are not well characterized. We believe the other foam models in LS-DYNA are superior in their performance and are recommended over this model which simulates the crushing through the volumetric deformations. If the yield stress is too low, this foam model gives nearly fluid like behavior.

A pressure-dependent flow rule governs the deviatoric behavior:

$$\phi_s = \frac{1}{2} s_{ij} s_{ij} - \left(a_0 + a_1 p + a_2 p^2 \right) \qquad (19.5.1)$$

where a_0, a_1, and a_2 are user-defined constants. Volumetric yielding is determined by a tabulated curve of pressure versus volumetric strain. Elastic unloading from this curve is assumed to a tensile cutoff as illustrated in Figure 19.5.1.

Implementation of this model is straightforward. One history variable, the maximum volumetric strain in compression, is stored. If the new compressive volumetric strain exceeds the stored value, loading is indicated. When the yield condition is violated, the updated trial stresses, s_{ij}^*, are scaled back using a simple radial return algorithm:

$$s_{ij}^{n+1} = \left(\frac{a_0 + a_1 p + a_2 p^2}{\frac{1}{2} s_{ij} \, s_{ij}} \right)^{1/2} s_{ij}^* \qquad (19.5.2)$$

If the hydrostatic tension exceeds the cutoff value, the pressure is set to the cutoff value and the deviatoric stress tensor is zeroed.

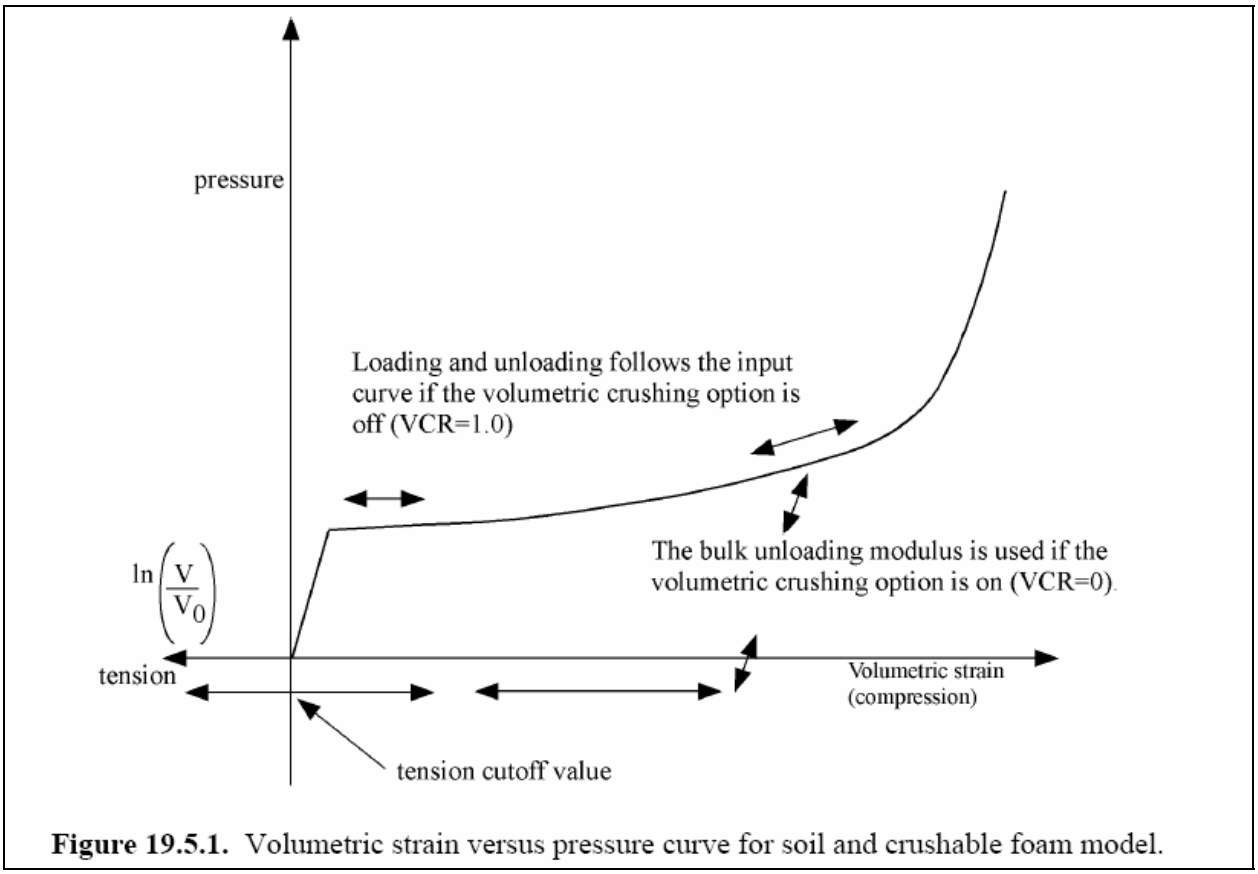

Figure 19.5.1. Volumetric strain versus pressure curve for soil and crushable foam model.

Krieg, R. D., "A Simple Constitutive Description for Cellular Concrete," Sandia National Laboratories, Albuquerque, NM, Rept. SC-DR-72-0883 (1972).

Appendix B: Field Report

The ARA field report is included as Appendix B.

Field Report February 24-26, 2008
Constitutive Soil Properties for NASA Langley

Kennedy Space Center, Florida

ARA was on site at the NASA Kennedy Space Center (KSC) by request of Dr. Ralph Buehrle to collect soil samples for geotechnical lab analysis. The lab analysis was conducted at the ARA New England Division Rock and Soil Test Laboratory in South Royalton, Vermont.

Dr. Buehrle of NASA Langley was onsite to facilitate entry to the site and observe the field activities. Mike Thomas and Casey T'Kindt were onsite representing the ARA Capital Area Division and the Shock Physics Division, respectively. Mike and Casey were onsite to collect the soil samples and take note of the conditions and locations of the sampled soils.

Dynamac is a company that provides environmental services to NASA and is housed at KSC. Paul Schmalzer and Tammy Foster of Dynamac accompanied us as security escorts and were generous in sharing knowledge of the site history and makeup.

Overall the soil across the site was very similar mostly made up fine to medium sand with up to 30% shell fragment content. The site is generally flat with elongated dune deposits that parallel the shoreline. Most of the site is covered with vegetation and or water. In the areas of vegetation the bushes and grasses are generally growing out of sand soil without much organic soil overburden. The thickest organic soil observed during this field visit was 7 inches of organic silt over sand at the shoreline of one of the inland ponds/lakes. The vast majority of that soil was covered with water and make up the mucky bottom of the lakes.

ARA sampled the soils using a shovel to dig shallow holes to expose the soil for logging. The soil was logged and photographs were taken of the sample locations to describe the native condition of the soils. Soil samples were collected by filling plastic bags with a shovel and sealing the bags with a wire tie and duct tape. The bags were placed into plastic 5-gal buckets for shipment to the lab. The soils were grab sampled and none of them were sampled intact. The laboratory will reconstitute the samples into various densities and water contents based on density measurements conducted on site by Dynamac during their environmental baseline site analysis.

Soil was sampled from five locations. Three of the samples of the samples were taken for testing and two addition samples were taken for reference. The samples for testing were taken from 1) the 39B Launch Pad area, 2) the beach near dune deposits and 3) the beach in the surf zone during low tide. Additionally, two samples were taken at the beach near the Pad 39A Camera Pad halfway between the dune and the shore on the beach and again in the surf zone for reference. Those samples were very similar to the beach samples taken for testing at the north end of the beach near the northern border of NASA-KSC.

Below are a map of the sample locations, photos of the sampling, and a log of soil descriptions.

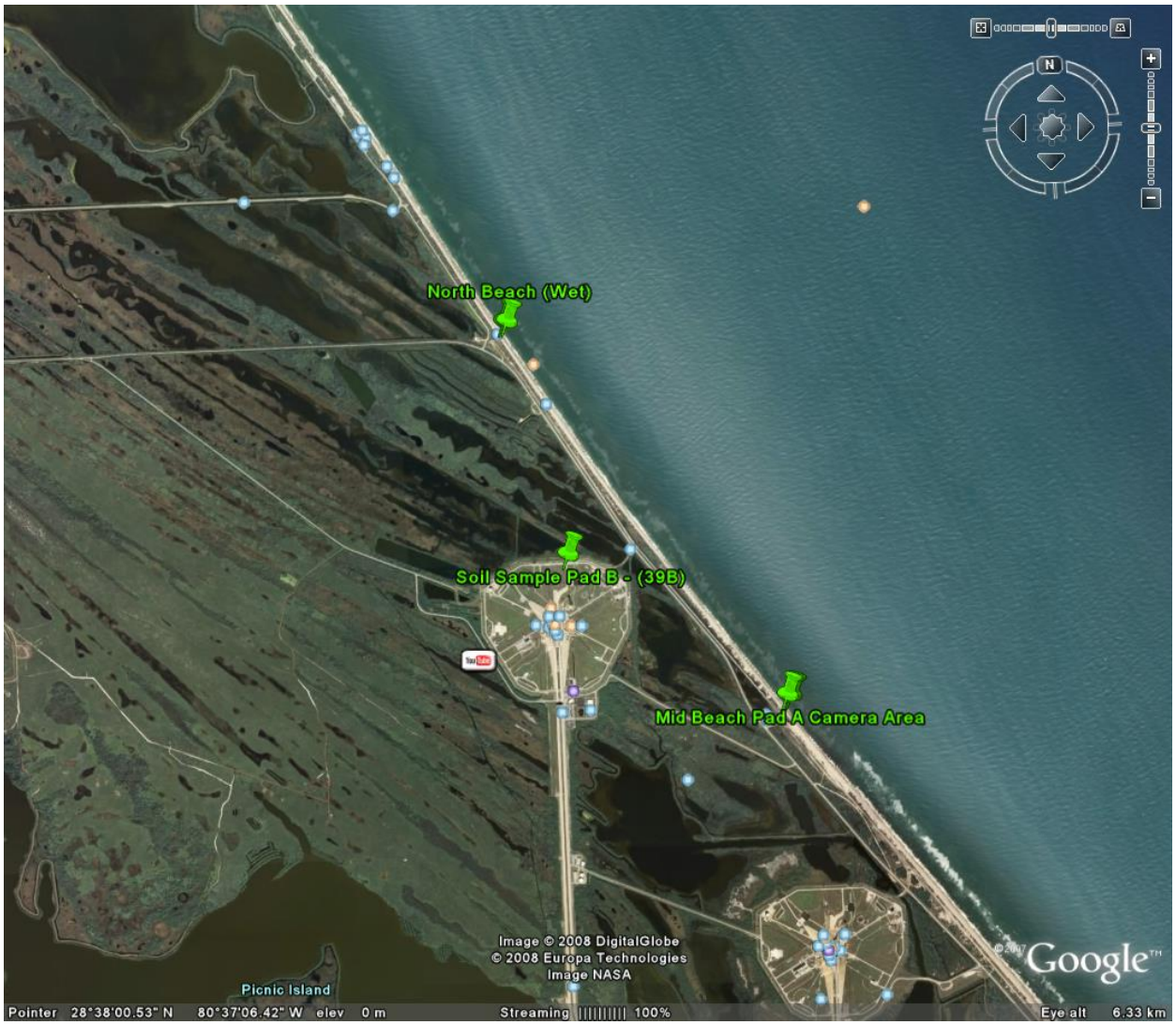

Figure B4 NASA Kennedy Space Center Sample Locations

Figure B5 Soil Sample Location - Pad 39B (KSC HDI Sand source)

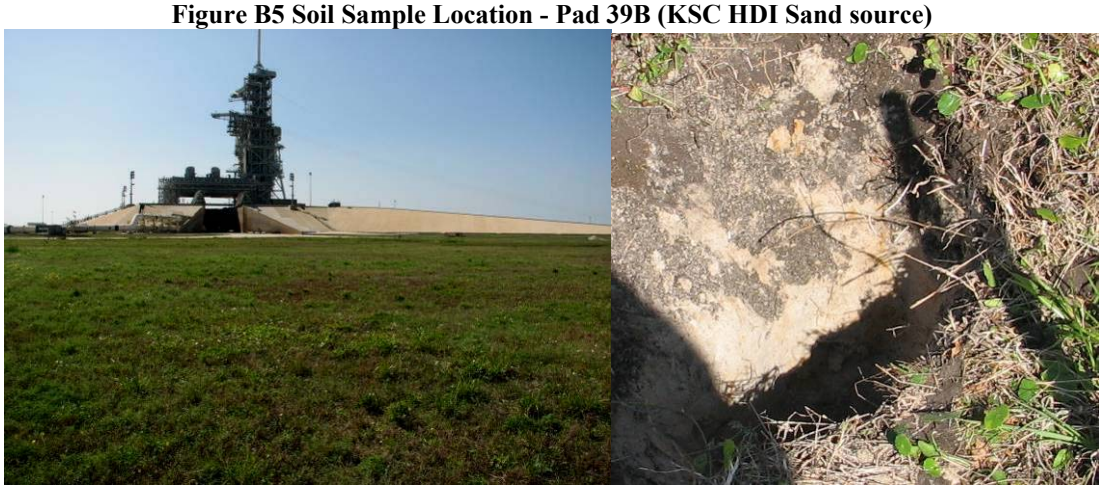

Figure B6 Soil Sample Location - North Beach (KSC LDD Sand source)

Figure B7 Soil Sample Location - North Beach Surf Zone (KSC HDF Sand source)

Table B1 Soil Log

Purpose	Kennedy Space Center (KSC) Location		Soil Description	UTM WSG 84 (m)	Coordinates (m)	Sample Volume
TEST	**Pad 39B**		Grassy Lawn Surface	537116	3167098	9 bags in 2 buckets
		0-4"	Dark Brown Sandy Organic Silt with occ Grass roots (OL)			
		4-24"	light brown fine to medium sand w/silt, orange mottling, med dense to dense and moist (SP-SM)			
			(placed fill, source was likely dredged from nearby source)			
TEST	**North End Beach (dry)** (area out of normal surf near dunes)	0-24"	light brown fine to medium sand, dense to very dense (0-2" loose beach sand), moist (SP) **(Surface was wind blown sand deposits with very occasional plants, grassy inland from here.** **Soil is approximately 70% rock mineral e.g. quartz, 30% clear to amber colored shell fragments.)**	536776	3168563	9 bags in 2 buckets
TEST	**North End Beach (wet)** (soil sampled in surf zone at lowering tide)	0-24"	light brown fine to medium sand, very dense, saturated (SP) **(hole filled with water during sampling. Two bags with native water was sampled other** **bags slightly drained. Soil is approximately 70% rock mineral e.g. quartz, 30% clear to amber** **colored shell fragments.)**	536790	3168562	10 bags in 2 buckets
Reference	**Beach east of PAD A Camera Pad (dry)** (soil sampled from mid beach, halfway between dunes and surf)	0-6"	light brown fine with black flecks to medium sand, medium dense, moist (SP)	539723	3164530	5-6 bags in 1 bucket
		6-24"	light reddish brown fine to medium sand, dense, moist (SP)			
			(Black flecks may be charcoal deposited by wind in periodic controlled burns. Surface was wind blown sand deposits with very occasional plants. Soil is approximately 70% rock mineral e.g. quartz, **30% clear to amber colored shell fragments.)**			
Reference	**Beach east of PAD A Camera Pad (wet)** (soil sampled in surf zone during out going tide)	0-24"	light brown fine to coarse sand, very dense and saturated, occasional live ocean organisms (worm, snails) (SP) **(30% clear to amber shell fragments)**	539745	3164578	5 bags in 1 bucket
Reference	**shoreline of swamp/pond**	0-7"	dark brown organic silt with sand and white shell fragments, soft and saturated	537439	3167103	None
		7-15"	light brown fine to medium sand with shell fragments, dense and moist to wet			

Appendix C: Laboratory data

Because of the volume of laboratory data generated, all of the raw lab data could not be combined into this report without due encumbrance. The test log, individual triaxial tests, tabular values for all test plots, and other laboratory data can be made available on disk or as a separate file.

REPORT DOCUMENTATION PAGE

Form Approved
OMB No. 0704-0188

1. REPORT DATE *(DD-MM-YYYY)*	2. REPORT TYPE	3. DATES COVERED *(From - To)*
01- 07 - 2008	Contractor Report	

4. TITLE AND SUBTITLE
Constitutive Soil Properties for Unwashed Sand and Kennedy Space Center

5a. CONTRACT NUMBER
NNL07AA00B

5b. GRANT NUMBER

5c. PROGRAM ELEMENT NUMBER

6. AUTHOR(S)
Thomas, Michael A.; Chitty, Daniel E.; Gildea, Martin L.; and T'Kindt, Casey M.

5d. PROJECT NUMBER

5e. TASK NUMBER

5f. WORK UNIT NUMBER
644423.04.31.04.40.42

7. PERFORMING ORGANIZATION NAME(S) AND ADDRESS(ES)
NASA Langley Research Center
Hampton, VA 23681-2199

Applied Research Associates, Inc.
4300 San Mateo Blvd. NE, Suite A-220
Albuquerque, NM 87110

8. PERFORMING ORGANIZATION REPORT NUMBER

9. SPONSORING/MONITORING AGENCY NAME(S) AND ADDRESS(ES)
National Aeronautics and Space Administration
Washington, DC 20546-0001

10. SPONSOR/MONITOR'S ACRONYM(S)
NASA

11. SPONSOR/MONITOR'S REPORT NUMBER(S)
NASA/CR-2008-215334

12. DISTRIBUTION/AVAILABILITY STATEMENT
Unclassified - Unlimited
Subject Category 39
Availability: NASA CASI (301) 621-0390

13. SUPPLEMENTARY NOTES
Langley Technical Monitor: Ralph D. Buehrle
An electronic version can be found at http://ntrs.nasa.gov

14. ABSTRACT

Accurate soil models are required for numerical simulations of land landings for the Orion Crew Exploration Vehicle. This report provides constitutive material models for one soil, unwashed sand, from NASA Langley's gantry drop test facility and three soils from Kennedy Space Center (KSC). The four soil models are based on mechanical and compressive behavior observed during geotechnical laboratory testing of remolded soil samples. The test specimens were reconstituted to measured in situ density and moisture content. Tests included: triaxial compression, hydrostatic compression, and uniaxial strain. A fit to the triaxial test results defines the strength envelope. Hydrostatic and uniaxial tests define the compressibility. The constitutive properties are presented in the format of LS-DYNA Material Model 5: Soil and Foam. However, the laboratory test data provided can be used to construct other material models. The four soil models are intended to be specific to the soil conditions discussed in the report. The unwashed sand model represents clayey sand at high density. The KSC models represent three distinct coastal sand conditions: low density dry sand, high density in-situ moisture sand, and high density flooded sand. It is possible to approximate other sands with these models, but the results would be unverified without geotechnical tests to confirm similar soil behavior.

15. SUBJECT TERMS
LSDYNA; Consitutive properties; Impact; Soil models

16. SECURITY CLASSIFICATION OF:			17. LIMITATION OF ABSTRACT	18. NUMBER OF PAGES	19a. NAME OF RESPONSIBLE PERSON
a. REPORT	b. ABSTRACT	c. THIS PAGE			STI Help Desk (email: help@sti.nasa.gov)
					19b. TELEPHONE NUMBER *(Include area code)*
U	U	U	UU	100	(301) 621-0390